Brief Communication

Cell Chemical Biology

CLK2 and CLK4 are regulators of DNA damage-induced NF-κB targeted by novel small molecule inhibitors

Graphical abstract

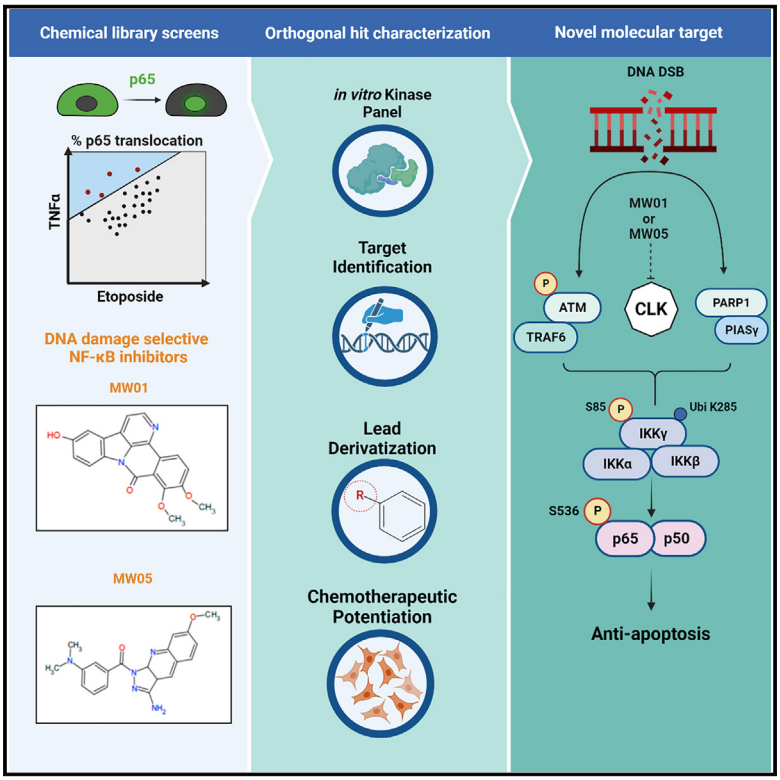

Highlights

- Discovery of pathway selective chemical NF-κB inhibitors for genotoxic cancer therapy
- CLK2 and 4 serve as drug targets and transmit signaling from ATM and PARP1 to IKKγ
- The lead compounds strongly synergize with chemotherapeutics to kill cancer cells

Authors

Patrick Mucka, Peter Lindemann, Bartolomeo Bosco, ..., Jens Peter von Kries, Marc Nazaré, Claus Scheidereit

Correspondence

nazare@fmp-berlin.de (M.N.), scheidereit@mdc-berlin.de (C.S.)

In brief

DNA-damaging cancer therapies activate transcription factor NF-κB, counteracting tumor cell killing. Using high-throughput screening, Mucka et al. identified compounds that selectively inhibit NF-κB following DNA damage and potentiate chemotherapy-induced apoptosis. The drugs target the kinases CLK2 and CLK4, which transfer genotoxic stress signaling to the IκB kinase complex.

Mucka et al., 2023, Cell Chemical Biology *30*, 1303–1312
October 19, 2023
https://doi.org/10.1016/j.chembiol.2023.06.027

CellPress

Cell Chemical Biology

CellPress
OPEN ACCESS

Brief Communication

CLK2 and CLK4 are regulators of DNA damage-induced NF-κB targeted by novel small molecule inhibitors

Patrick Mucka,[1] Peter Lindemann,[2,4] Bartolomeo Bosco,[1,4] Michael Willenbrock,[1,4] Silke Radetzki,[3] Martin Neuenschwander,[3] Cristina Brischetto,[1] Jens Peter von Kries,[3,5] Marc Nazaré,[2,*] and Claus Scheidereit[1,6,*]

[1]Laboratory of Signal Transduction in Tumor Cells, Max Delbrück Center for Molecular Medicine, 13125 Berlin, Germany
[2]Laboratory of Medicinal Chemistry, Leibniz Forschungsinstitut für Molekulare Pharmakologie, 13125 Berlin, Germany
[3]Screening Unit, Leibniz Forschungsinstitut für Molekulare Pharmakologie, 13125 Berlin, Germany
[4]These authors contributed equally
[5]Senior author
[6]Lead contact
*Correspondence: nazare@fmp-berlin.de (M.N.), scheidereit@mdc-berlin.de (C.S.)
https://doi.org/10.1016/j.chembiol.2023.06.027

SUMMARY

Transcription factor NF-κB potently activates anti-apoptotic genes, and its inactivation significantly reduces tumor cell survival following genotoxic stresses. We identified two structurally distinct lead compounds that selectively inhibit NF-κB activation by DNA double-strand breaks, but not by other stimuli, such as TNFα. Our compounds do not directly inhibit previously identified regulators of this pathway, most critically including IκB kinase (IKK), but inhibit signal transmission in-between ATM, PARP1, and IKKγ. Deconvolution strategies, including derivatization and *in vitro* testing in multi-kinase panels, yielded shared targets, cdc-like kinase (CLK) 2 and 4, as essential regulators of DNA damage-induced IKK and NF-κB activity. Both leads sensitize to DNA damaging agents by increasing p53-induced apoptosis, thereby reducing cancer cell viability. We propose that our lead compounds and derivatives can be used in context of genotoxic therapy-induced or ongoing DNA damage to increase tumor cell apoptosis, which may be beneficial in cancer treatment.

INTRODUCTION

Therapeutic resistance is a major hurdle to the treatment of cancer. However, drugs intervening in the molecular pathways regulating resistance remain elusive.[1,2] Traditional cancer treatments, such as chemo- and radiotherapies, generate DNA lesions leading to activation of anti-apoptotic and pro-survival genetic programs, a major regulator of which is transcription factor NF-κB.[3] Despite this well-established role within the broader DNA damage response (DDR) pathway, pharmacological inhibition of NF-κB activity specifically following DNA damage has not been previously achieved.

DNA double-strand breaks (DSBs), as induced by chemotherapeutics or γ-irradiation, are sensed by two sensors, ATM and PARP1, whose activation is required for triggering of the IκB kinase (IKK)/NF-κB pathway. PARP1 is recruited to DNA lesions within seconds and synthesizes poly(ADP-ribose) (PAR), attached to itself and other proteins, dissociates, and assembles a nucleoplasmic complex with IKKγ, ATM, and PIASy, in which IKKγ is phosphorylated and SUMOylated. Subsequently, *p*-ATM and modified IKKγ are exported to the cytoplasm.[4–6] Within the cytoplasm, an ATM-TRAF6-cIAP1 axis and PTM-modified IKKγ lead to IKK activation and to nuclear translocation of NF-κB.[7] Once in the nucleus, NF-κB potently upregulates the expression of anti-apoptotic genes, leading to tumor cell survival and thus therapeutic resistance to standard cancer therapies.[3,8,9]

Considering IKK's critical role as NF-κB master regulator, it would seem an attractive therapeutic target.[10] However, previous attempts to develop clinically applicable IKK inhibitors were unsuccessful due to widespread toxicity.[3,11] This is explained by the role of IKK-controlled NF-κB in integrating multiple stimuli, in addition to NF-κB-independent functions of IKK, including mRNA stability regulation.[12–14] Reflecting this broad role, deregulated IKK and NF-κB contribute to numerous pathological conditions including cancer and chronic inflammation.[15–17] Therefore, NF-κB inhibition remains conceptually attractive, but inhibitors must be developed that block IKK and NF-κB in a pathway selective manner upstream of IKK.

In this study, we differentially screened a chemical library with etoposide and TNFα and identified two structurally distinct selective inhibitors of DNA damage-induced NF-κB activity. CLK2 and CLK4 are targets of these compounds, which sensitize tumor cells to DNA-damaging agents. We propose that our compounds be used in the context of therapy-induced or ongoing genotoxic stress to reduce chemotherapeutic burden while treating cancer in the clinic.

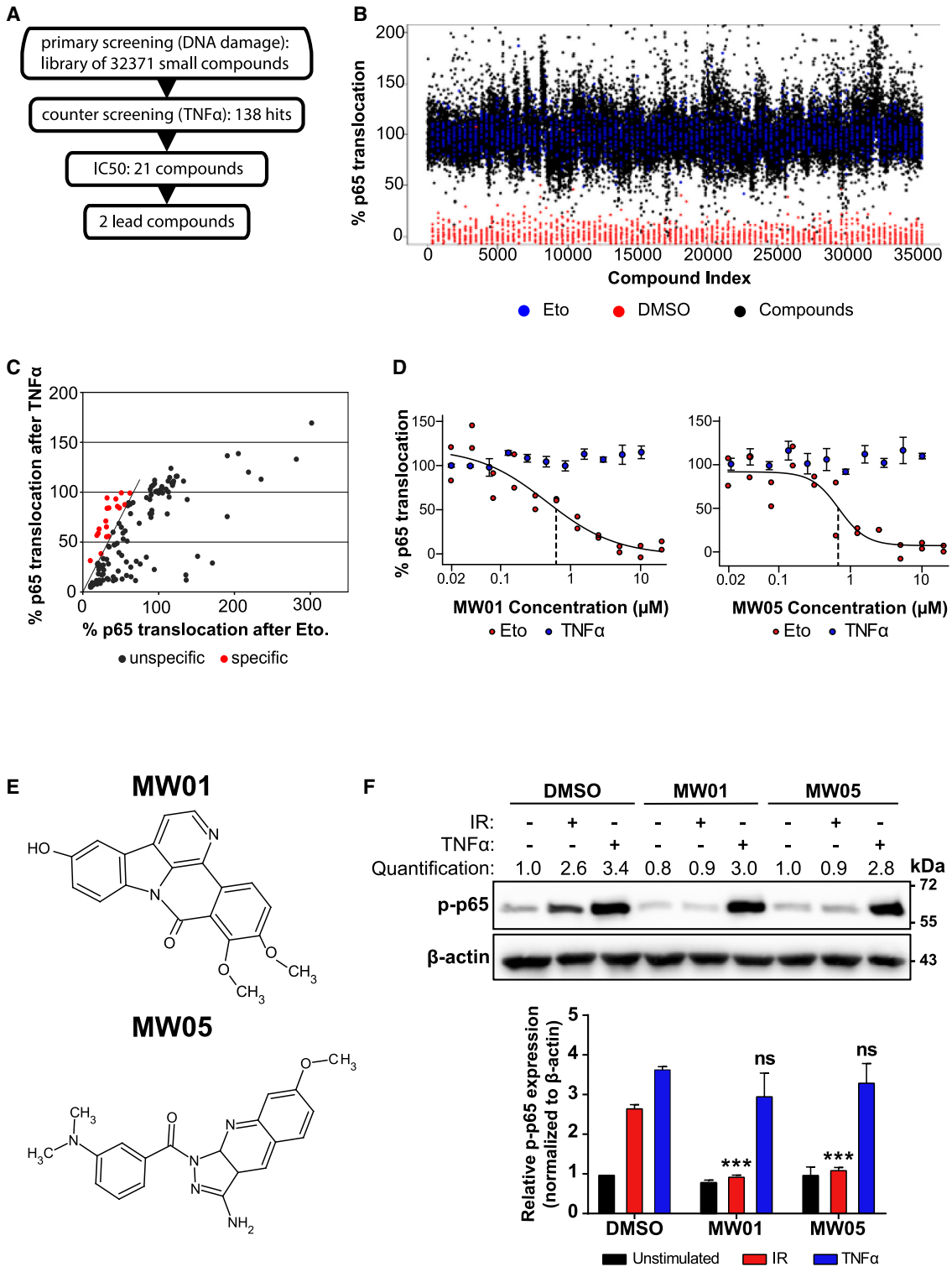

Figure 1. Identification of inhibitors specific for DNA damage-induced NF-κB activity

(A) Flowchart, high-throughput chemical library screening performed on U2-OS cells.

(B) Distribution of all compounds tested in etoposide-stimulated primary screen. Black dots represent individual compounds, blue dots etoposide-stimulated positive controls, and red dots DMSO-treated negative controls.

(C) Mean p65 nuclear translocation following etoposide or TNFα stimulation after treatment with each counter-screened hit compound. Values were normalized to etoposide or TNFα positive controls. Specific inhibitors (red) of DNA damage-induced NF-κB were defined by setting cut-off criteria (black line).

(legend continued on next page)

RESULTS

Identification of inhibitors specific for DNA damage-induced NF-κB activity

To identify inhibitors that selectively prevent DNA damage-induced NF-κB activation, we established a high-throughput screen quantifying p65 nuclear translocation, an essential step in NF-κB activation.[18] A chemical library of over 32,000 compounds was screened and 138 small molecule inhibitors of etoposide-induced p65 nuclear translocation were identified. These hit compounds were used in a subsequent TNFα-induced counter-screen and 21 compounds that inhibited NF-κB only after DNA damage were selected for IC50 determination (Figures 1A–1C). Among them, two promising structurally distinct compounds, MW01 and MW05, inhibited p65 translocation at sub-micromolar concentrations following etoposide treatment, without affecting p65 translocation upon TNFα stimulation, were selected for further investigation (Figures 1D and 1E). We synthesized both compounds and unambiguously characterized them by NMR and LC-MS/MS prior to further evaluation (Figures S1A and S1B and Data S1). Moreover, using epithelial CaCo2 cells, we found that both MW01 and MW05 show a sufficiently high rate of cellular absorption with low enough apparent permeability coefficients (P_{app}) to reach effective intracellular concentrations (Figure S1C). Both compounds significantly reduced p65 phosphorylation at serine 536, the substrate site of IKK,[19] only after DNA damage generation while leaving TNFα-stimulated and unstimulated levels untouched compared to DMSO-treated control (Figure 1F). We first re-confirmed the inhibition of p65 nuclear translocation by our two lead compounds (Figure S2A). In addition, other critical events in the genotoxic stress-induced NF-κB pathway, such as IR-induced IKKγ S85-phosphorylation and K285-monoubiquitination, were also inhibited by both lead compounds while others, such as PARP1 activation and PAR formation or nuclear ATM activation, were not (Figures S2B–S2E).[7,20–22] Furthermore, cleavage of PARP1, as apoptotic marker, was potentiated, while upregulation of anti-apoptotic NF-κB target gene BIRC3 was abolished by MW01 or MW05 following irradiation (Figures S2F and S2G). Thus, both compounds act downstream of the DNA sensors ATM and PARP1 and upstream of IKK. We therefore proceeded to investigate the molecular target, mechanism of action, and antitumor properties of our structurally distinct leads MW01 and MW05.

MW01 and MW05 are potent and selective kinase inhibitors

Based on their similar effects in our screen and molecular signaling pathway analysis, MW01 and MW05 were used in comparative target deconvolution studies seeking common targets. To eliminate previously identified kinases regulating NF-κB activity, such as IKK as possible targets, an *in vitro* kinase inhibition assay was performed. We tested 275 different kinases and found that both MW01 and MW05 are kinase inhibitors with distinct kinase inhibition profiles (Table S1). Importantly, no previously known kinases within the DNA damage-induced NF-κB pathway were inhibited (Table S1). IC50 values were determined for all strongly inhibited kinases contained in the broad panel for both compounds (Figure S3A). Interestingly, several hits shared by both lead compounds were found despite the more selective kinase inhibition profile of MW05, including various phosphatidylinositol phosphate kinases and CLK2 (Figure S3B). We next investigated if any of the shared kinase targets of MW01 and MW05 play a role in genotoxic stress-induced NF-κB activity. Based on the CaCo2 recovery values and experimental treatment concentration of 10 μM, the putative target kinase should have a low IC50 of, at most, 2000 nM for both lead compounds in the *in vitro* kinase panel (Figure S3A). Based on this criterion alone, we arrived at a relatively short list of potential targets for further analysis, leaving only PIK3CG, PIK3C2G, and CLK2 (Figure S3B). PIK3C2G was eliminated from further analysis since RNA expression data indicated high tissue specificity and lack of expression in our U2-OS model cell line.[23] DNA-PK and mTOR failed to meet the sub-2000 nM IC50 criteria for MW05 and MW01, respectively, but were scrutinized experimentally (Figure S3B). Importantly, CLK2 shared the most similar and second-lowest combined IC50 values, suggesting that strong inhibition is likely reached at 10 μM in cell-based assays, so we carried out further analysis on PIK3CG, CLK2, DNA-PK, and mTOR.

CLK2 and CLK4 are the shared targets of MW01 and MW05

To confirm kinase inhibition by MW01 and MW05 in our cell-based assays and to investigate their shared kinases, we tested PI-103, NU-7441, and MU-1210 as PI3K, DNA-PK, and CLK inhibitors, respectively, based on similar or lower IC50s for the shared target kinases of MW01 and MW05.[24–26] In addition, PI-103 also inhibits DNA-PK and mTOR with low nanomolar IC50s,[24] and therefore, this compound can be used to test if PI3K, DNA-PK, or mTOR are involved in NF-κB activation. As expected, based on the low nanomolar PI3K IC50s of MW01 and PI-103, we observed a complete reduction of *p*-Akt by either compound and a partial reduction by MW05, in agreement with its comparatively higher PI3K IC50 (Figure 2A).[24] In addition, DNA-PK inhibitor NU-7441 did not reduce p-p65 following either stimulation. We observed a reduction in p65 phosphorylation by MW01, MW05, and, interestingly, CLK inhibitor MU1210, but not its negative control MU140[27] (not shown), only after irradiation, suggesting experimentally for the first time that CLKs regulate irradiation-induced NF-κB activity (Figure 2A).

We determined potency and isoform specificity of all four CLKs for both MW01 and MW05, finding that MW01 is a CLK1, CLK2, and CLK4 inhibitor and MW05 is relatively less potent and displays selectivity toward CLK4, while both compounds

(D) IC50 determination for MW01 (left) and MW05 (right) of p65 nuclear translocation, following etoposide (red dots) or TNFα treatment (blue dots). MW01 etoposide-stimulated IC50: 460 nM MW05 etoposide-stimulated IC50: 690 nM. TNFα-stimulated for each: not determined. IC50 indicated by black dotted line.
(E) Structures of lead compounds MW01 (5-Hydroxy-10,11-dimethoxy-9H-benzo[*c*]indolo[3,2,1-ij][1,5]naphthyridin-9-one) and MW05 (3-Amino-7-methoxypyrazolo[3,4-*b*]quinolin-1-yl)-[3-(dimethylamino)phenyl]methanone).
(F) Western blot analysis (top) and quantification (bottom) of U2-OS cells following pre-treatment with DMSO, MW01 (10 μM), or MW05 (10 μM), unstimulated, after irradiation (IR), or after TNFα treatment. β-actin was used as loading control. ns: not significant; ***: $p < 0.001$.

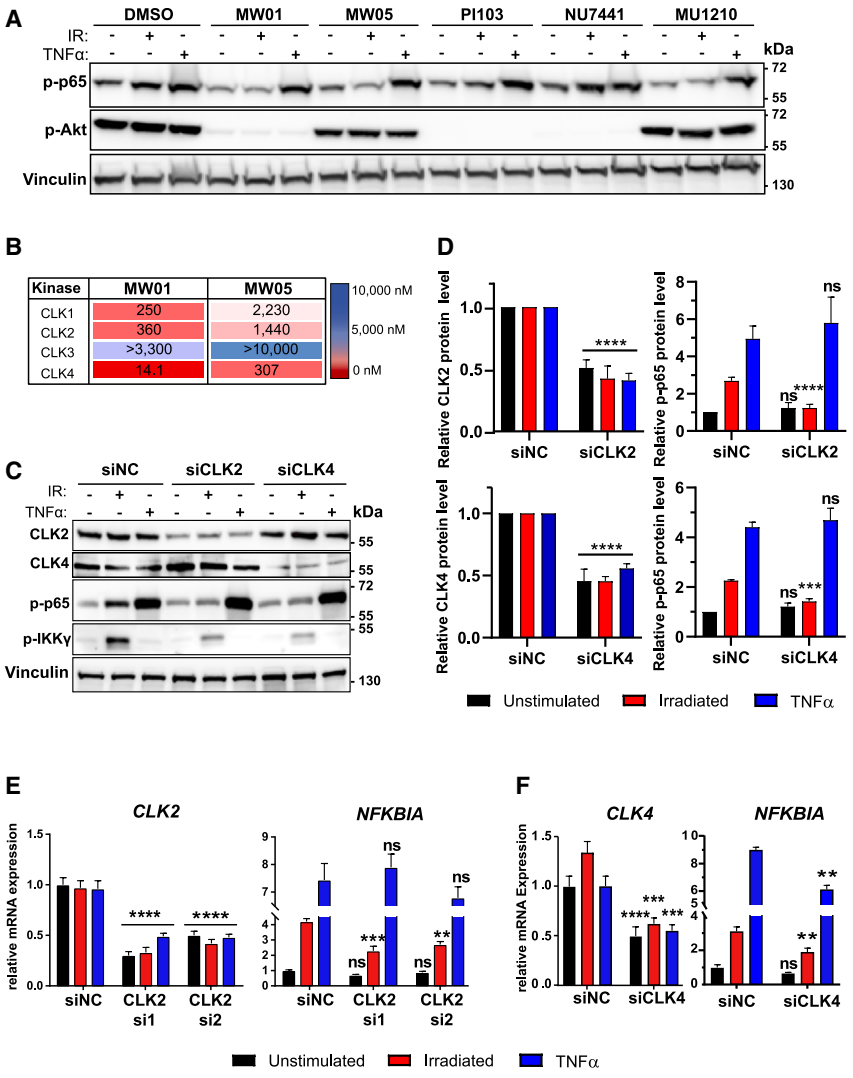

Figure 2. MW01 and MW05 are potent and selective kinase inhibitors

(A) Western blot analysis of U2-OS cells following pre-treatment with DMSO, MW01 (10 μM), MW05 (10 μM), PI-103 (1 μM), NU7441 (1 μM), or MU1210 (1 μM) unstimulated, after irradiation (IR), or after TNFα treatment.

(B) IC50 (nM) of MW01 and MW05 for all CLK isoforms. Lower IC50 is indicated by red color, higher by blue.

(C) Western blot analysis of U2-OS cells after transfection with siNC or CLK2 si2 unstimulated, after irradiation (IR), or after TNFα treatment. Vinculin used as loading control.

(D) Quantification from (C) with CLK2 knockdown and p-p65 quantification (top left and top right, respectively) and CLK4 knockdown and p-p65 (bottom left and bottom right, respectively. ns: not significant; **, ***, ****: $p < 0.01$, $p < 0.001$, $p < 0.0001$.

(E) mRNA expression of CLK2 (left) and NFKBIA (right) after transfection with siNC, CLK2 si1, or CLK2 si2. ns: not significant; **, ***, ****: $p < 0.01$, $p < 0.001$, $p < 0.0001$.

(F) mRNA expression analysis of CLK4 (left) and NFKBIA (right), with same experimental conditions and quantification as (E). ns: not significant; **, ***, ****: $p < 0.01$, $p < 0.001$, $p < 0.0001$. Western blots are representative images of three independent experiments. mRNA expression analyses are expressed as mean of three independent experiments with three technical replicates each.

largely spare CLK3 (Figure 2B). Importantly, with the CLK2 IC50 of 360 nM for MW01 and of 1,440 nM for MW05, and the CLK4 IC50 of 14.1 nM for MW01 and 307 nM for MW05, we expect sufficient levels of CLK2 and CLK4 inhibition at 10 μM in cell-based assays. To investigate the role of CLKs in regulating DNA damage-induced NF-κB activity, siRNAs were used to knockdown CLK2 and CLK4. Recapitulating the effect of MW01 and MW05, CLK2 or CLK4 knockdown produced a significant irradiation-specific reduction in p-p65 level and NFKBIA expression, (Figures 2C–2F). Furthermore, knockdown of CLK2 or 4 produced a strong reduction in IKKγ-S85 phosphorylation, mirroring the ablation of this DNA damage-specific, ATM dependent IKKγ PTM by MW01 and MW05, and localizing CLKs upstream of IKK (Figures 2C and S2B). Taken together, these data suggest that CLK2 and 4 are the functional targets of MW01 and MW05.

CLKs are the shared targets of active derivatives of MW01 and MW05

To validate the structural backbones of MW01 and MW05 and leverage additional structures in discerning on- and off-target activity, we screened more than 30 structural derivatives (Table S2) for similar NF-κB pathway inhibition compared to our lead compounds. Several active derivatives of each lead compound were identified, which reduced p-p65 and NFKBIA expression in an irradiation-specific manner, along with numerous weakly active or inactive derivatives. (Figures 3A–3C and S4). We selected two most active and two least active compounds for an *in vitro* kinase panel containing all kinases strongly inhibitable by MW01 and MW05 (Table S3). The profiles of active derivatives were similar to the respective lead compounds, validating the chemotypes of each as kinase inhibitors. However, inhibition of several kinases, except CLKs, was lost in the active derivatives of MW01 and MW05, including PI3K isoforms (Table S3). Crucially, all active compounds inhibited CLK2 with IC50 values of less than 2000 nM and CLK4 with IC50 values less than 300 nM, while three of four inactive compounds very weakly inhibited CLK2 (Figure 3D and Table S3). The fourth inactive compound, MW05-E2, inhibited both CLK2 and CLK4 despite lacking activity in cell-based NF-κB activation assays, likely due to poor cellular uptake, an issue absent under *in vitro* kinase assay conditions (Table S3). Moderate CLK4 inhibition was noted for three of four inactive derivatives while one, MW05-E10, inhibited CLK4 comparably to the active compounds. However, none of the inactive compounds share a CLK2 and 4 inhibition profile comparable to the leads or their active derivatives. Considering the phenotypic similarity between

CellPress
OPEN ACCESS

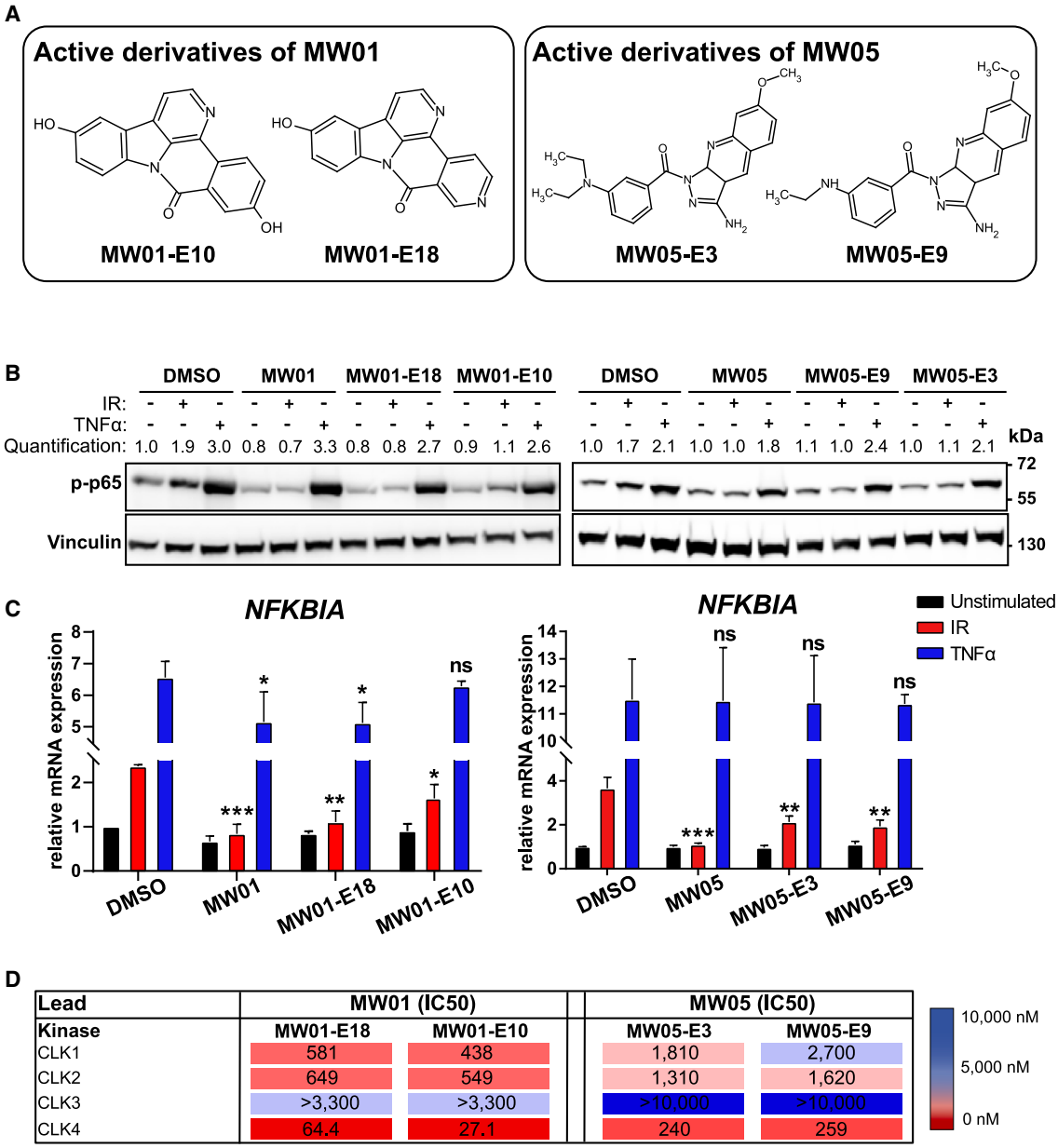

Figure 3. CLKs are the shared targets of active derivatives of MW01 and MW05

(A) Selected active structural derivatives of MW01 and MW05. MW01-E10: (5,16-dihydroxy-1,11-diazapentacyclo[10.7.1.0^{2,7}.0^{8,20}.0^{13,18}]icosa-2(7),3,5,8(20),9,11,13(18),14,16-nonaen-19-one); MW01-E18: (5-hydroxy-1,11,16-triazapentacyclo[10.7.1.0^{2,7}.0^{8,20}.0^{13,18}]icosa-2(7),3,5,8(20),9,11,13(18),14,16-nonaen-19-one); MW05-E3: 1-[3-(diethylamino)benzoyl]-7-methoxy-1H-pyrazolo[3,4-*b*]quinolin-3-amine; MW05-E9: 7-methoxy-1-[3-(methylamino)benzoyl]-1H-pyrazolo[3,4-*b*]quinolin-3-amine.

(B) Western blot analysis of U2-OS cells following pre-treatment with DMSO, MW01 (10 μM), MW01-E18 (10 μM), or MW01-E10 (10 μM) unstimulated, after irradiation (IR), or after TNFα conditions (left). Western blot analysis of U2-OS following pre-treatment with DMSO, MW05 (10 μM), MW05-E9 (10 μM), or MW05-E3 (10 μM) under the same conditions (right). Vinculin was the loading control.

(C) mRNA expression analysis using the same experimental conditions as in (B) for MW01 and active derivatives (left), or MW05 and active derivatives (right). ns: not significant; *, **, ***: $p < 0.05$, $p < 0.01$, $p < 0.001$.

(D) IC50 (nM) of MW01-E10 and MW01-E18 (left), and MW05-E3 and MW05-E9 (right) for all CLK isoforms. Western blots are representative images of three independent experiments. mRNA expression analyses are expressed as mean of three independent experiments with three technical replicates each.

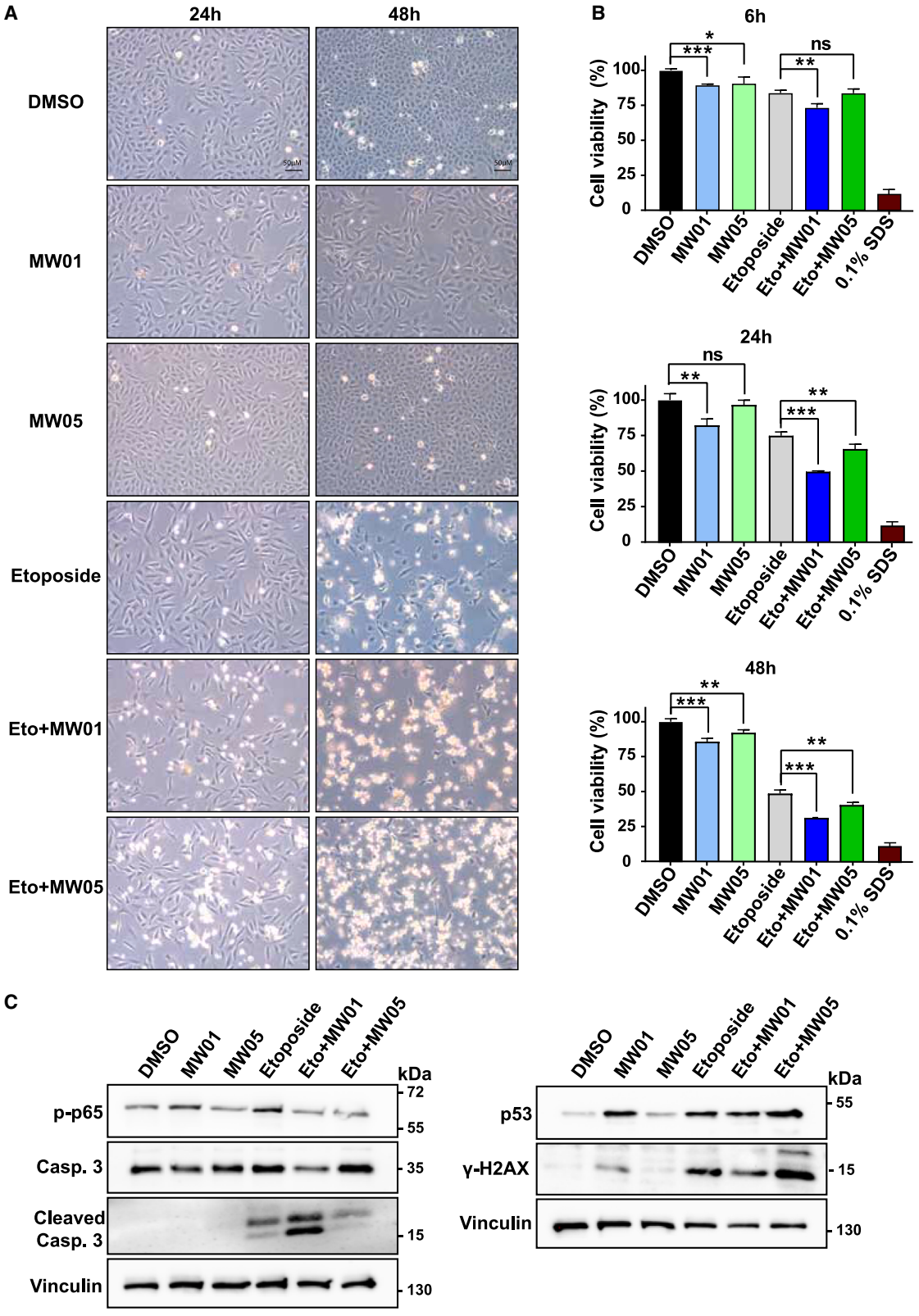

Figure 4. MW01 and MW05 reduce cell viability and increase p53-mediated apoptosis upon etoposide co-treatment

(A) Representative light microscopy images of U2-OS cells following treatment with DMSO, MW01 (10 μM), MW05 (10 μM), or etoposide (50 μM), or co-treatment at 24 (left) and 48 h (right), as indicated.

(legend continued on next page)

the structurally distinct lead compounds, the agreement of all active derivatives with our kinase IC50 criteria, and significant results following siRNA knockdown of CLK2 and CLK4, we proceeded to further characterize our lead compounds.

MW01 and MW05 potentiate cell killing effects of chemotherapeutic agents

Since the DNA double strand break-induced IKK-NF-κB pathway strongly suppresses apoptosis,[6] both MW01 and MW05 should sensitize cells to DNA damaging agents. To characterize the effect of MW01 and MW05 on viability, cells were treated with each compound alone or in combination with etoposide (Figure 4A). MW05 or MW01 only slightly reduced cell viability after 6, 24, and 48 h compared to DMSO-treated controls (Figures 4A and 4B). Importantly, at 48 h, MW01 or MW05 treated cells did not display characteristics of cell death, suggesting that the compounds are not grossly toxic (Figures 4A and 4B). Co-treatment of inhibitors with etoposide significantly reduced cell viability after 6 h for MW01 and 24 h for MW05, compared to etoposide alone (Figure 4B). Interestingly, 24 h after co-treatment of either MW01 or MW05 with etoposide, attached cells were visibly distressed and the number of floating cells was drastically increased (Figure 4A). This effect was greatly increased at 48 h, with relatively fewer attached cells and more floating cells, indicating cell death. The same effect in cell viability reduction was confirmed for MW01 and MW05 in co-treatment with cisplatin, another widely used chemotherapeutic drug (data not shown).

To investigate the underlying molecular causes of this phenotype, we analyzed markers of NF-κB and p53 activation, DNA damage, and apoptosis after single and co-treatment with MW01, MW05, and etoposide (Figure 4C). MW01 and MW05 reduced etoposide-stimulated p65 phosphorylation, as expected. Interestingly, MW01 alone caused a weak activation of γH2AX. Moreover, γH2AX activation was persistent in all etoposide treated samples, as expected, indicating an accumulation of DNA damage. Treatment with MW01 or MW05 alone did not cause an increase in cleaved caspase-3. Notably, this apoptosis marker was increased following etoposide co-treatment. Interestingly, we also observed a stabilization of p53 following MW01 treatment alone and, as expected, in all etoposide containing samples. We suspect a disparity in γH2AX, p53, and cleaved caspase-3 levels between MW01 and MW05 in etoposide co-treatment is due to MW01 co-treated cells more quickly undergoing p53-mediated cell death compared to MW05. Thus, in the co-treatment at 24 h, γH2AX levels were comparatively lower and cleaved caspase-3 higher for MW01 than MW05 because the apoptotic cells no longer repair DNA damage. Taken together, all these results indicate that MW01 and MW05 may be promising lead compounds for cancer treatment, reducing the expression of pro-survival NF-κB target genes and increasing the expression of pro-apoptotic p53 target genes in co-administration with chemo- or radiotherapy.

DISCUSSION

The wide-reaching physiological roles and deregulation in numerous disease states suggest the IκB kinase (IKK)/NF-κB pathways as attractive therapeutic targets.[3,11] However, only few therapeutics targeting components of IKK/NF-κB signaling cascades have reached the clinic. In this study, we identified MW01 and MW05, novel small molecule inhibitors specifically of DNA DSB-induced NF-κB activity, by differential chemical library screening. Through *in vitro* kinase profiling, structural derivatization, and siRNA-mediated silencing, we identified CLK2 and 4 as functional drug targets for MW01 and MW05. We show that both compounds strongly impair tumor cell survival when combined with chemotherapeutic agents.

Due to the nuclear origin of genotoxic stress compared to cell surface-initiated stimuli, a deeper understanding of the DNA damage-induced NF-κB pathway was required to identify pathway-specific druggable regulators of this pathway. Considering the essential role of PARP1 and PAR in the DNA damage-induced IKK/NF-κB pathway previously established by our group,[6,28] PARP inhibition would appear promising to achieve DNA damage-specific NF-κB inhibition. However, clinically used PARP inhibitors have not been shown to effectively inhibit NF-κB following standard chemo- and radiotherapies and therefore may lack the tumor-killing effect resulting from abrogated NF-κB-mediated pro-survival gene expression. Critically, MW01 and MW05 do not inhibit PARP activity and as such represent a new therapeutic modality to achieve DNA damage-specific NF-κB inhibition.

The identification of CLK2 and 4 as shared targets of our active compounds was surprising, since the kinases had no previously documented role in genotoxic stress signaling or NF-κB pathways. It has been reported that CLKs phosphorylate SR proteins that modulate RNA splicing.[29–31] However, a splicing-related function of CLK2 and 4 in our context can be excluded, because short time pre-incubation with the inhibitors is sufficient to block DNA damage-induced NF-κB activation. On re-inspection of our recent genome-wide siRNA screen global data for regulators of etoposide-induced NF-κB,[28] we noted that CLK2 and CLK4 scored similar to IKK or ATM, additionally confirming a function for CLK2/CLK4 in NF-κB signaling. Based on our study of post-translational modifications using MW01 and MW05, CLK2 and 4 act downstream of ATM and PARP1, but not directly at IKKα/CHUK or IKKβ, as indicated by the *in vitro* kinase data (Figures S2A–S2D and Table S1) and abrogate the signature Ser-85 phosphorylation of IKKγ. Silencing of the CLKs revealed that they are essential to promote the phosphorylation at Ser-85 by ATM, perhaps through a priming phosphorylation for ATM. Thus, it remains to be clarified which protein-associations CLK2 and 4 undergo in the pathway and what their substrates are.

The clinical implications of deregulated CLKs in a variety of cancers have been illuminated by numerous recent studies. CLK2 has an oncogenic role in many cancers, such as colorectal

(B) Quantification of cell viability at 6, 24, and 48 h. 0.1% SDS was used as positive cell death control. Results are expressed as mean of three independent experiments with three technical replicates each. ns: not significant; *, **, ***: $p < 0.05$, $p < 0.01$, $p < 0.001$.
(C) Western blot analysis of U2-OS cells 24 h following treatment as in (A), as indicated, with vinculin as loading control. Representative images of three independent experiments.

cancer, non-small cell lung cancer, glioblastoma, and breast cancer, and elevated CLK2 expression is associated with their occurrence, progression, and poor prognosis.[32–34] In addition, pharmacological abrogation of CLK2 inhibits tumor xenografts *in vivo* in breast cancer models.[29,30,35] CLK4 is comparatively less well understood, but recent studies have illustrated a role in breast cancer as well as downstream targets which are not splicing factors.[4,36,37] These data suggest that CLK2 and 4 are promising targets for the development of cancer drugs in the context of DNA damage-induced IKK/NF-κB and in a wider array of tumors. To that end, several CLK inhibitors have been recently reported, in addition to the novel inhibitors we identified here, providing multiple chemotypes as starting points for further pharmacokinetic optimization.[26,27,38,39]

Our compounds offer differing possibilities for therapeutic development, the direction of which will largely be determined by their differential kinase specificities. Therefore, to fully determine the kinase inhibition profiles of both MW01 and MW05 and address any additional identified off-targets, we envision a kinome-wide inhibition profile to be performed. In the case of MW01, the current kinase inhibition profile presents notable PI3K isoform off-targets, which may be beneficial depending on the context and could guide future pharmacological repositioning of this compound. Despite several reports claiming a relationship between PI3K/Akt and NF-κB, we note that these studies focus on canonical NF-κB stimuli and not DNA damage.[40–42] In the case of MW05, the more specific kinase profile of the lead compound and improved specificity of equally active derivatives points toward the possibility of a specific CLK inhibitor with selectivity toward CLK2 and CLK4. However, the affinity for these targets by MW05, especially CLK2, would need to be further improved for *in vivo* contexts. Additional pharmacokinetic parameters, such as solubility and cell permeability, should also be addressed for both compounds, especially MW01, in consideration of its relatively short half-life in liver microsomes and *in vivo*, which should be improved prior to *in vivo* studies.

In conclusion, we show the potency of two lead compounds able to inhibit NF-κB activation only upon DNA DSBs. Since NF-κB blocks apoptosis, its inhibition following DNA damage drastically reduces cancer cell viability. We showed that a combinatorial treatment between our lead compounds and chemotherapeutic drugs resulted in an accumulation of DNA damage, activation of the tumor suppressor p53, and subsequently cell death by unbalancing the NF-κB-p53 axis. These effects make MW01 and MW05 valuable leads for drug development in the treatment of many aggressive tumors, sensitizing them to genotoxic chemotherapies that are otherwise less effective. Finally, the successful identification of our drug targets opens the possibility to screen for additional specific kinase inhibitors to exploit the same genotoxic stress-induced NF-κB inhibition strategy and pharmacological repositioning.

Limitations of the study

We cannot formally exclude that at least a part of the pathway inhibitory effect is due to other proteins targeted by the lead compounds and their active derivatives, in addition to CLK2 and CLK4, or by additional substrates of CLKs outside of the ATM-IKKγ axis.

SIGNIFICANCE

The IKK-NF-κB cascade that is activated by chemo- and irradiation therapies strongly counteracts cell death induction by these genotoxic agents. Considering the pervasive role of NF-κB in multiple physiological processes, the development of novel classes of sub-pathway-selective inhibitors that exclusively block NF-κB activation by genotoxic stress is lacking, but critically needed. Here, we identified two lead compounds that only affect NF-κB activity and tumor cell viability after DNA double-strand break induction and identified their target kinases, CLK2 and 4, as new regulators of the genotoxic stress-induced IKK pathway. Our data also call for repurposing of already available clinical CLK2 or 4 inhibitors for cancer therapies.

STAR★METHODS

Detailed methods are provided in the online version of this paper and include the following:

- KEY RESOURCES TABLE
- RESOURCE AVAILABILITY
  - Lead contact
  - Materials availability
  - Data and code availability
- EXPERIMENTAL MODEL AND STUDY PARTICIPANT DETAILS
  - Cell culture
- METHOD DETAILS
  - HCS screening of NF-κB inhibitor library
  - NF-κB stimulation
  - siRNA transfection
  - Drug treatment
  - Nuclear/cytoplasm fractionation
  - Whole cell lysate preparation and immunoblot analysis
  - Immunoprecipitation
  - Kinase panel study
  - RNA extraction and RT-qPCR
  - Cell viability assay
  - Compound characterization (performed by Enamine Ltd.)
- QUANTIFICATION AND STATISTICAL ANALYSIS

SUPPLEMENTAL INFORMATION

Supplemental information can be found online at https://doi.org/10.1016/j.chembiol.2023.06.027.

ACKNOWLEDGMENTS

We thank Kamil Paruch, Masaryk University, Brno, for providing the inhibitor MU1210 and Davide Cirillo for compound characterization. We thank Sandra Miksche and Jessica Przygodda, for chemical syntheses. Special thanks to Enamine Ltd. in Kyiv for substance library synthesis. This work was supported in part by general funding of the Bundesministerium für Bildung und Forschung (BMBF) and the Helmholtz Association Wirkstoffinitiative to JP. vK., by the BMBF grant 0316047A, ProSiTu, to C.S., and by the European Union Regional Development Funds (ERDF Berlin 1.8/16). Graphical Abstract was created with BioRender.com.

AUTHOR CONTRIBUTIONS

P.M., B.B., and M.W.: Formal analysis, investigation, validation, visualization, writing original draft. P.L.: Formal analysis, investigation, visualization, and resources. S.R.: Data curation, formal analysis, investigation, and visualization. M. Ne.: Data curation, formal analysis. C.B.: Formal analysis, investigation, and visualization. JP. vK.: Conceptualization, funding and methodology. M.N.: Conceptualization, funding acquisition, methodology, project administration, resources, supervision. C.S.: Conceptualization, funding acquisition, formal analysis, investigation, methodology, project administration, resources, supervision, writing. All authors: reviewing and editing.

DECLARATION OF INTERESTS

C.S., M.W., P.L., S.R., JP. vK., and M.N. are listed as inventors on patents for MW01 and, together with P.M. and B.B., as inventors on patent applications for MW05.

Received: September 28, 2022
Revised: April 20, 2023
Accepted: June 29, 2023
Published: July 27, 2023

REFERENCES

1. Ellis, L.M., and Hicklin, D.J. (2009). Resistance to targeted therapies: refining anticancer therapy in the Era of molecular oncology. Clin. Cancer Res. *15*, 7471–7478. https://doi.org/10.1158/1078-0432.ccr-09-1070.
2. Labrie, M., Brugge, J.S., Mills, G.B., and Zervantonakis, I.K. (2022). Therapy resistance: opportunities created by adaptive responses to targeted therapies in cancer. Nat. Rev. Cancer *22*, 323–339. https://doi.org/10.1038/s41568-022-00454-5.
3. Baud, V., and Karin, M. (2009). Is NF-κB a good target for cancer therapy? Hopes and pitfalls. Nat. Rev. Drug Discov. *8*, 33–40. https://doi.org/10.1038/nrd2781.
4. Huang, T.T., Wuerzberger-Davis, S.M., Wu, Z.-H., and Miyamoto, S. (2003). Sequential modification of NEMO/IKKγ by SUMO-1 and ubiquitin mediates NF-κB activation by genotoxic stress. Cell *115*, 565–576. https://doi.org/10.1016/s0092-8674(03)00895-x.
5. Mabb, A.M., Wuerzberger-Davis, S.M., and Miyamoto, S. (2006). PIASy mediates NEMO sumoylation and NF-κB activation in response to genotoxic stress. Nat. Cell Biol. *8*, 986–993. https://doi.org/10.1038/ncb1458.
6. Stilmann, M., Hinz, M., Arslan, S.C., Zimmer, A., Schreiber, V., and Scheidereit, C. (2009). A nuclear poly(ADP-ribose)-dependent signalosome confers DNA damage-induced IkappaB kinase activation. Mol. Cell *36*, 365–378. https://doi.org/10.1016/j.molcel.2009.09.032.
7. Hinz, M., Stilmann, M., Arslan, S.Ç., Khanna, K.K., Dittmar, G., and Scheidereit, C. (2010). A cytoplasmic ATM-TRAF6-cIAP1 module links nuclear DNA damage signaling to ubiquitin-mediated NF-kappaB activation. Mol. Cell *40*, 63–74. https://doi.org/10.1016/j.molcel.2010.09.008.
8. Nakanishi, C., and Toi, M. (2005). Nuclear factor-κB inhibitors as sensitizers to anticancer drugs. Nat. Rev. Cancer *5*, 297–309. https://doi.org/10.1038/nrc1588.
9. Tergaonkar, V., Pando, M., Vafa, O., Wahl, G., and Verma, I. (2002). p53 stabilization is decreased upon NFκB activation. Cancer Cell *1*, 493–503. https://doi.org/10.1016/s1535-6108(02)00068-5.
10. Scheidereit, C. (2006). IkappaB kinase complexes: gateways to NF-kappaB activation and transcription. Oncogene *25*, 6685–6705. https://doi.org/10.1038/sj.onc.1209934.
11. Gilmore, T.D., and Herscovitch, M. (2006). Inhibitors of NF-κB signaling: 785 and counting. Oncogene *25*, 6887–6899. https://doi.org/10.1038/sj.onc.1209982.
12. Antonia, R.J., Hagan, R.S., and Baldwin, A.S. (2021). Expanding the view of IKK: new substrates and new biology. Trends Cell Biol. *31*, 166–178. https://doi.org/10.1016/j.tcb.2020.12.003.
13. Hinz, M., and Scheidereit, C. (2014). The IκB kinase complex in NF -κB regulation and beyond. EMBO Rep. *15*, 46–61. https://doi.org/10.1002/embr.201337983.
14. Mikuda, N., Kolesnichenko, M., Beaudette, P., Popp, O., Uyar, B., Sun, W., Tufan, A.B., Perder, B., Akalin, A., Chen, W., et al. (2018). The IκB kinase complex is a regulator of mRNA stability. EMBO J. *37*, e98658. https://doi.org/10.15252/embj.201798658.
15. Karin, M., and Greten, F.R. (2005). NF-κB: linking inflammation and immunity to cancer development and progression. Nat. Rev. Immunol. *5*, 749–759. https://doi.org/10.1038/nri1703.
16. Rayet, B., and Gélinas, C. (1999). Aberrant rel/nfkb genes and activity in human cancer. Oncogene *18*, 6938–6947. https://doi.org/10.1038/sj.onc.1203221.
17. Taniguchi, K., and Karin, M. (2018). NF-κB, inflammation, immunity and cancer: coming of age. Nat. Rev. Immunol. *18*, 309–324. https://doi.org/10.1038/nri.2017.142.
18. Hayden, M.S., and Ghosh, S. (2008). Shared principles in NF-κB signaling. Cell *132*, 344–362. https://doi.org/10.1016/j.cell.2008.01.020.
19. Kolesnichenko, M., Mikuda, N., Höpken, U.E., Kärgel, E., Uyar, B., Tufan, A.B., Milanovic, M., Sun, W., Krahn, I., Schleich, K., et al. (2021). Transcriptional repression of NFKBIA triggers constitutive IKK- and proteasome-independent p65/RelA activation in senescence. EMBO J. *40*, e104296. https://doi.org/10.15252/embj.2019104296.
20. Li, N., Banin, S., Ouyang, H., Li, G.C., Courtois, G., Shiloh, Y., Karin, M., and Rotman, G. (2001). ATM is required for IκB kinase (IKK) activation in response to DNA double strand breaks. J. Biol. Chem. *276*, 8898–8903. https://doi.org/10.1074/jbc.M009809200.
21. Piret, B., Schoonbroodt, S., and Piette, J. (1999). The ATM protein is required for sustained activation of NF-κB following DNA damage. Oncogene *18*, 2261–2271. https://doi.org/10.1038/sj.onc.1202541.
22. Wu, Z.-H., Shi, Y., Tibbetts, R.S., and Miyamoto, S. (2006). Molecular linkage between the kinase ATM and NF-κB signaling in response to genotoxic stimuli. Science *311*, 1141–1146. https://doi.org/10.1126/science.1121513.
23. Uhlén, M., Fagerberg, L., Hallström, B.M., Lindskog, C., Oksvold, P., Mardinoglu, A., Sivertsson, Å., Kampf, C., Sjöstedt, E., Asplund, A., et al. (2015). Proteomics. Tissue-based map of the human proteome. Science *347*, 1260419. https://doi.org/10.1126/science.1260419.
24. Raynaud, F.I., Eccles, S., Clarke, P.A., Hayes, A., Nutley, B., Alix, S., Henley, A., Di-Stefano, F., Ahmad, Z., Guillard, S., et al. (2007). Pharmacologic characterization of a potent inhibitor of class I phosphatidylinositide 3-kinases. Cancer Res. *67*, 5840–5850. https://doi.org/10.1158/0008-5472.Can-06-4615.
25. Leahy, J.J.J., Golding, B.T., Griffin, R.J., Hardcastle, I.R., Richardson, C., Rigoreau, L., and Smith, G.C.M. (2004). Identification of a highly potent and selective DNA-dependent protein kinase (DNA-PK) inhibitor (NU7441) by screening of chromenone libraries. Bioorg. Med. Chem. Lett. *14*, 6083–6087. https://doi.org/10.1016/j.bmcl.2004.09.060.
26. Němec, V., Hylsová, M., Maier, L., Flegel, J., Sievers, S., Ziegler, S., Schröder, M., Berger, B.T., Chaikuad, A., Valčíková, B., et al. (2019). Furo[3,2-b]pyridine: a privileged scaffold for highly selective kinase inhibitors and effective modulators of the Hedgehog pathway. Angew. Chem. Int. Ed. Engl. *58*, 1062–1066. https://doi.org/10.1002/anie.201810312.
27. Martín Moyano, P., Němec, V., and Paruch, K. (2020). Cdc-like kinases (CLKs): biology, chemical probes, and therapeutic potential. Int. J. Mol. Sci. *21*, 7549. https://doi.org/10.3390/ijms21207549.
28. Tufan, A.B., Lazarow, K., Kolesnichenko, M., Sporbert, A., von Kries, J.P., and Scheidereit, C. (2022). TSG101 Associates with PARP1 and is essential for PARylation and DNA damage-induced NF-κB activation. EMBO J. *41*, e110372. https://doi.org/10.15252/embj.2021110372.
29. Iwai, K., Yaguchi, M., Nishimura, K., Yamamoto, Y., Tamura, T., Nakata, D., Dairiki, R., Kawakita, Y., Mizojiri, R., Ito, Y., et al. (2018). Anti-tumor efficacy of a novel CLK inhibitor via targeting RNA splicing and MYC-dependent

vulnerability. EMBO Mol. Med. *10*, e8289. https://doi.org/10.15252/emmm.201708289.

30. Salvador, F., and Gomis, R.R. (2018). CLK2 blockade modulates alternative splicing compromising MYC-driven breast tumors. EMBO Mol. Med. *10*, e9213. https://doi.org/10.15252/emmm.201809213.
31. Yoshida, T., Kim, J.H., Carver, K., Su, Y., Weremowicz, S., Mulvey, L., Yamamoto, S., Brennan, C., Mei, S., Long, H., et al. (2015). CLK2 is an oncogenic kinase and splicing regulator in breast cancer. Cancer Res. *75*, 1516–1526. https://doi.org/10.1158/0008-5472.CAN-14-2443.
32. Lin, J., Lin, G., Chen, B., Yuan, J., and Zhuang, Y. (2022). CLK2 expression is associated with the progression of colorectal cancer and is a prognostic biomarker. BioMed Res. Int. *2022*, 7250127. https://doi.org/10.1155/2022/7250127.
33. Liu, B., Kong, X., Wang, R., and Xin, C. (2021). CLK2 promotes occurrence and development of non-small cell lung cancer. J buon *26*, 58–64.
34. Park, S.Y., Mittal, S., Dong, J., Jeong, K., Martinez-Ledesma, E., Piao, Y., Khan, S., Henry, V., Verhaak, R.G., Majd, N., et al. (2020). Depletion of CLK2 sensitizes glioma stem-like cells to PI3K/mTOR and FGFR inhibitors. Am. J. Cancer Res. *10*, 3765–3783.
35. Riggs, J.R., Nagy, M., Elsner, J., Erdman, P., Cashion, D., Robinson, D., Harris, R., Huang, D., Tehrani, L., Deyanat-Yazdi, G., et al. (2017). The discovery of a dual TTK protein kinase/CDC2-like kinase (CLK2) inhibitor for the treatment of triple negative breast cancer initiated from a phenotypic screen. J. Med. Chem. *60*, 8989–9002. https://doi.org/10.1021/acs.jmedchem.7b01223.
36. Kang, E., Kim, K., Jeon, S.Y., Jung, J.G., Kim, H.K., Lee, H.B., and Han, W. (2022). Targeting CLK4 inhibits the metastasis and progression of breast cancer by inactivating TGF-beta pathway. Cancer Gene Ther. *29*, 1168–1180. https://doi.org/10.1038/s41417-021-00419-0.
37. Huang, J., Wang, L., Shen, Y., Zhang, S., Zhou, Y., Du, J., Ma, X., Liu, Y., Liang, D., Shi, D., et al. (2022). CDC-like kinase 4 deficiency contributes to pathological cardiac hypertrophy by modulating NEXN phosphorylation. Nat. Commun. *13*, 4433. https://doi.org/10.1038/s41467-022-31996-9.
38. Kim, H., Choi, K., Kang, H., Lee, S.Y., Chi, S.W., Lee, M.S., Song, J., Im, D., Choi, Y., and Cho, S. (2014). Identification of a novel function of CX-4945 as a splicing regulator. PLoS One *9*, e94978. https://doi.org/10.1371/journal.pone.0094978.
39. Walter, A., Chaikuad, A., Helmer, R., Loaëc, N., Preu, L., Ott, I., Knapp, S., Meijer, L., and Kunick, C. (2018). Molecular structures of cdc2-like kinases in complex with a new inhibitor chemotype. PLoS One *13*, e0196761. https://doi.org/10.1371/journal.pone.0196761.
40. Ahmad, A., Biersack, B., Li, Y., Kong, D., Bao, B., Schobert, R., Padhye, S.B., and Sarkar, F.H. (2013). Targeted regulation of PI3K/Akt/mTOR/NF-κB signaling by indole compounds and their derivatives: mechanistic details and biological implications for cancer therapy. Anti Cancer Agents Med. Chem. *13*, 1002–1013. https://doi.org/10.2174/18715206113139990078.
41. Bai, D., Ueno, L., and Vogt, P.K. (2009). Akt-mediated regulation of NFκB and the essentialness of NFκB for the oncogenicity of PI3K and Akt. Int. J. Cancer *125*, 2863–2870. https://doi.org/10.1002/ijc.24748.
42. Gustin, J.A., Ozes, O.N., Akca, H., Pincheira, R., Mayo, L.D., Li, Q., Guzman, J.R., Korgaonkar, C.K., and Donner, D.B. (2004). Cell type-specific expression of the IkappaB kinases determines the significance of phosphatidylinositol 3-kinase/Akt signaling to NF-kappa B activation. J. Biol. Chem. *279*, 1615–1620. https://doi.org/10.1074/jbc.M306976200.

STAR★METHODS

KEY RESOURCES TABLE

REAGENT or RESOURCE	SOURCE	IDENTIFIER
Antibodies		
p-p65 (Ser536)	Cell Signaling Technology	Cat#3039; RRID: AB_330579
p65	Santa Cruz Biotechnology	Cat#Sc-372; RRID: AB_632037
p-Akt	Cell Signaling Technology	Cat#4060; RRID: AB_2315049
IKKγ	Santa Cruz Biotechnology	Cat#Sc-8256; RRID: AB_2264738
IKKγ S85	Abcam	Cat#Ab63551; RRID: AB_1140634_
PAR	Abcam	Cat#ab14459; RRID: AB_301239
Tubulin	Sigma Aldrich	Cat#T6074; RRID: AB_477582
Clk2	Abcam	Cat#Ab86147; RRID: AB_10674956
Clk4	Abcam	Cat#Ab67936; RRID: AB_1140224
p-ATM(Ser1981)	Abcam	Cat#Ab36810; RRID: AB_725573
LDH-A	Santa Cruz Biotechnology	Cat#Sc-137243; RRID: AB_2137192
PARP1	Santa Cruz Biotechnology	Cat#Sc-8007; RRID: AB_628105
Caspase 3	Abcam	Cat#Ab4051; RRID: AB_304243
Cleaved Caspase 3	Abcam	Cat#Ab2302; RRID: AB_302962
p53	Santa Cruz Biotechnology	Cat#Sc-126; RRID: AB_628082
γH2A.X (Ser139)	Abcam	Cat#Ab11174; RRID: AB_297813
β-actin	Cell Signaling Technology	Cat#4970; RRID: AB_2223172
Vinculin	Cell Signaling Technology	Cat#4650; RRID: AB_10559207
Secondary anti-mouse conjugated HRP	Jackson ImmunoResearch	Cat#115-035-003; RRID: AB_10015289
Secondary anti-rabbit conjugated HRP	Jackson ImmunoResearch	Cat#111-035-003; RRID: AB_2313567
Goat anti-mouse IgG conjugated Alexa Fluor 488	Thermo Fisher Scientific	Cat#A-11001; RRID: AB_2534069
Critical commercial assays		
SelectScreen Kinase Panel Assay	Thermo Fischer Scientific	N/A
CellTiter-Glo Luminescence Cell Viability Assay	Promega	Cat#G7570
Oligonucleotides		
Primer: Clk2 Forward: TTCGGCCGAGTTGTACAATG	This paper	N/A
Primer: Clk2 Reverse: AGCACGTTGATCTCAAGTCG	This paper	N/A
Primer: Clk4 Forward: CGAGCTCGTTCAGAAATCCAAG	This paper	N/A
Primer: Clk4 Reverse: TAGCATCTGGACACATCGGAA	This paper	N/A
Primer: NFKBIA Forward: TTGGGTGCTGATGTCAATGC	This paper	N/A
Primer: NFKBIA Reverse: ACACCAGGTCAGGATTTTGC	This paper	N/A
Primer: GAPDH Forward: AATTCCATGGCACCGTCAAG	This paper	N/A
Primer: GAPDH Reverse: ATCGCCCCACTTGATTTTGG	This paper	N/A
Primer: B2M Forward: TACACTGAATTCACCCCCACTG	This paper	N/A
Primer: B2M Reverse: TGCTGCTTACATGTCTCGATCC	This paper	N/A
siRNA targeting sequence: Clk2 #1: GCUGCAUCAUC UUUGAAUA	This Paper	N/A
siRNA targeting sequence: Clk2 #2	Invitrogen	Cat#43929
siRNA targeting sequence: Clk4	Invitrogen	Cat#s32987
AllStars Negative Control siRNA	Qiagen	Cat#1027281
Software and algorithms		
Bio-Rad CFX Maestro	Bio-Rad	CFX Maestro
Image-Lab 3.0	Bio-Rad	image lab
Prism 7.04	GraphPad	https://www.graphpad.com/features

RESOURCE AVAILABILITY

Lead contact

Further information and requests for resources and reagents should be directed to and will be fulfilled by the lead contact, Claus Scheidereit (scheidereit@mdc-berlin.de).

Materials availability

Available materials will be shared on request for academic research. Commercial applications might require a Material Transfer Agreement and/or a contract.

Data and code availability

- Requests for further information and data should be addressed to the lead contact, Claus Scheidereit (scheidereit@mdc-berlin.de)
- This paper does not report original code.
- Any additional information required to reanalyze the data reported in this paper is available from the lead contact upon request

EXPERIMENTAL MODEL AND STUDY PARTICIPANT DETAILS

Cell culture

U2-OS cells originating from a female patient were obtained from Leibnitz-Institute DSMZ - German Collection of Microorganisms and Cell Cultures (ACC 785) and were authenticated by the supplier by STR analysis according to the global standard ANSI/ATCC ASN-0002.1-2021 (2021), which resulted in an authentic STR profile of the reference STR database. U2-OS cells (DSMZ) were propagated in DMEM medium supplemented with 10% FBS, 1% pen-strep, and 1% L-glutamine at 37°C and 5% CO2.

METHOD DETAILS

HCS screening of NF-κB inhibitor library

U2-OS cells were seeded in a 384-well microplate (Corning) (750 cells/well), and after 48 h they were treated with a library of about 32,000 compounds concentrated 10 μM in DMSO. After 2 h of treatment, DNA damage was induced using 50 μM etoposide (Sigma Aldrich, E1383) for 2 h. Cells were washed with PBS 1X, fixed with PFA 4% (Sigma Aldrich, 158127) for 10 minutes and washed again with PBS 1X. Subsequently, cells were incubated with a solution of 0.12% glycine/0.2% saponin in PBS for 10 min and blocked with 10% FCS/0.2% saponin in PBS for 1 h. Primary antibody anti-p65 (Santa Cruz Biotechnologies, sc-372) was incubated for 1 h at room temperature (1:500 dilution in 0.2% saponin in PBS). Cells were washed four times with washing solution (0.2% saponin in PBS). Following washing steps, incubation with the secondary antibody anti mouse conjugated with Alexa 488 (Thermo Fisher Scientific, A-11001) (1:1000 diluted in 0.2% saponin in PBS) was carried out for 1 h at room temperature. Cells were washed again four times with washing solution and nuclei were stained by incubation with 10 μM Hoechst 33342 (Sigma Aldrich, B2261) in washing solution for 10 min. For data acquisition, 36 images per well were taken using the automated wide field fluorescence microscope ArrayScan VTI HCS reader (Thermo Fisher Scientific) and p65 nuclear translocation rates were calculated by applying masks to define the nuclear and cytoplasmic areas. Hits were counter-screened with TNFα (10 ng/ml, 20 min). Cells were pre-treated with compounds (10 μM, 2h) before stimulation, fixed, and percent p65 nuclear translocation measured by fluorescence microscopy. IC50 values were used for final selection.

NF-κB stimulation

NF-κB was stimulated by DNA damage through 20 Gy irradiation (IR) or by etoposide and analyzed after 90 minutes, or as indicated, or cells were stimulated by 10 ng/ml TNFα and analyzed after 20 minutes unless otherwise noted.

siRNA transfection

Cells were silenced with 50 nM of CLK2 or CLK4 siRNAs and transfected using Lipofectamine RNAiMAX Transfection Reagent (Thermo Fisher Scientific, 13778100). All experiments were performed 48 h post-silencing.

Drug treatment

All compounds were pre-treated for 1-hour prior to NF-κB stimulation unless otherwise noted.

Nuclear/cytoplasm fractionation

Initially, cells were lysed with Buffer A (20 mM Tris-HCl pH 7.9, 1.5 mM $MgCl_2$, 10 mM KCl, 8 mM β-Glycerol, 20 mM NaF, 200 mM Na_3VO_4, 1 mM DTT, 0.2% NP-40) supplemented with Protease (Thermo Fisher Scientific, 78429) and Phosphatase (Thermo Fisher Scientific, 78420) inhibitors and 50 nM Calyculin A. Lysate was vortexed for 10 second and centrifuged. The supernatant, representing the cytoplasm extract (CE), was collected, while the pellet was washed with Buffer A and the suspended with Buffer C (40 mM Tris-HCl

pH 7.9, 25% Glycerol, 420 mM NaCl, 1.5 mM $MgCl_2$, 8 mM β-Glycerol, 20 mM NaF, 1mM DTT) supplemented with Protease (Thermo Fisher Scientific, 78429) and Phosphatase (Thermo Fisher Scientific, 78420) inhibitors. The pellet was incubated for 20 minutes at 4°C under shaking, centrifuged for 10 minutes at 14,000 rpm and the supernatant, representing the nuclear extract (NE) was collected.

Whole cell lysate preparation and immunoblot analysis

Cells were collected by scraping and lysed in Baeuerle lysis buffer (20 mM HEPES, 350 mM NaCl, 20% Glycerin, 1 mM $MgCl_2$, 0.5 mM EDTA, 0.1 mM EGTA, 1% NP-40, 1 mM DTT) supplemented with Protease (Thermo Fisher Scientific, 78429) and Phosphatase (Thermo Fisher Scientific, 78420) inhibitors after the appropriate treatment and time point. Proteins were quantified by Bradford assay (Bio-Rad, 5000006) and 20–50 μg of extracted proteins were loaded on 4–20% Protein Gel (Bio-Rad, 4568096) and then transferred onto a PVDF membrane (Bio-Rad, 1620177) using Tris-Glycine buffer with 20% of methanol. Blocking was performed for 1h with 5% not-fat dry milk in PBS 1X. Immunodetection was obtained using primary and secondary antibodies reported in Key Resources Table. The membranes were analyzed by ECL (Thermo Fisher Scientific, 34580) and detected by ChemiDoc XRS+ (Bio-Rad) using ImageLab software (Bio-Rad).

Immunoprecipitation

1.5 mg of protein lysate was used for pulldown. Lysates were precleared with 30 μl Sepharose G beads for 30 min and centrifuged for 5 min at 1,500 × *g*. Primary antibody was added to the supernatant for immunoprecipitation overnight while rotating at 4°C. The next day 30 μl of Sepharose beads per sample were used for immobilization of antibodies. IP wash buffer was used to wash the beads four times and precipitated proteins were then eluted by mixing with 3X SDS-buffer and heating to 95°C for 4min.

Kinase panel study

The kinase panel analysis (Tables S1 and S3) was provided by Thermo Fisher Scientific using the two lead compounds MW01 and MW05 as well as their active (MW01-E10, MW01-E18, MW05-E3, MW05-E9) and inactive (MW01-E6, MW01-E14, MW05-E2, MW05-E10) derivatives. The experiment was performed using the ZLyte or Adapta protocol according to manufacturer standard operating procedures.

RNA extraction and RT-qPCR

$3.5x10^5$ cells per well were seeded in a 6-well plate and incubated overnight. The day after, the appropriate treatment at the appropriate time point was performed and cells were scraped and lysed with β-mercaptoethanol and total RNA was extracted using an RNeasy kit (Qiagen, 74004) following the kit protocol. Then, 500 ng of RNA were retro-transcribed using the iScript cDNA synthesis kit (Bio-Rad, 1708890). Finally, RT-qPCR was performed using 5 ng of cDNA and SYBR Green PCR Master Mix (Thermo Fisher Scientific, 4309155) in Cfx96 Real-Time System Thermocycler (Bio-Rad).

Cell viability assay

$1x10^4$ cells per well were seeded in a 96-well plate and incubated overnight. The day after, cells were treated with 10 μM of compounds under investigation, 50 μM Etoposide or 10 μM Cisplatin, alone or in combination, for appropriate time points. DMSO and 10% of Triton-X100 were used as negative and positive control respectively. Luminescent staining was performed using CellTiter-Glo Luminescent Cell Viability Assay (Promega, G7570), adding in each well a volume of CellTiter-Glo reagent equal to the volume of cell culture medium present into the well. After 1 h of incubation at 37°C, luminescence was read by BioTek Cytation 1 Cell Imaging Multimode Reader (Agilent).

Compound characterization (performed by Enamine Ltd.)

The following LCMS conditions were used: Column: Agilent Poroshell 120 SB-C18 4.6 × 30mm 2.7 μm; Column temperature: 60°C; Mobile phase: A – water (0.1% formic acid), B – acetonitrile (0.1% formic acid); Flow rate: 3 ml/min; Gradient: 0.01 min – 1% B, 1.5 min – 100% B, 1.73 min – 100% B; MS Ionization mode: Electrospray ionization (ESI); MS Scan range: 83 – 600 m/z; UV detection: 215 nm, 254nm, 280 nm.

Nuclear Magnetic Resonance (NMR) mono-1H were recorded on Bruker AV spectrometers. All chemical shifts are reported in ppm relative to tetramethylsilane (δ = 0.00 ppm) and were calibrated with respect to their respective deuterated solvents.

QUANTIFICATION AND STATISTICAL ANALYSIS

The results are expressed as mean ± SD of three independent experiments. Graphpad Prism 7.04 was used for statistical analysis using the two-way ANOVA multiple comparison with the default setting (Tukey hypothesis testing with 95% confidence interval). All western blot quantifications were normalized to their respective loading controls. Protein level knockdown efficiency was determined by comparing siCLK2 or siCLK4 to paired siNC-expressing control. Relative NF-κB activation was calculated by comparing the p-p65 signal (for protein level analysis) or *NFKBIA* expression (for RNA expression analysis) of each sample to the unstimulated control.

Cell Chemical Biology, Volume *30*

Supplemental information

CLK2 and CLK4 are regulators of DNA damage-induced NF-κB targeted by novel small molecule inhibitors

Patrick Mucka, Peter Lindemann, Bartolomeo Bosco, Michael Willenbrock, Silke Radetzki, Martin Neuenschwander, Cristina Brischetto, Jens Peter von Kries, Marc Nazaré, and Claus Scheidereit

Supplemental Item Legends

Figure S1: Synthesis strategies and cell permeabilities of lead compounds MW01 and MW05, related to Figure 1

(A) Synthetic scheme for MW01, as previously published in [1].

(B) Synthetic scheme for MW05, as previously published in [2].

(C) Mean apparent permeability (P_{app}) of MW01, MW05, or positive control propranolol in CaCo2 cells.

Figure S2: MW01 and MW05 inhibit critical NF-κB pathway steps leading to apoptosis, related to Figure 1

(A) MW01 and MW05 are inhibitors of DNA damage-induced p65 nuclear translocation. U2-OS cells were pre-treated with DMSO, MW01 or MW05. Etoposide was added and after 2 hours cells were fixed and nuclei stained with DAPI. p65 and γH2AX were stained by immunofluorescence and images taken at a confocal Zeiss 710 LSM microscope with a 40x oil objective.

(B) Immunoprecipitation of IKKγ from HEK293 lysates pre-treated for 1 hour with 10 μM MW01 or MW05, then irradiated (IR) and lysed.

(C) Western blot analysis, using an IKKγ S85-specific antibody, of U2-OS cells pre-treated with 10 μM MW01, MW05 or ATM inhibitor KU55933 for 1 hour and irradiated (IR). The specific IKKγ S85 band was confirmed by induction following irradiation and by sensitivity to ATMi treatment.

(D) Western blot analysis of U2-OS cells pre-treated for 1 hour with 10 μM of the indicated substances, irradiated (IR) and whole cell lysates probed for poly(ADP)-ribose.

(E) Western blot analysis of cytoplasmic and nuclear fractions from U2-OS cells after 1 hour pre-treatment with DMSO, MW01 (10 μM), or MW05 (10 μM) and 45 min following irradiation (IR). PARP1 and LDHA are used as loading controls for nuclear and cytoplasmic fractions, respectively.

(F) Western blot analysis of U2-OS cells 8 hours after 10 Gy irradiation following 1 hour pre-treatment with 10 μM DMSO, MW01, or MW05. Tubulin was used loading control.

(G) mRNA expression analysis of BIRC3 in U2-OS cells 8 hours after 10 Gy irradiation following 1 hour pre-treatment with 10 μM DMSO, MW01, or MW05 and. Values were normalized to DMSO-treated unstimulated cells.

Figure S3: MW01 and MW05 inhibit shared kinase targets, related to Figure 2

(A) IC50 (nM) of all kinases strongly inhibited by MW01 and MW05. Heatmap indicates lower IC50 by red color, higher by blue.

(B) Venn diagram depicting strongly inhibited kinases for MW01 (orange) and MW05 (green), with shared hits.

Figure S4: Inactive derivatives of MW01 and MW05 do not inhibit CLK, related to Figure 3

(A) Selected inactive structural derivatives of MW01 and MW05, as indicated. MW01-E6: (5,15-dimethoxy-1,11,14-triazapentacyclo[10.7.1.0^{2},^{7}.0^{8},^{20}.0^{13},^{18}]icosa-2(7),3,5,8(20),9,11,13(18),14,16-nonaen-19-one); and MW01-E14: (5,17-dimethoxy-1,11,16-triazapentacyclo[10.7.1.0^{2},^{7}.0^{8},^{20}.0^{13},^{18}]icosa-2(7),3,5,8(20),9,11,13(18),14,16-nonaen-19-one); MW05-E2: (1-[3-(dimethylamino)benzoyl]-6-methoxy-1H-pyrazolo[3,42uinolinelin-3-amine); MW05-E10: (1-[3-(dimethylamino)benzoyl]-7-methoxy-N,N-dimethyl-1H-pyrazolo[3,42uinolinelin-3-amine).

(B) (left) Western blot analysis of U2-OS cells following pre-treatment with DMSO, MW01 (10 μM), MW01-E6 (10 μM), or MW01-E14 (10 μM) in unstimulated, after irradiation (IR), or after TNFα conditions. (right) Western blot analysis following pre-treatment with DMSO, MW05 (10 μM), MW05-E2 (10 μM), or MW05-10 (10 μM) under the same conditions. Vinculin is used as loading control.

(C) mRNA expression analysis of NFKBIA using same experimental conditions as in (B) for MW01 and inactive derivatives (left) and MW05 and inactive derivatives (right). ns: not significant; *, **, ***: $p<0.05$, $p<0.01$, $p<0.001$.

(D) Percent inhibition of all CLK isoforms by derivatives MW01-E6 and MW01-E14, and MW05-E2 and MW05-E10, which were inactive in cell-based assays. Higher inhibition is indicated by red color, moderate by white, and low by blue.

Western blots are representative images of three independent experiments. mRNA expression analyses are expressed as mean of three independent experiments with three technical replicates each.

Table S3: Percentage of inhibition of the indicated kinases by active and inactive derivatives of MW01 or MW05, related to Figure 3

Data S1: Characterization of compounds and extended raw data, related to "Compound characterization" section in STAR Methods. Contains LCMS data and 1H NMR descriptions for the lead compounds and their chemical derivatives, as indicated.

Supplemental References

1. Sen'ko, O.A., Dybenko, A.G., Garazd, M.M., and Kartsev, V.G. (2017). Synthesis of Benzoannelated Canthin-6-One Analogs. Chemistry of Natural Compounds *53*, 523-528. 10.1007/s10600-017-2037-9.
2. Lapa, G.B., Bekker, O.B., Mirchink, E.P., Danilenko, V.N., and Preobrazhenskaya, M.N. (2013). Regioselective acylation of congeners of 3-amino-1H-pyrazolo[3,4-b]quinolines, their activity on bacterial serine/threonine protein kinases and in vitro antibacterial (including antimycobacterial) activity. J Enzyme Inhib Med Chem *28*, 1088-1093. 10.3109/14756366.2012.716056.

Figure S1

A

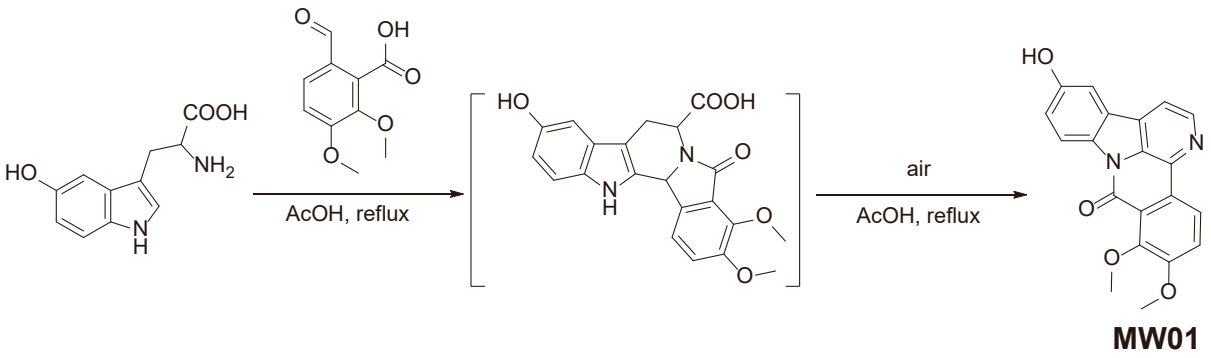

MW01

B

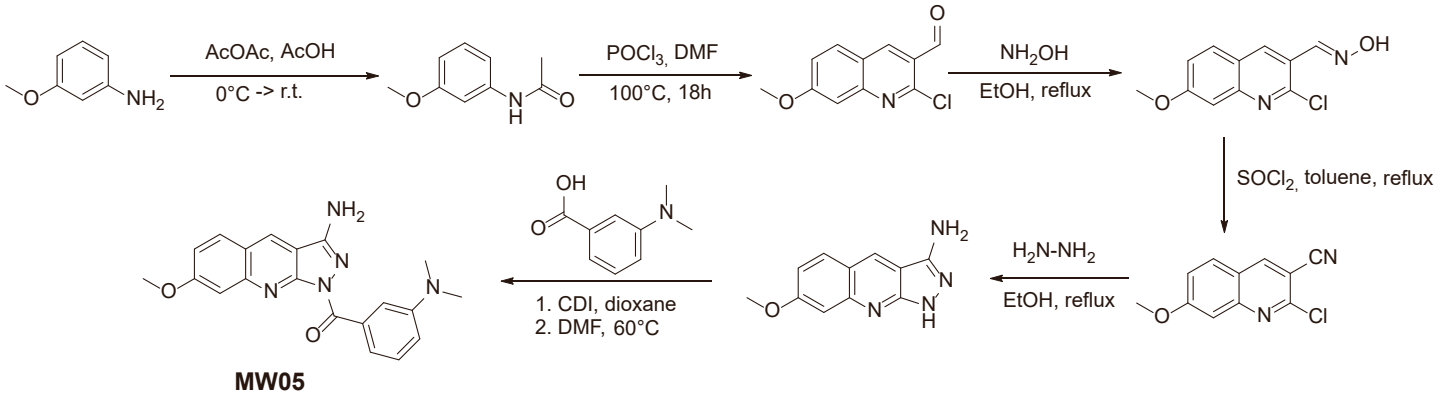

MW05

C

Compound	Mean P_{app} (× 10^{-6}cm/s)
MW01	12.60 ± 6.20
MW05	17.28 ± 2.65
Propranolol	33.43 ± 0.98

Figure S2

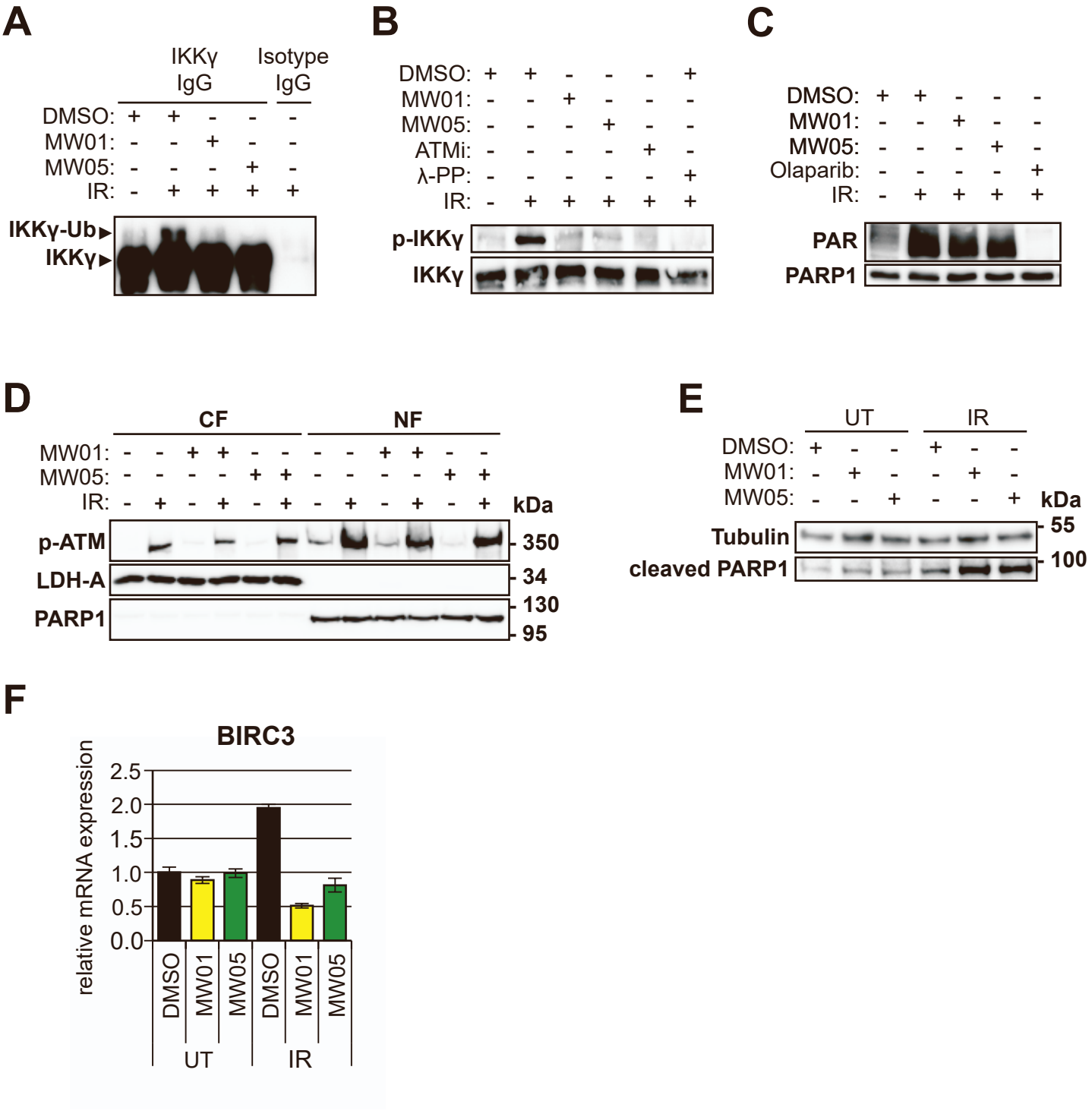
A
IKKγ IgG
Isotype IgG
DMSO: + + - - -
MW01: - - + - -
MW05: - - - + -
IR: - + + + +
IKKγ-Ub▶
IKKγ▶
B
DMSO: + + - - - +
MW01: - - + - - -
MW05: - - - + - -
ATMi: - - - - + -
λ-PP: - - - - - +
IR: - + + + + +
p-IKKγ
IKKγ
C
DMSO: + + - - -
MW01: - - + - -
MW05: - - - + -
Olaparib: - - - - +
IR: - + + + +
PAR
PARP1
D
CF
NF
MW01: - - + + - - - - + + - -
MW05: - - - - + + - - - - + +
IR: - + - + - + - + - + - +
kDa
p-ATM
LDH-A
PARP1
350
34
130
95
E
UT
IR
DMSO: + - - + - -
MW01: - + - - + -
MW05: - - + - - +
kDa
Tubulin
cleaved PARP1
55
100
F
BIRC3
relative mRNA expression
2.5
2.0
1.5
1.0
0.5
0.0
DMSO
MW01
MW05
DMSO
MW01
MW05
UT
IR

Figure S3

A

Kinase	MW01 IC50	MW05 IC50
CLK2	360	1440
CSF1R (FMS)	1,000	10,000
DNA-PK	150	2,930
DYRK1A	949	10,000
DYRK1B	4,630	10,000
FLT3	6,010	10,000
FRAP1 (mTOR)	2,630	1,920
GSG2 (Haspin)	72.5	10,000
LRRK2 FL	49.4	10,000
MAP4K2 (GCK)	877	10,000
MAP4K4 (HGK)	1,800	10,000
MINK1	1,420	10,000
PI4KB (PI4K beta)	11.6	10,000
PIK3C2B (PI3K-C2 beta)	283	10,000
PIK3C2G (PI3K-C2 gamma)	25.6	610
PIK3CA/PIK3R1 (p110 alpha/p85)	15	9,570
PIK3CA/PIK3R3 (p110 alpha/p55)	29.5	9,670
PIK3CB/PIK3R2 (p110 beta/p85)	1,710	4,760
PIK3CD/PIK3R1 (p110 delta/p85)	62.8	2,200
PIK3CG (p110 gamma)	22.7	1,440
PIP5K1A	7,730	10,000

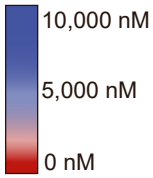

B

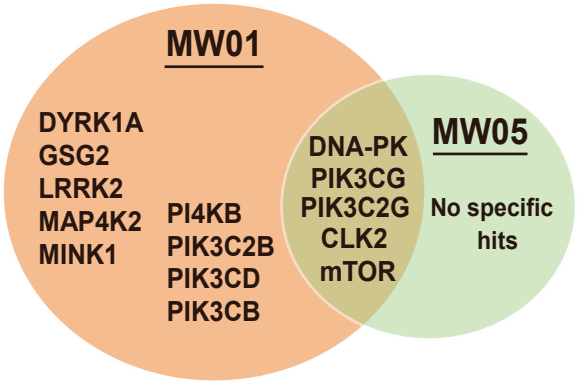

Figure S4

A

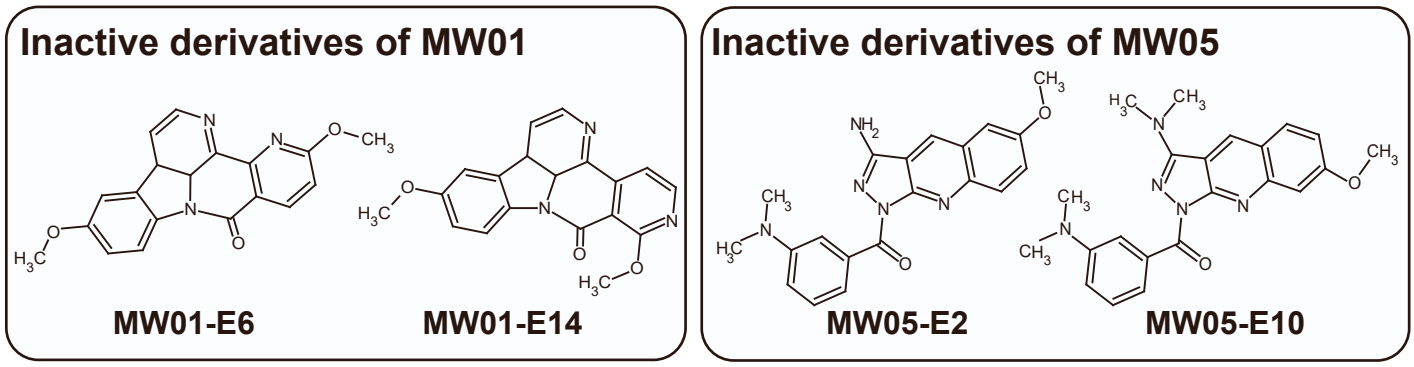

B

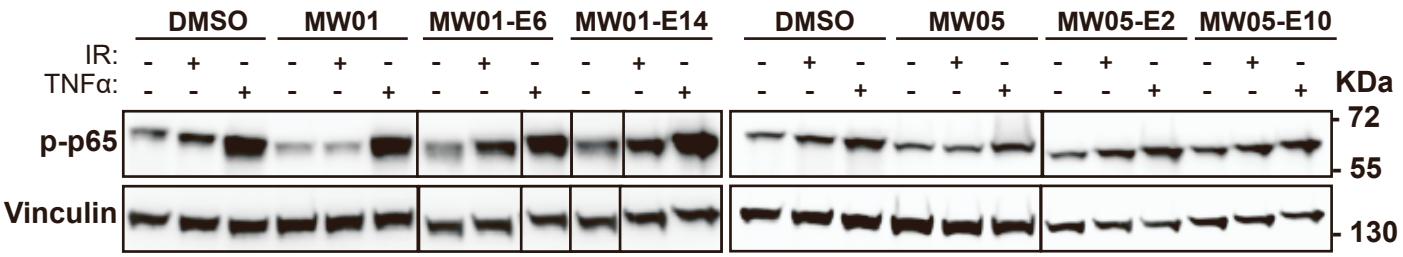

C

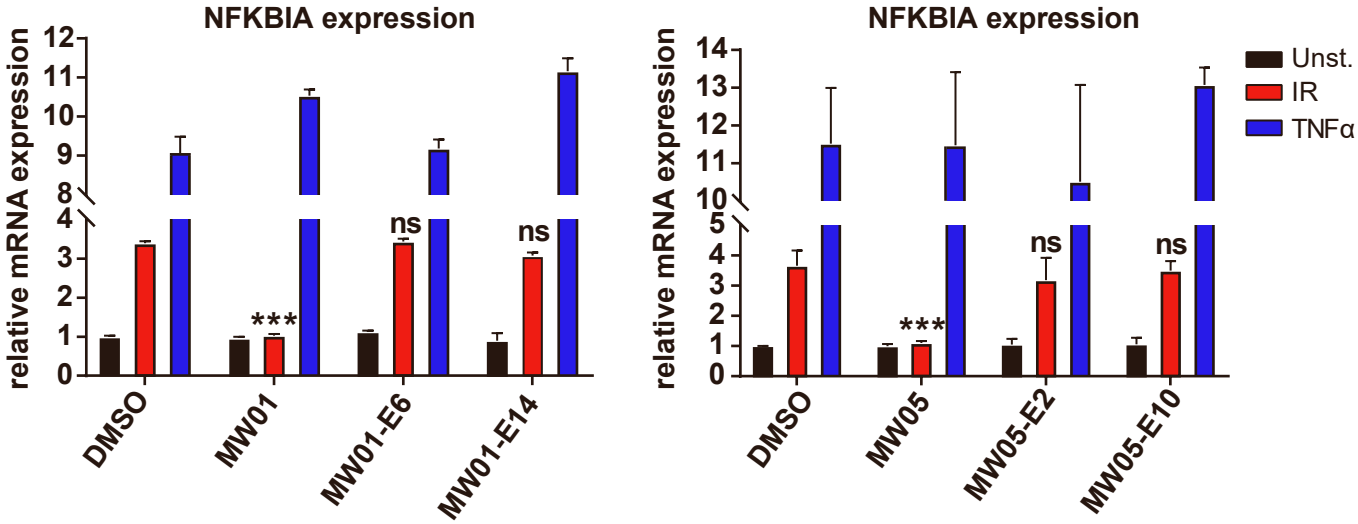

D

Lead	MW01		MW05	
Kinase	MW01-E14 (10μM)	MW01-E6 (10μM)	MW05-E10 (10μM)	MW05-E2 (10μM)
CLK1	6	10	35	16
CLK2	20	18	28	74
CLK3	7	9	2	5
CLK4	67	58	92	75

Percent inhibition
= low, 0-40%
= moderate, 40-70%
= high, 70-100%

Table S3

	% Inhibition							
Lead	**MW01**				**MW05**			
NF-kB Inhibition	**active**	**active**	**inactive**	**inactive**	**active**	**active**	**inactive**	**inactive**
Kinase	**MW01-E18 (10μM)**	**MW01-E10 (10μM)**	**MW01-E14 (10μM)**	**MW01-E6 (10μM)**	**MW05-E9 (10μM)**	**MW05-E3 (10μM)**	**MW05-E10 (10μM)**	**MW05-E2 (10μM)**
AKT1 (PKB alpha)	12	18	9	6	8	29	9	9
AKT2 (PKB beta)	3	18	14	4	5	20	7	8
AKT3 (PKB gamma)	19	24	23	12	14	33	12	11
ALK	35	75	15	19	20	19	9	24
BLK	23	42	9	23	5	30	17	10
BTK	30	69	29	30	7	37	12	7
CLK1	61	69	6	10	79	81	35	16
CLK2	70	70	20	18	87	86	28	74
CLK3	35	35	7	9	38	41	2	5
CLK4	98	99	67	58	84	99	92	75
CSF1R (FMS)	57	61	18	33	11	32	14	20
DNA-PK	94	62	43	9	64	67	8	16
DYRK1A	65	56	12	14	36	76	20	53
DYRK1B	68	81	23	20	46	58	14	84
EGFR (ErbB1)	14	15	9	11	5	12	6	33
FLT3	65	27	12	31	-4	22	9	17
FRAP1 (mTOR)	43	42	26	12	71	52	2	5
GSG2 (Haspin)	88	80	24	29	23	83	19	36
IKBKB (IKK beta)	16	31	16	10	7	23	10	12
IRAK1	69	71	9	56	6	37	-19	2
IRAK4	2	-186	-15	-9	-11	-13	-6	-3
LRRK2	75	86	-4	64	-1	37	-6	8
MAP4K2 (GCK)	93	98	81	70	0	51	5	2
MINK1	85	92	12	57	19	16	13	29
PI4K2A (PI4K2 alpha)	30	13	35	22	-7	4	-3	-4
PI4K2B (PI4K2 beta)	24	22	21	11	-6	3	1	8
PI4KB (PI4K beta)	81	90	36	12	-14	24	1	9
PIK3C2A (PI3K-C2 alpha)	44	31	23	26	-6	17	6	10
PIK3C2G (PI3K-C2 gamma)	81	81	50	35	41	72	10	27
PIK3CA/PIK3R1	90	90	80	38	21	51	-9	26
PIK3CA/PIK3R3	94	90	59	10	16	47	-3	8
PIK3CB/PIK3R1	62	34	26	13	19	40	4	1
PIK3CB/PIK3R2	63	35	12	12	22	34	2	7
PIK3CD/PIK3R1	77	87	84	34	25	55	6	28
PIK3CG	99	93	49	-1	40	56	-7	2
PIP4K2A	-1	-2	53	-4	-6	2	-14	-6
PIP5K1A	28	5	11	20	-16	-2	-8	-9
PIP5K1B	-3	5	26	14		29	-8	-12
PIP5K1C	27	33	8	14	-5	39	-4	-2
PRKCN (PKD3)	52	74	-1	-8	14	31	5	7

Data S1

MW01

==========

Acq. Operator : SYSTEM Seq. Line : 2
Acq. Instrument : LCMSD Location : P1-A-06
Injection Date : 23-Oct-17 13:21:44 Inj : 1
Inj Volume : 1.000 µl
Different Inj Volume from Sample Entry! Actual Inj Volume : 0.500 µl
Acq. Method : K:\DATA\DEF_LC 2017-10-23 13-16-07\ND_C18_ESI-_100-2000_5-99_0.8ML_2.5MIN.M
Last changed : 23-Oct-17 13:16:07 by SYSTEM
Analysis Method : C:\Users\Public\Documents\ChemStation\1\Methods\def_LC.M
Last changed :

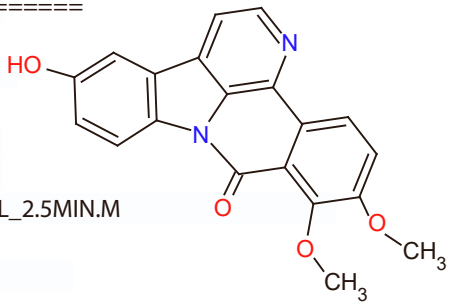

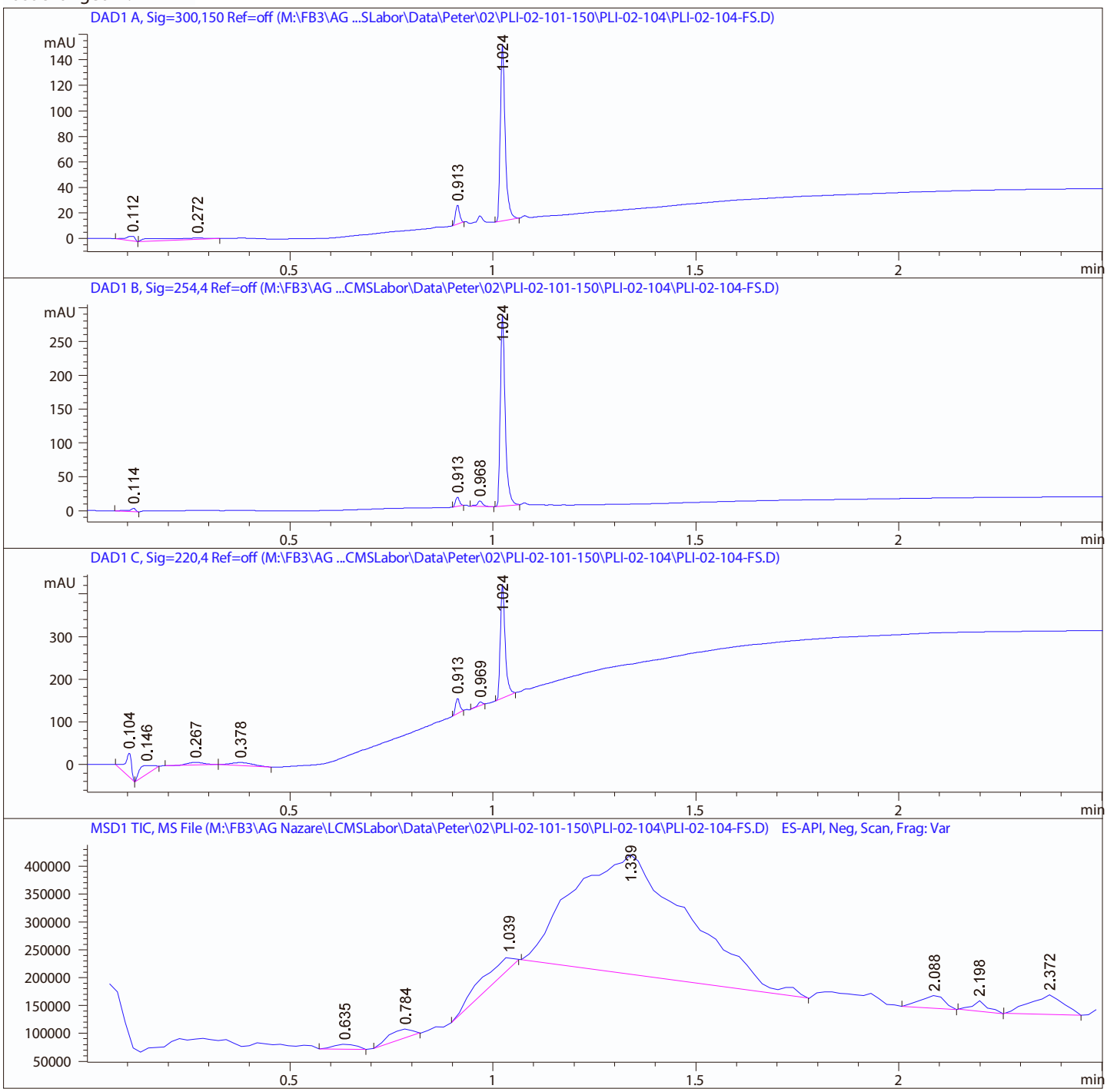

MaxPeak: 98.00%
Ret_Time: 3.253 min

MW01-E1
Z4613513986

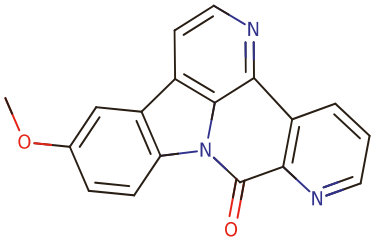

Mol Wt 301.3
Exact Mass 301.09

#	Time	Area%
1	2.718	2.00
2	3.253	98.00

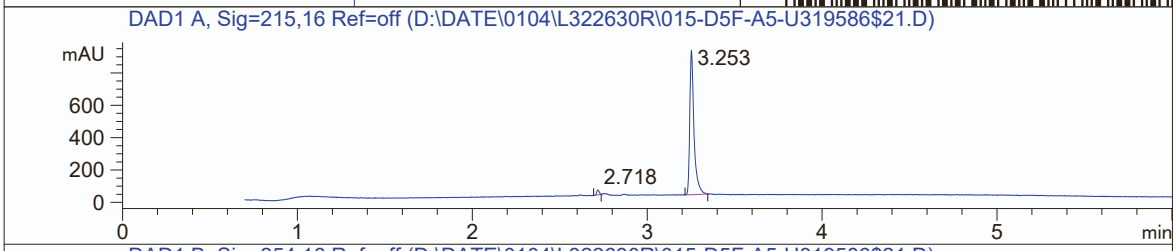

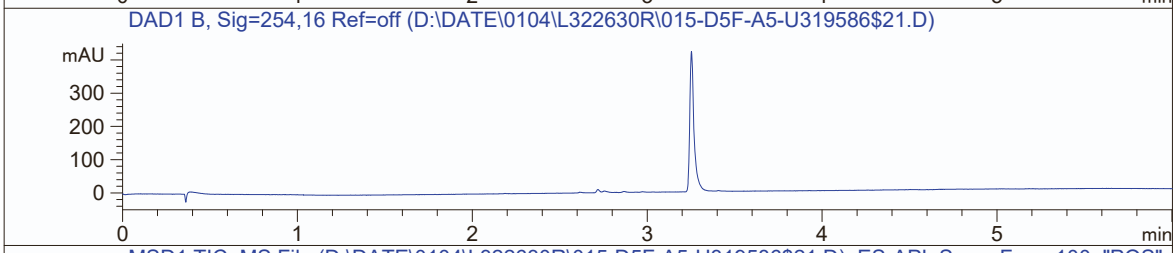

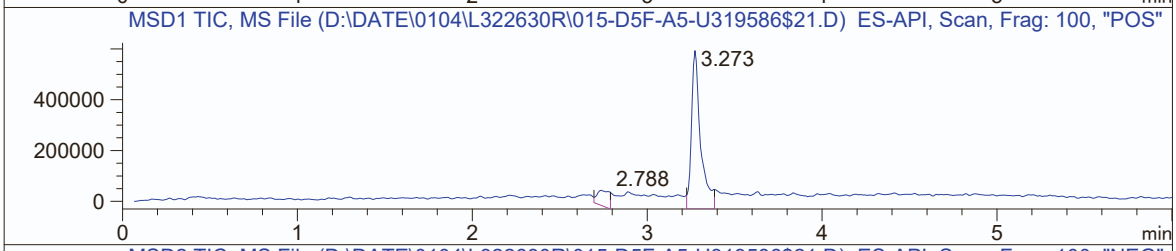

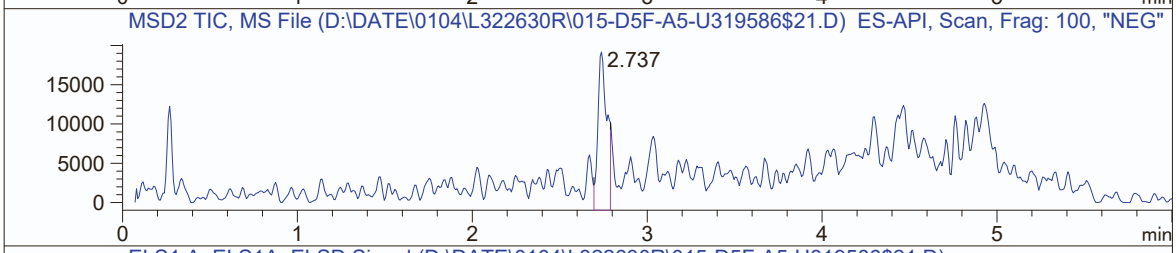

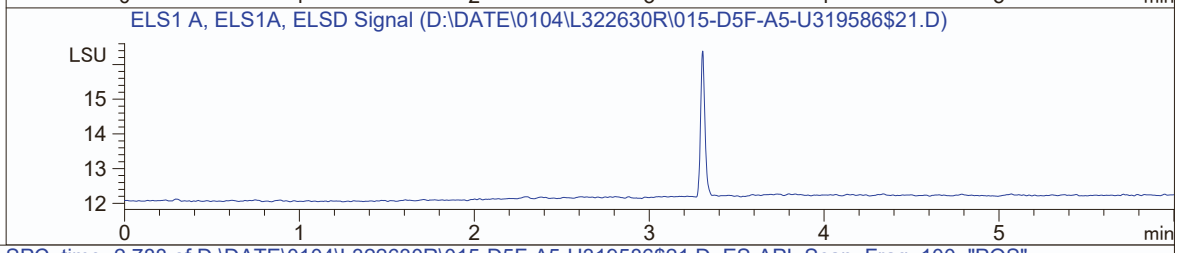

RT 2.788

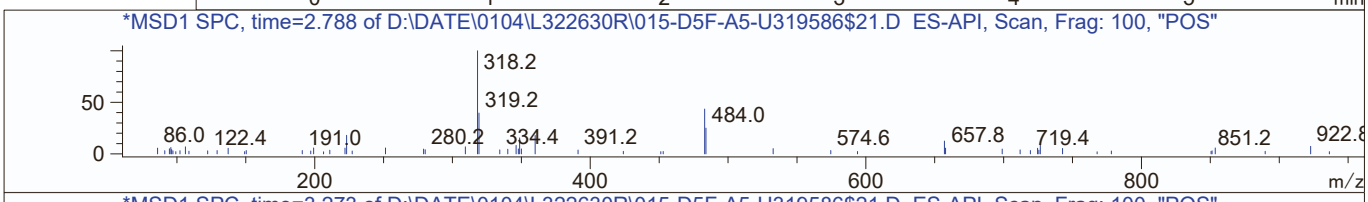

RT 3.273

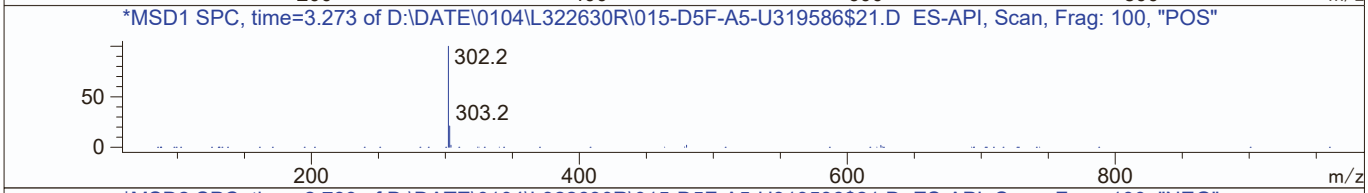

RT 2.737

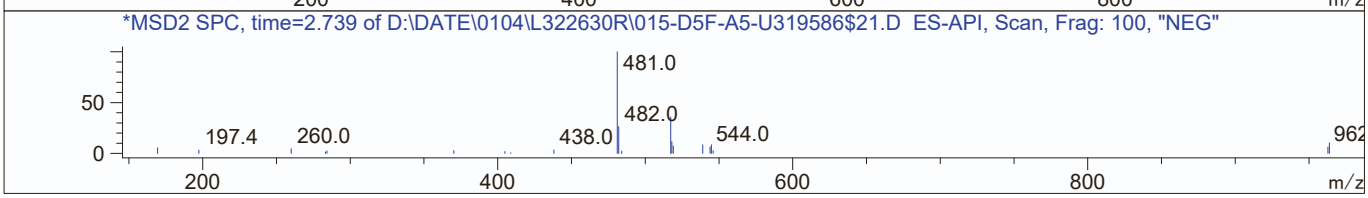

MW01-E2
Z4623297010

MaxPeak: 98.18%
Ret_Time: 2.436 min

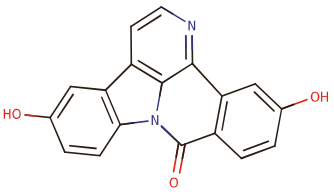

Mol Wt 302.28
Exact Mass 302.07

#	Time	Area%
1	2.436	98.18
2	2.671	1.82

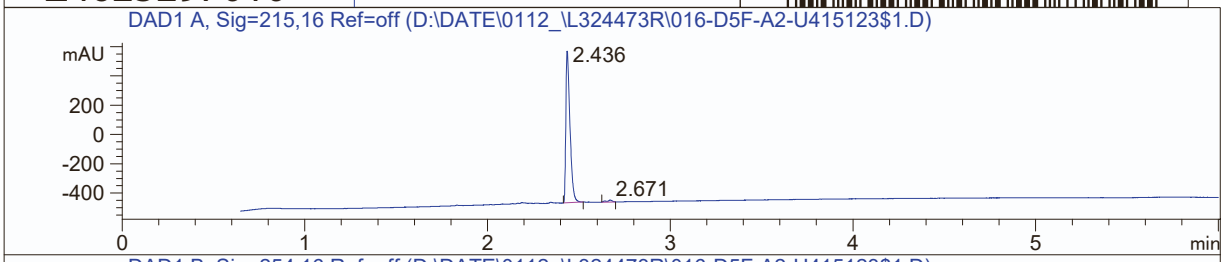

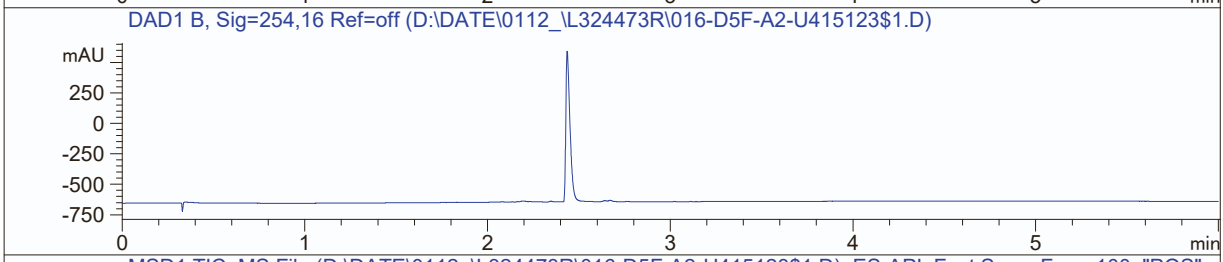

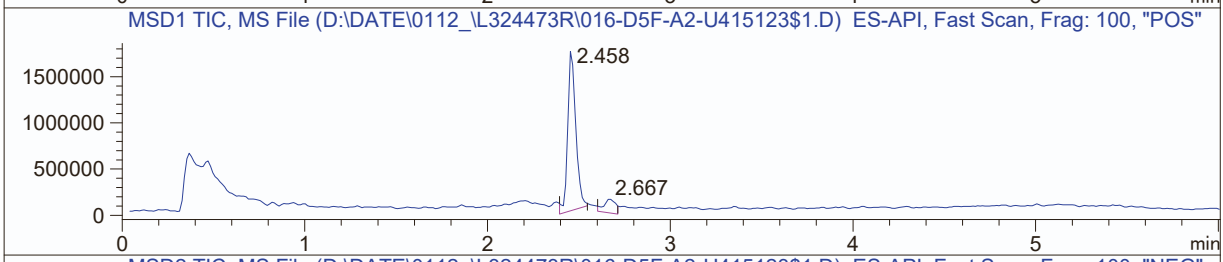

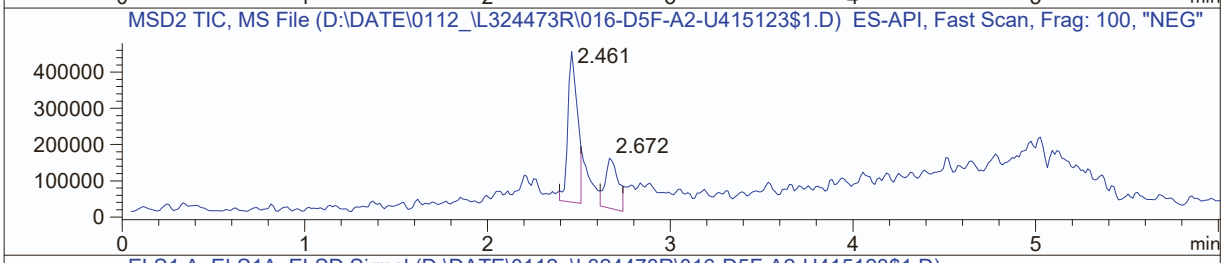

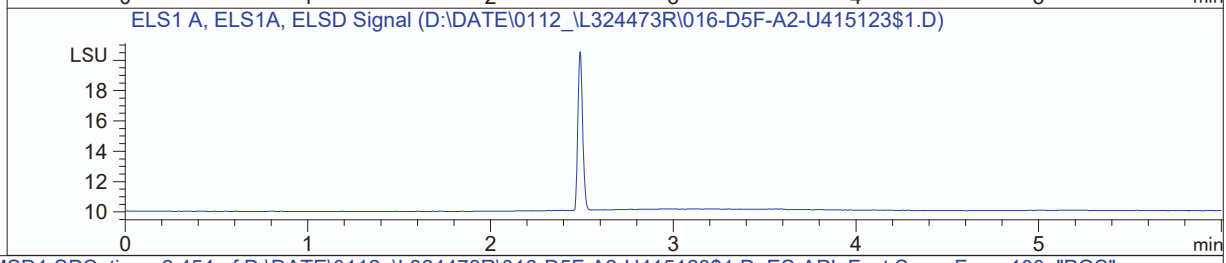

RT 2.458

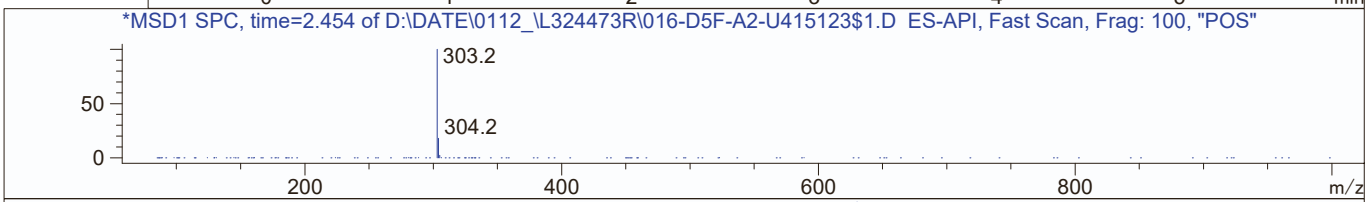

RT 2.667

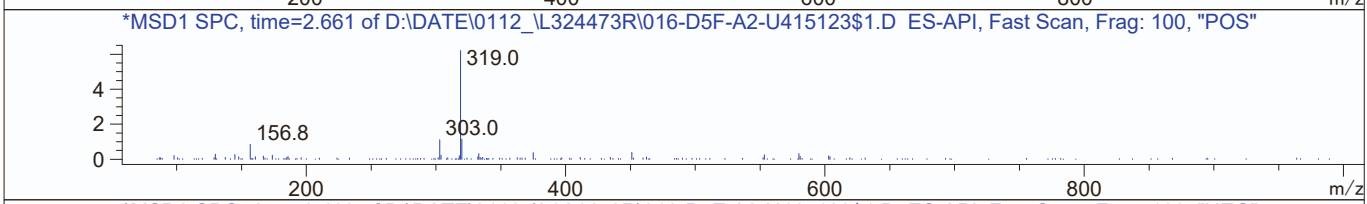

RT 2.461

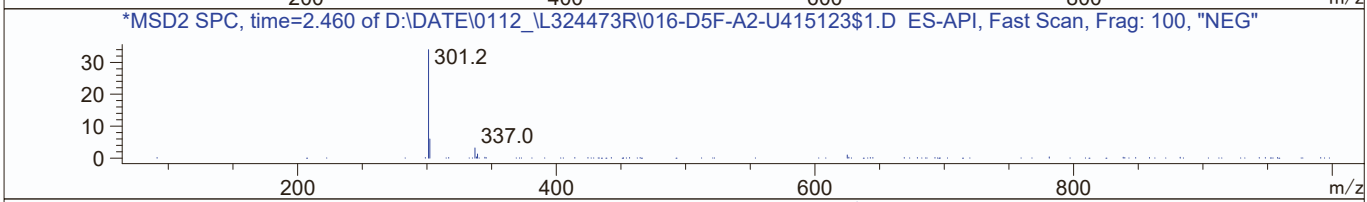

RT 2.672

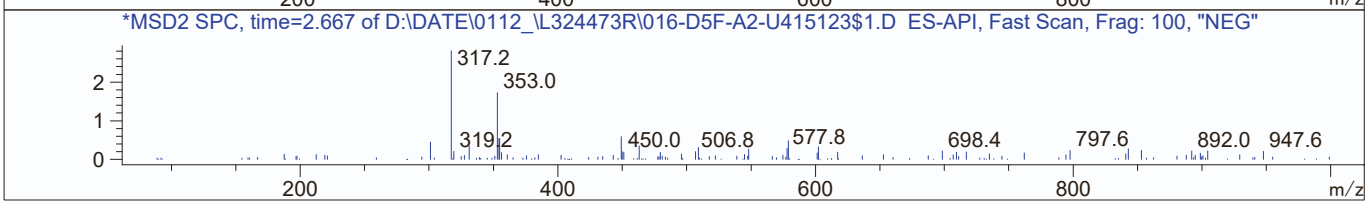

Inj.Date 1/12/2021 O Acq. Method C:\Users\ -> ->

MW01-E3
Z4613515656

MaxPeak: 100.00%
Ret_Time: 2.889 min

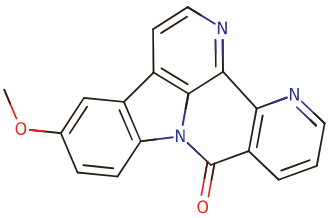

Mol Wt **301.3**
Exact Mass **301.09**

#	Time	Area%
1	2.889	100.00

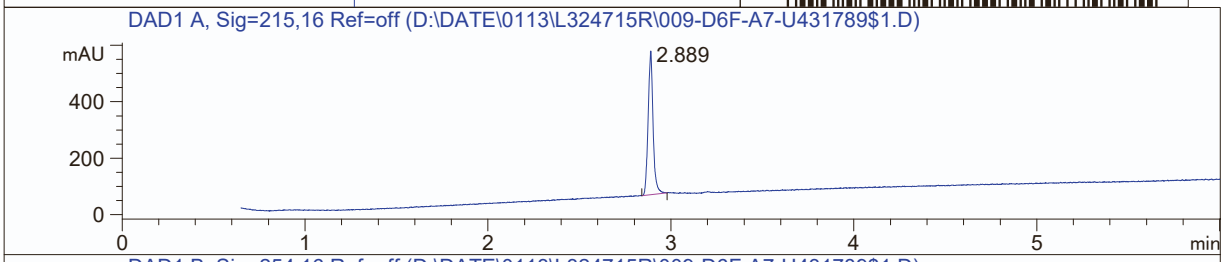

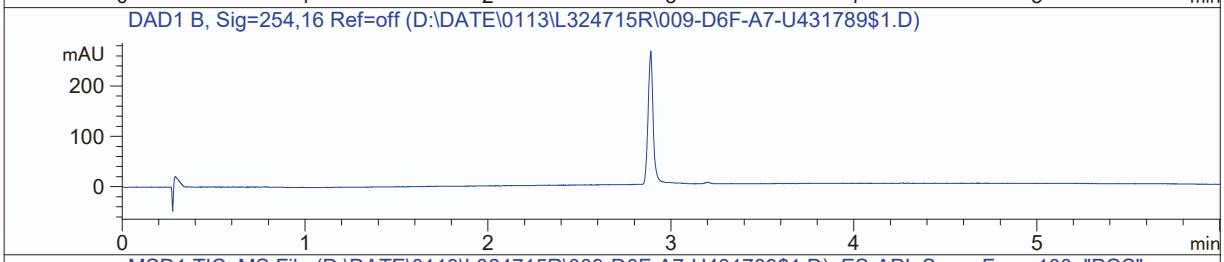

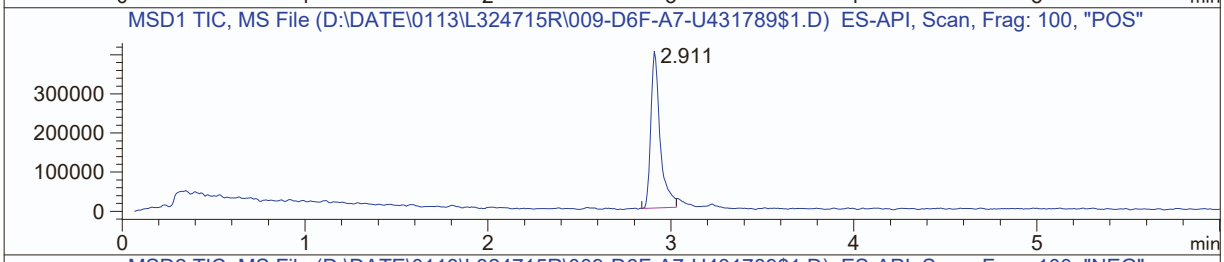

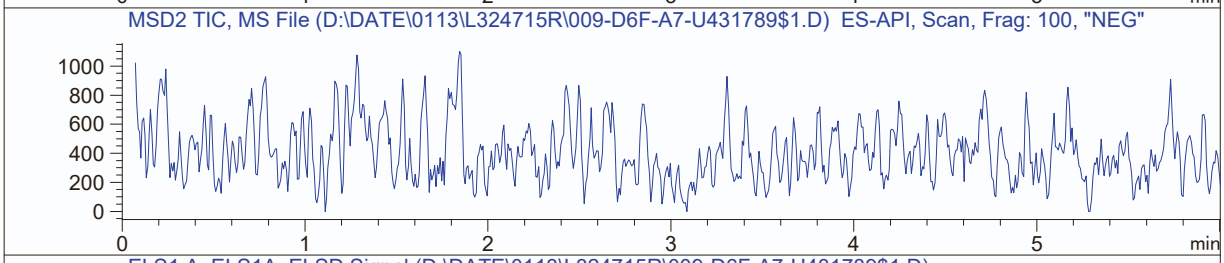

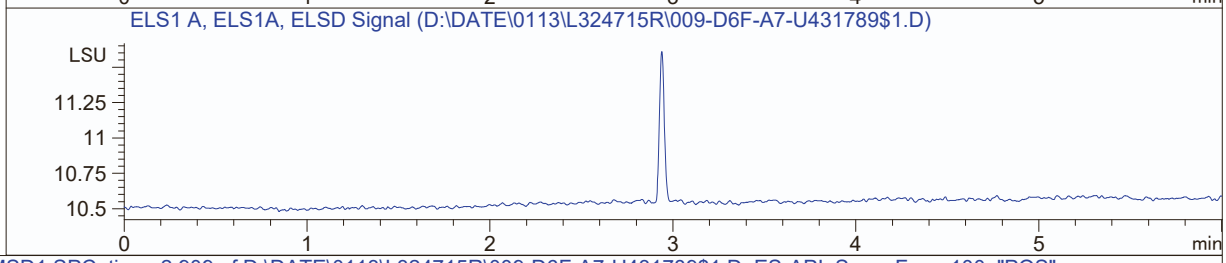

RT 2.911

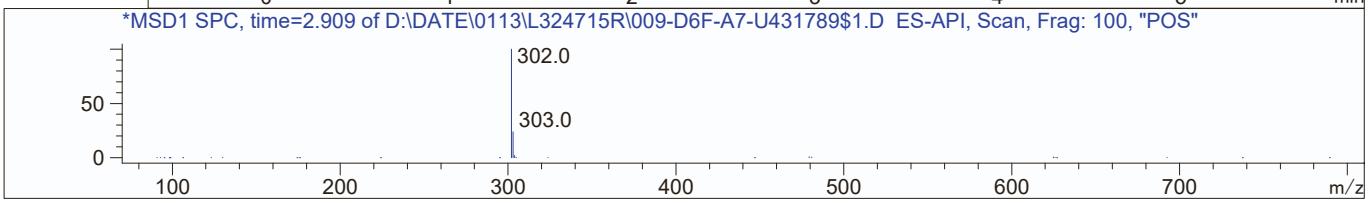

MaxPeak: 100.00%
Ret_Time: 3.255 min

MW01-E4
Z4613448788

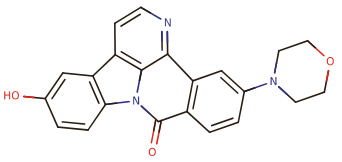

Mol Wt 371.39
Exact Mass 371.14

#	Time	Area%
1	3.255	100.00

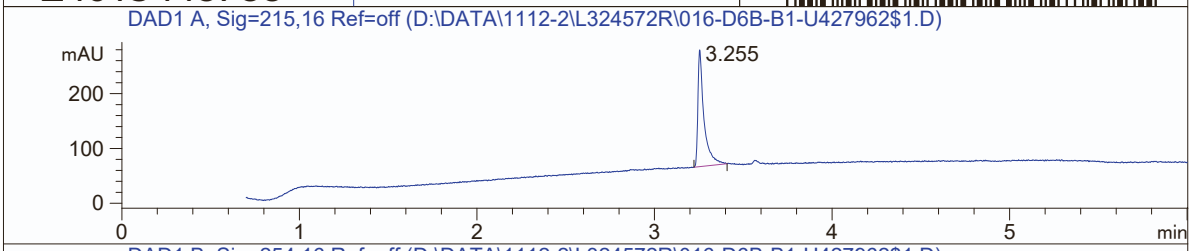

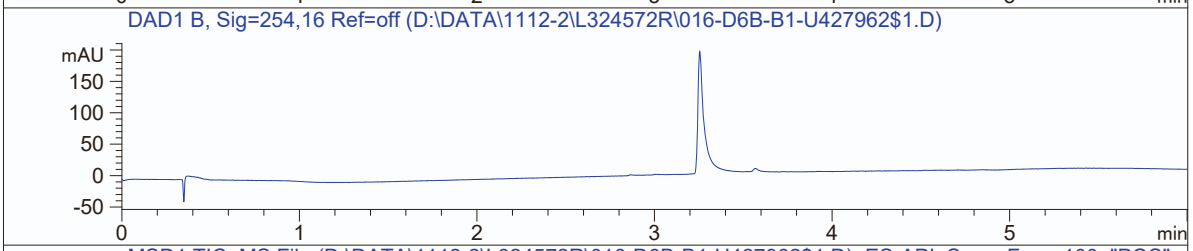

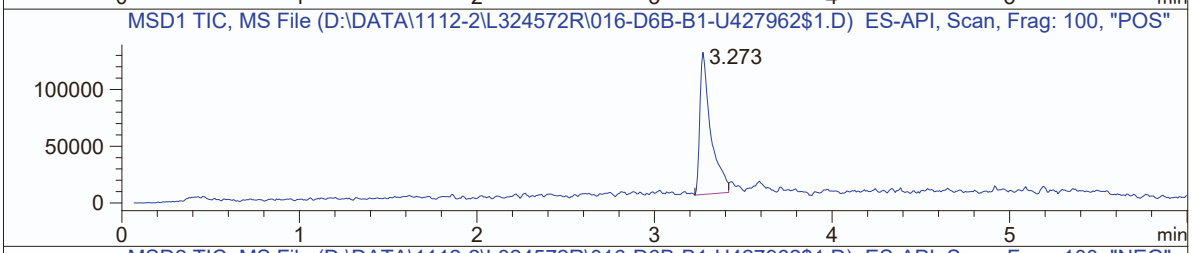

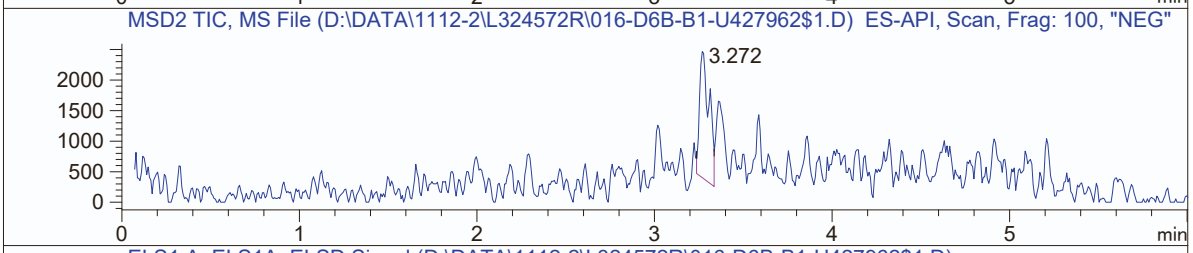

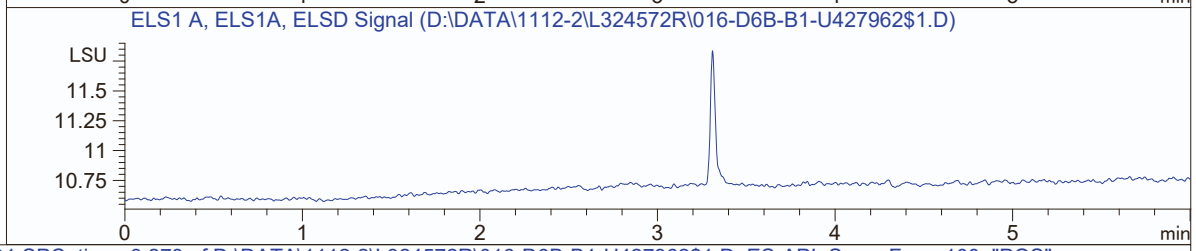

RT 3.273

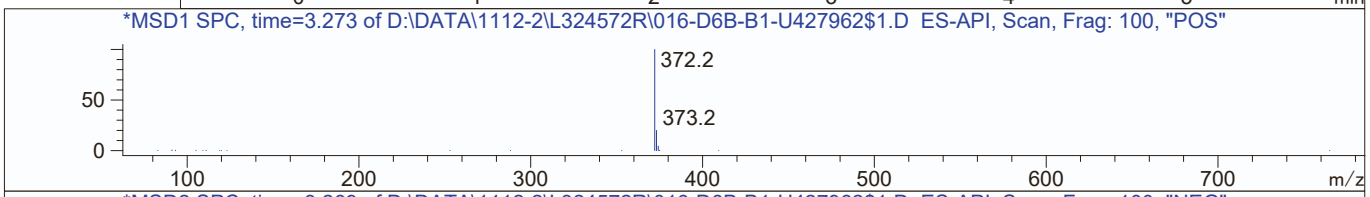

RT 3.272

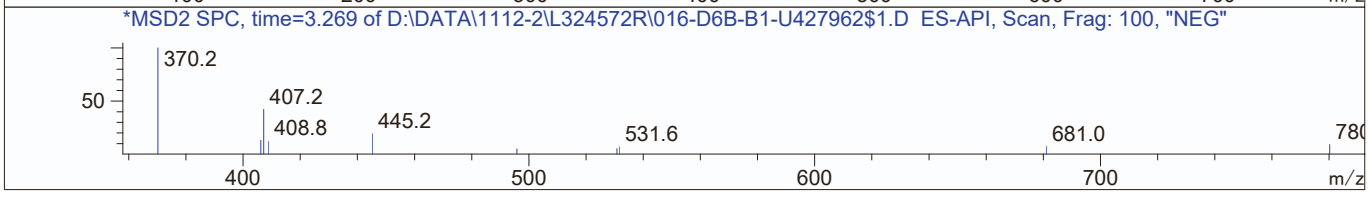

MaxPeak: 96.57%
Ret_Time: 3.247 min

MW01-E5
Z4623297025

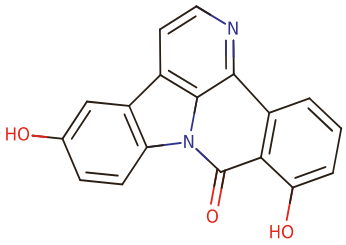

Mol Wt 302.28
Exact Mass 302.07

#	Time	Area%
1	3.247	96.57
2	3.382	3.43

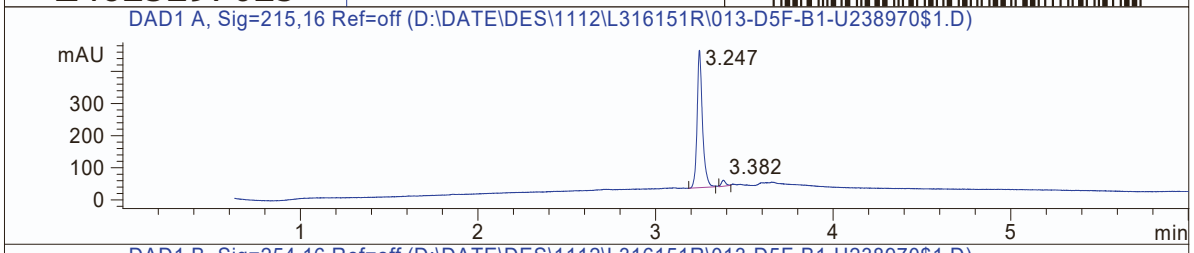

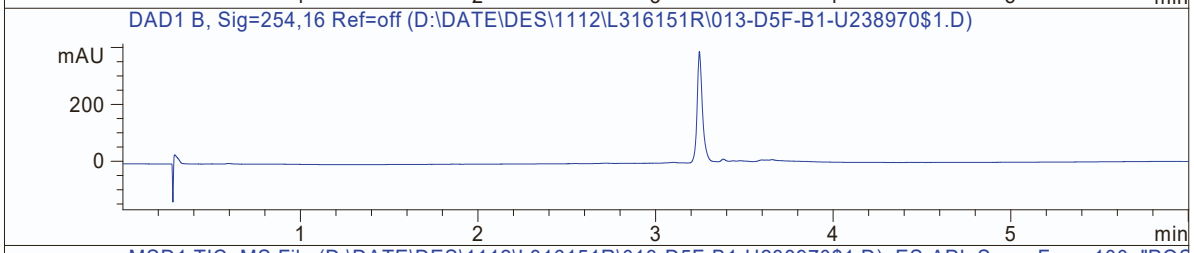

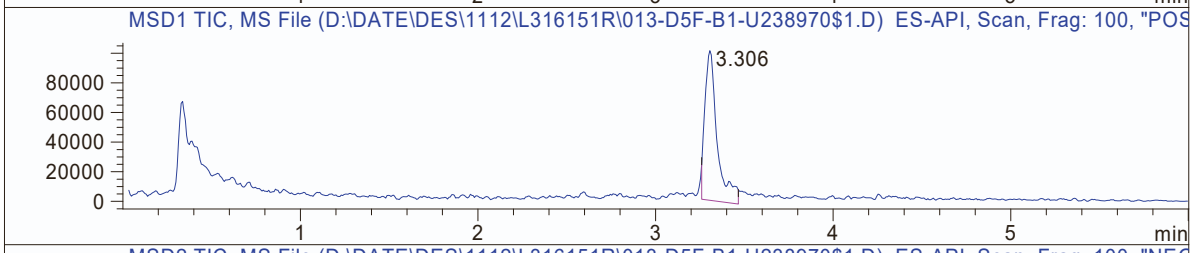

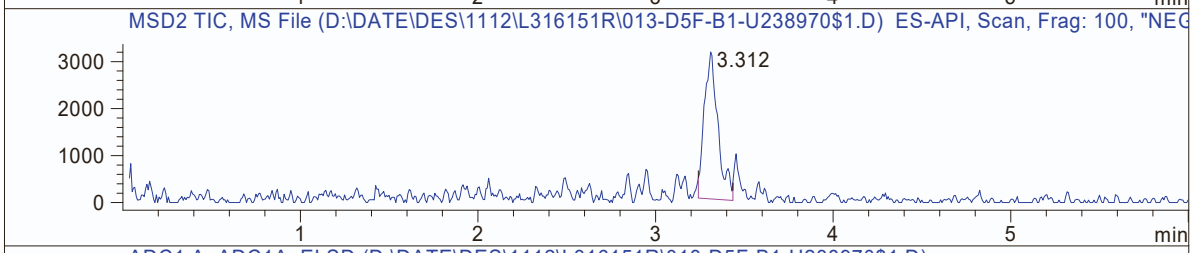

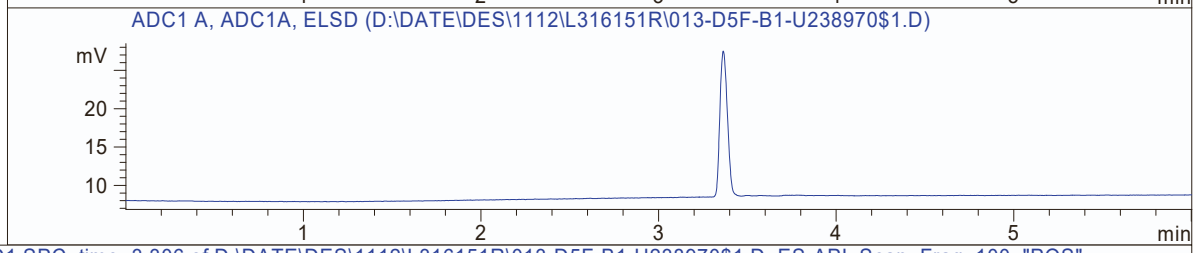

RT 3.306

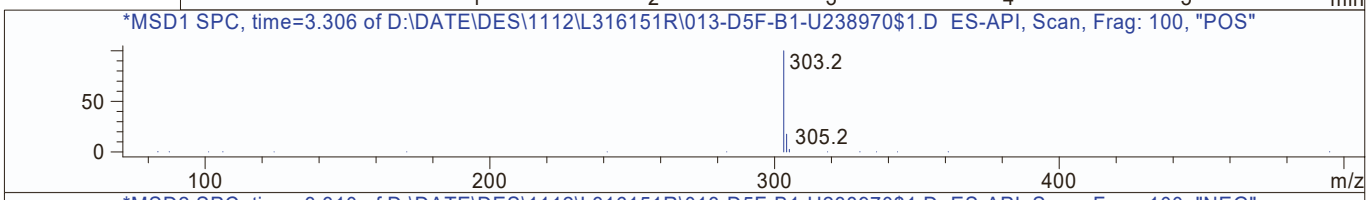

RT 3.312

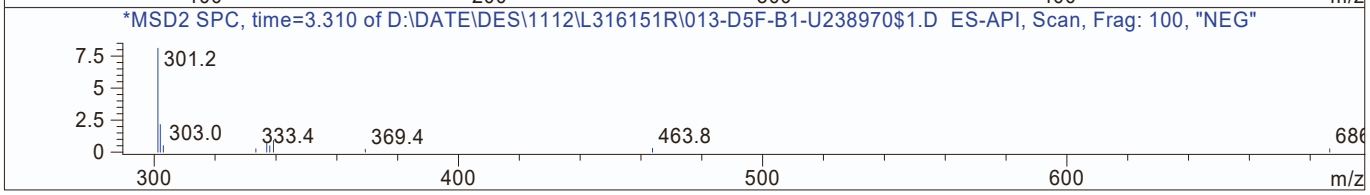

MaxPeak: 100.00%
Ret_Time: 3.524 min

MW01-E6
Z4613838256

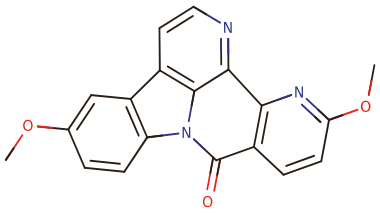

DAD1 A, Sig=215,16 Ref=off (D:\DATE\01 12\L324568R\015-D6B-A7-U425312$2.D)

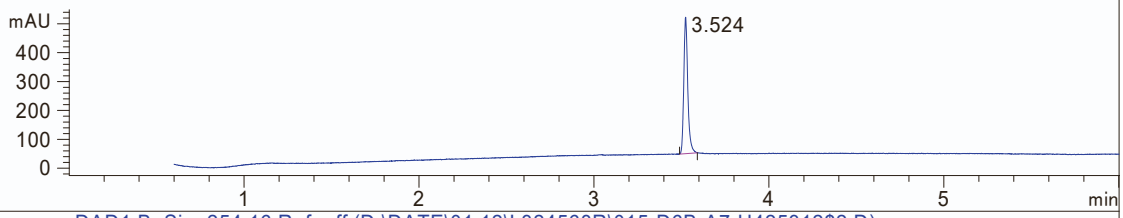

DAD1 B, Sig=254,16 Ref=off (D:\DATE\01 12\L324568R\015-D6B-A7-U425312$2.D)

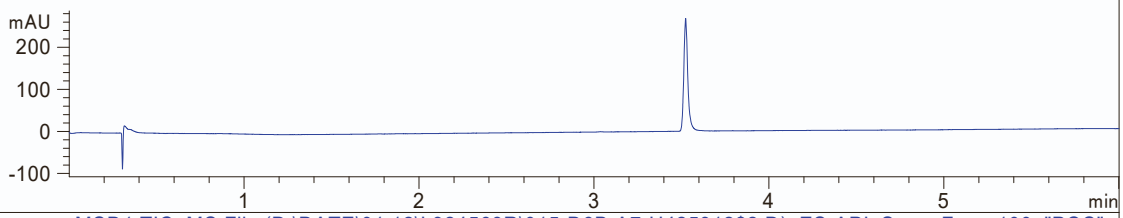

Mol Wt **331.32**
Exact Mass **331.1**

#	Time	Area%
1	3.524	100.00

MSD1 TIC, MS File (D:\DATE\01 12\L324568R\015-D6B-A7-U425312$2.D) ES-API, Scan, Frag: 100, "POS"

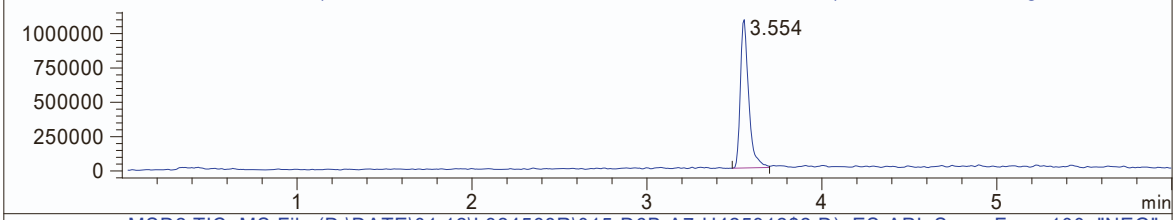

MSD2 TIC, MS File (D:\DATE\01 12\L324568R\015-D6B-A7-U425312$2.D) ES-API, Scan, Frag: 100, "NEG"

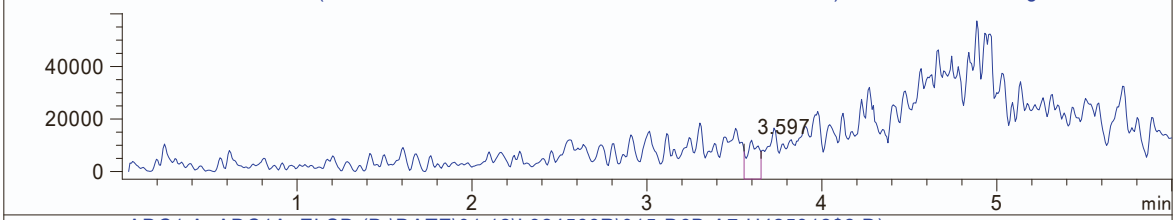

ADC1 A, ADC1A, ELSD (D:\DATE\01 12\L324568R\015-D6B-A7-U425312$2.D)

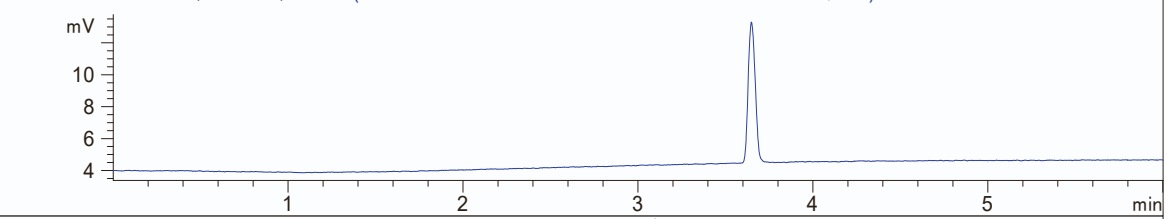

RT 3.554

*MSD1 SPC, time=3.556 of D:\DATE\01 12\L324568R\015-D6B-A7-U425312$2.D ES-API, Scan, Frag: 100, "POS"

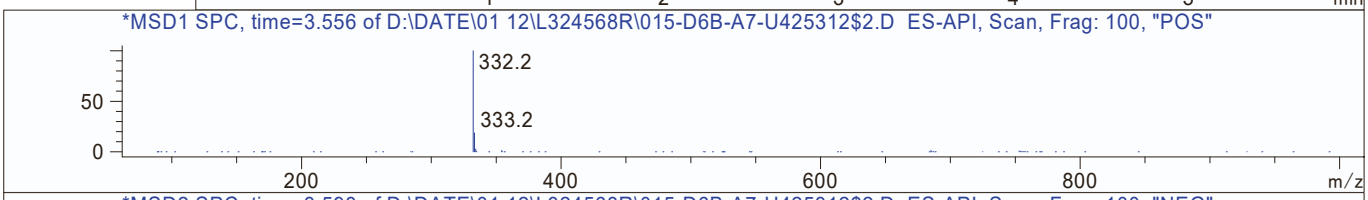

RT 3.597

*MSD2 SPC, time=3.598 of D:\DATE\01 12\L324568R\015-D6B-A7-U425312$2.D ES-API, Scan, Frag: 100, "NEG"

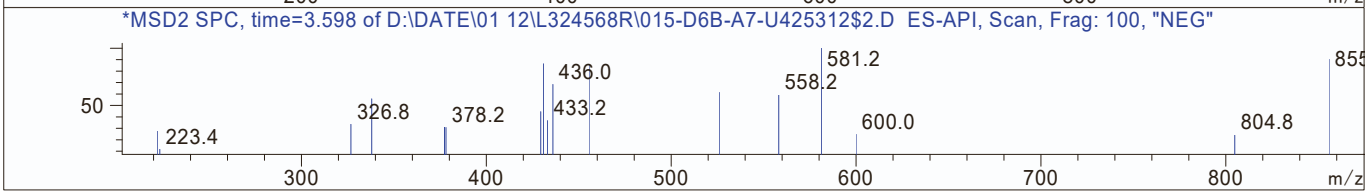

MaxPeak: 95.87%
Ret_Time: 2.030 min

MW01-E7
Z4613449330

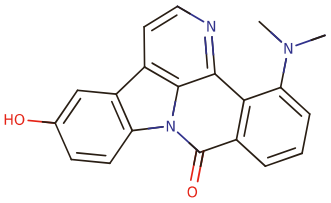

Mol Wt 329.35
Exact Mass 329.13

#	Time	Area%
1	1.580	0.64
2	2.030	95.87
3	2.624	3.50

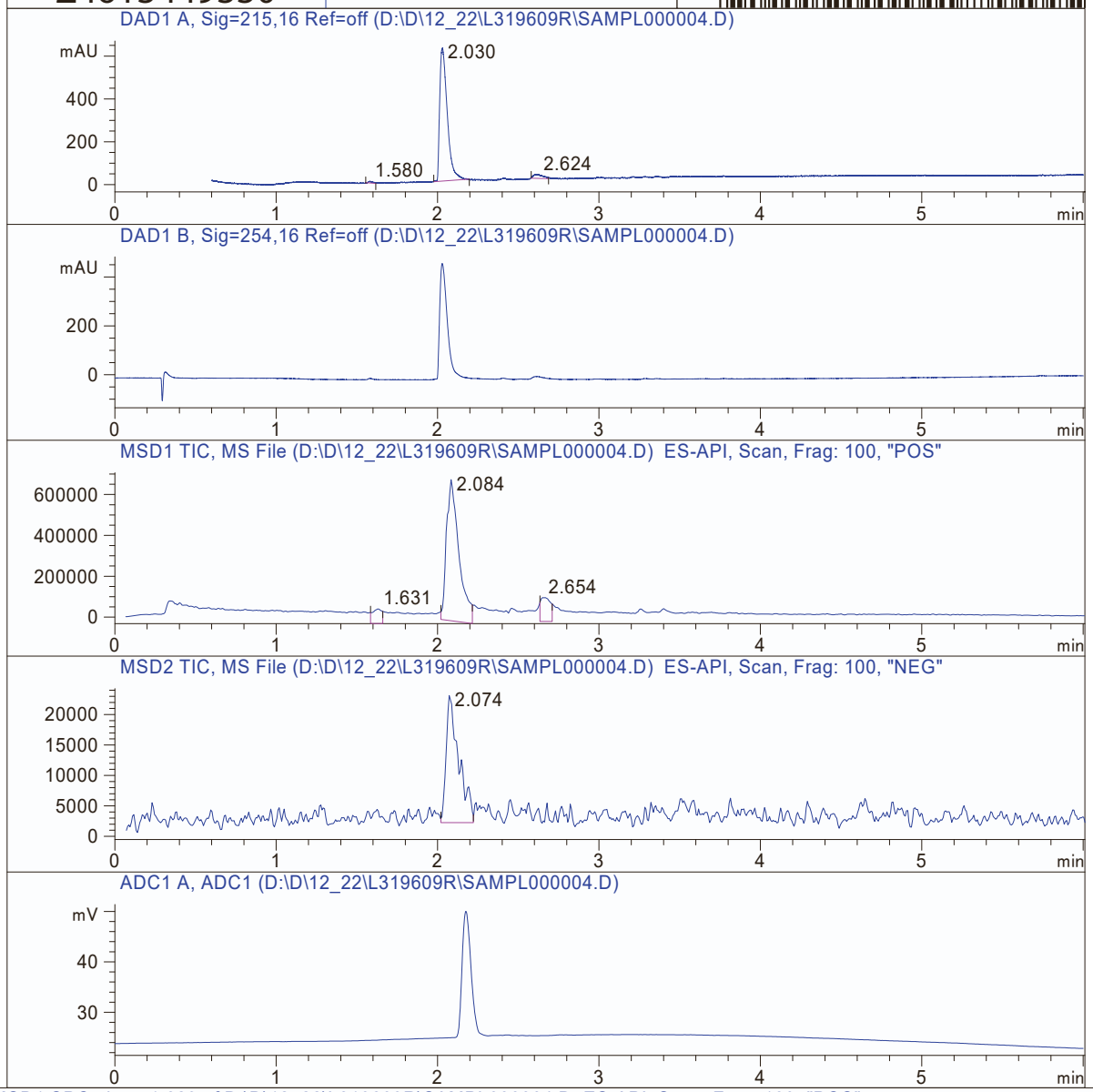

RT 1.631

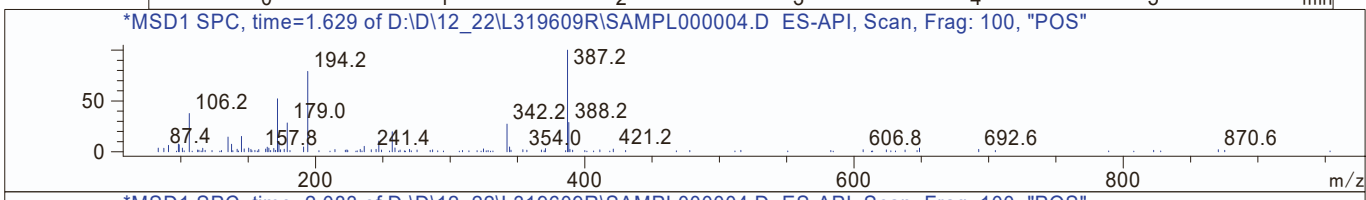

RT 2.084

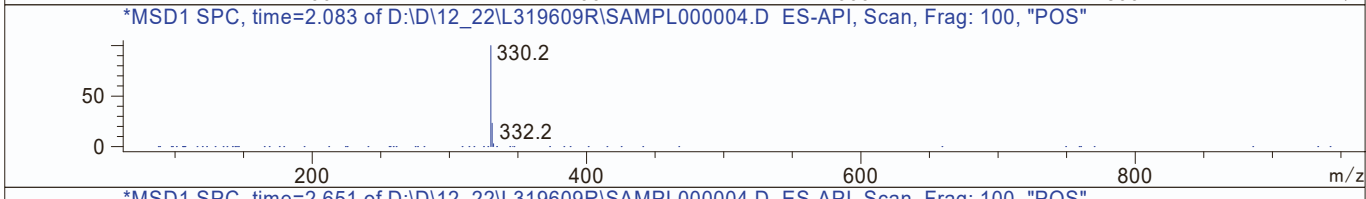

RT 2.654

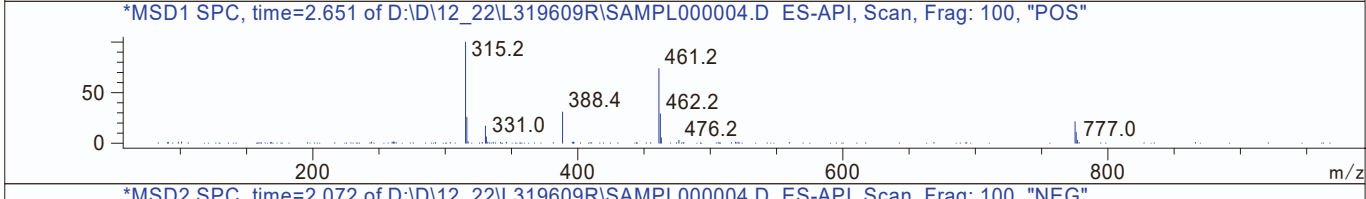

RT 2.074

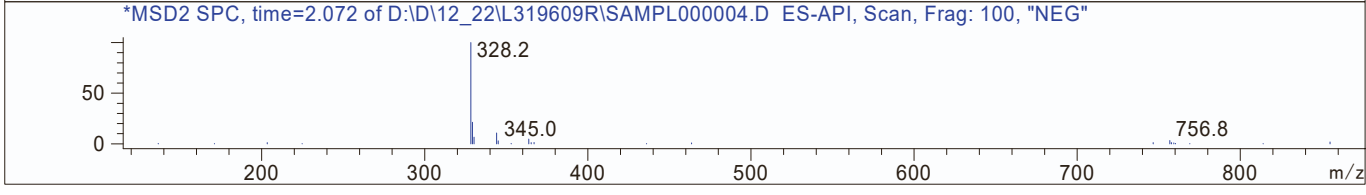

MaxPeak: 100.00%
Ret_Time: 3.844 min

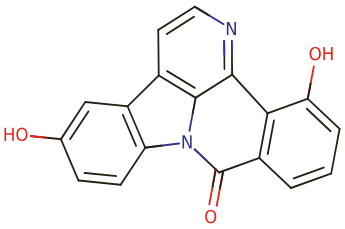

Mol Wt 302.28
Exact Mass 302.07

#	Time	Area%
1	3.844	100.00

MW01-E8
Z4623297004

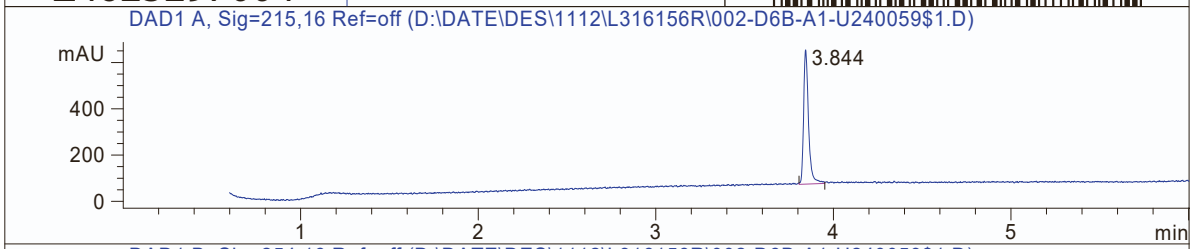

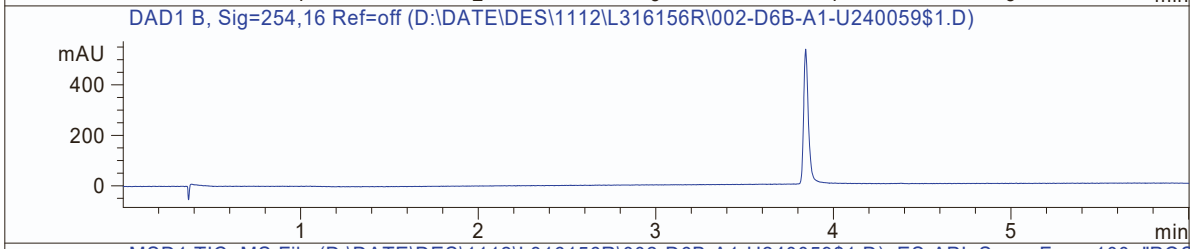

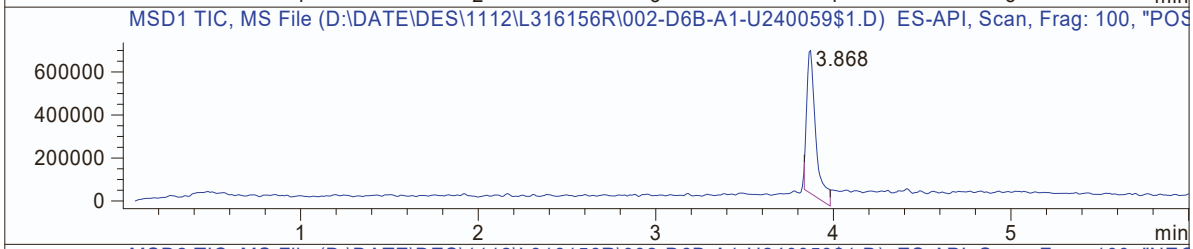

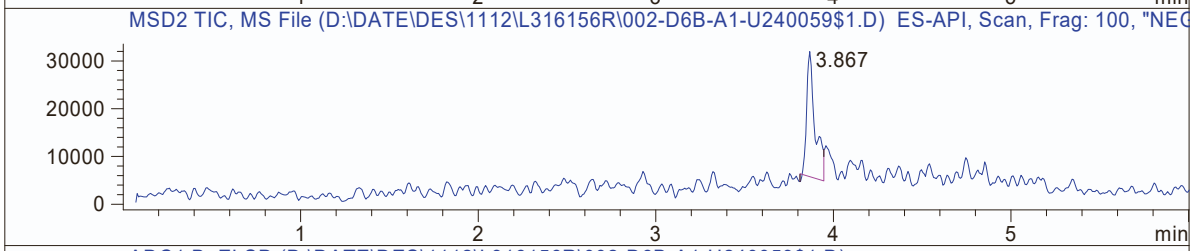

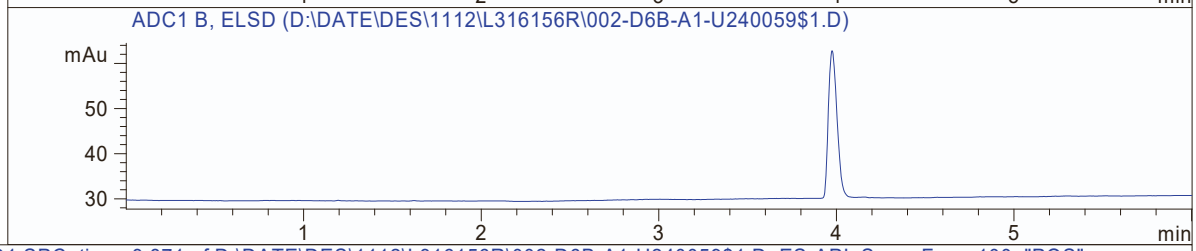

RT 3.868

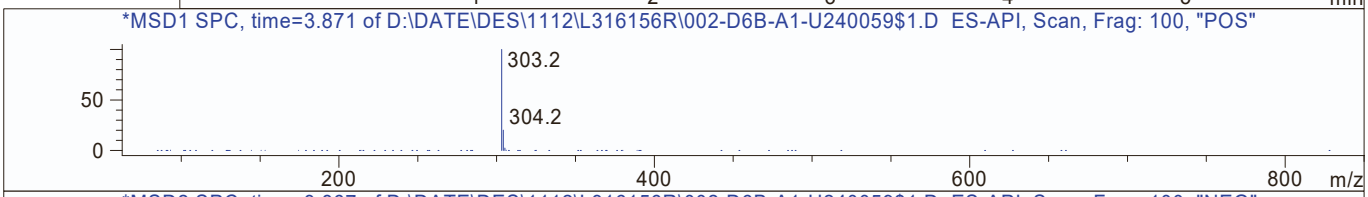

RT 3.867

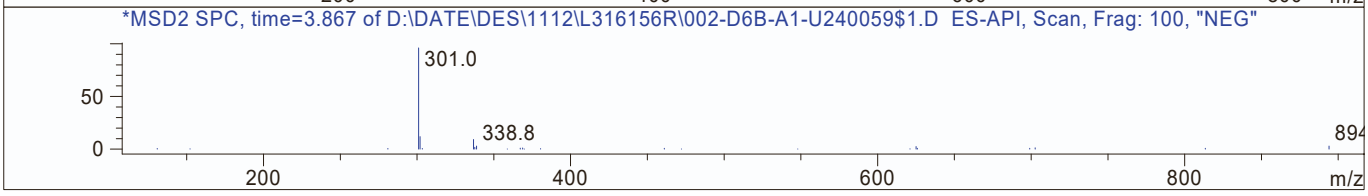

MaxPeak: 98.31%
Ret_Time: 3.186 min

MW01-E9
Z4613448981

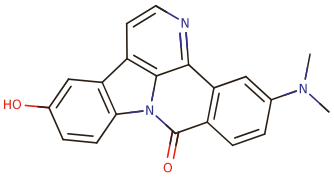

Mol Wt 329.35
Exact Mass 329.13

#	Time	Area%
1	2.892	1.69
2	3.186	98.31

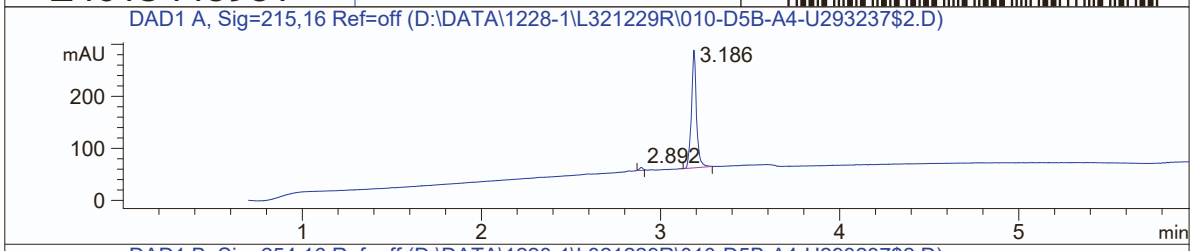

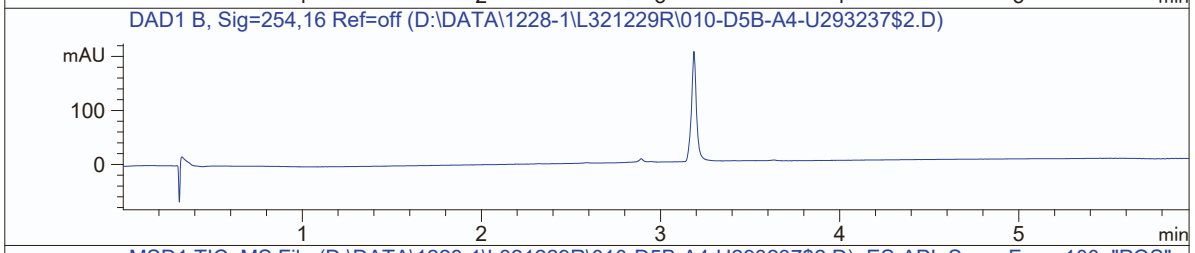

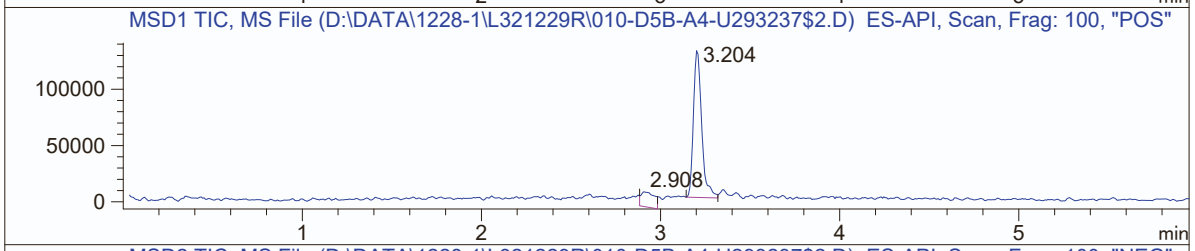

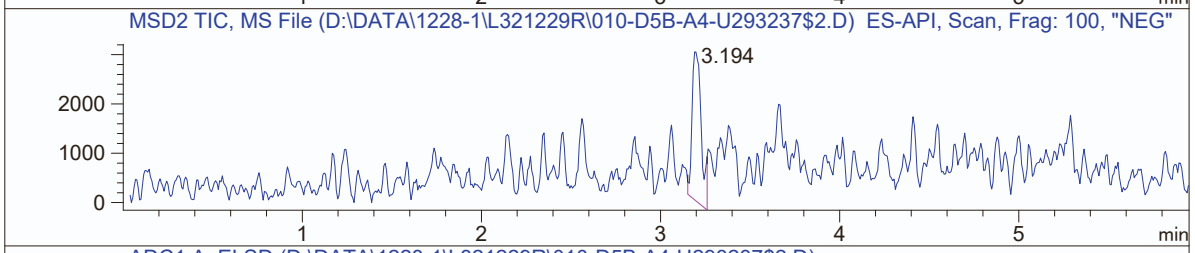

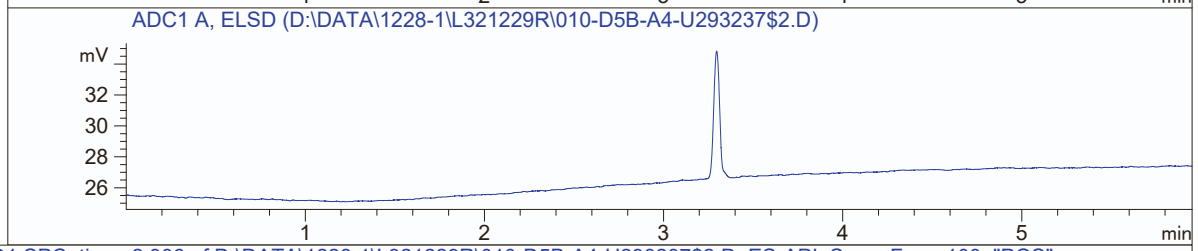

RT 2.908

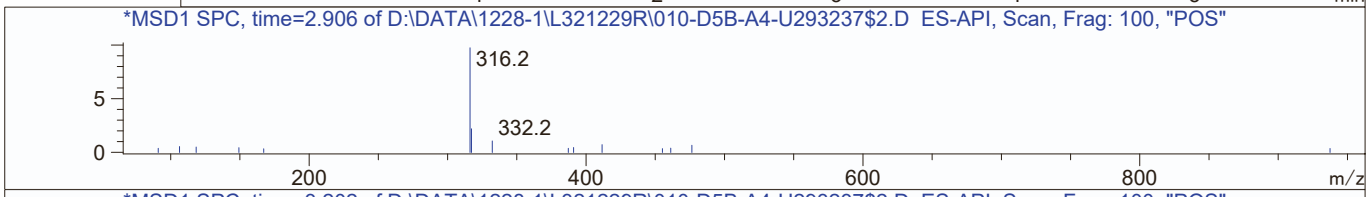

RT 3.204

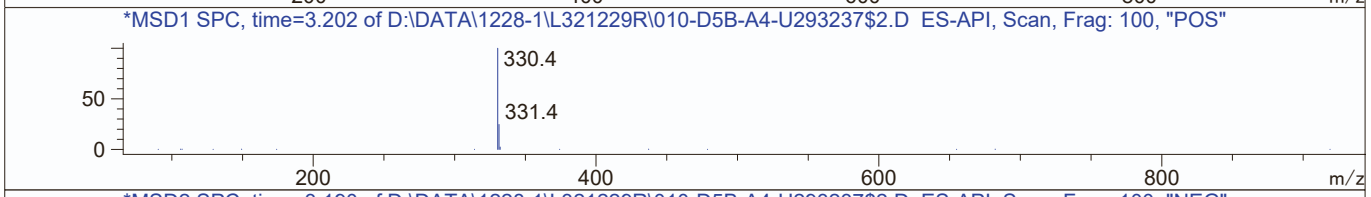

RT 3.194

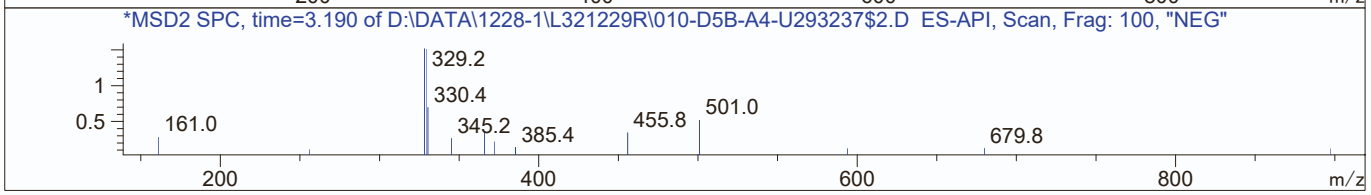

MaxPeak: 100.00%
Ret_Time: 2.882 min

MW01-E10
Z4623297012

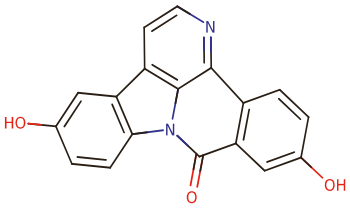

Mol Wt 302.28
Exact Mass 302.07

#	Time	Area%
1	2.882	100.00

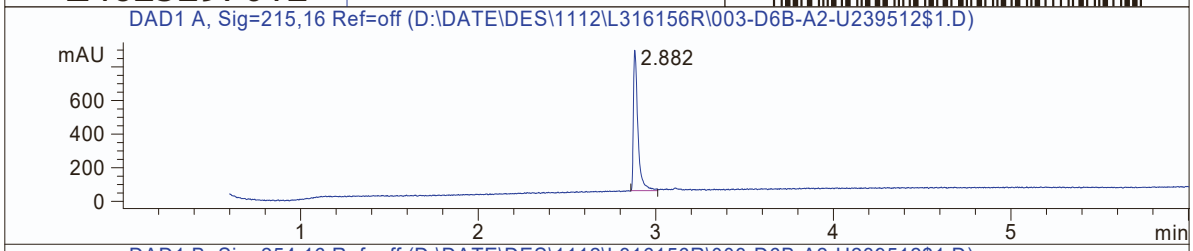

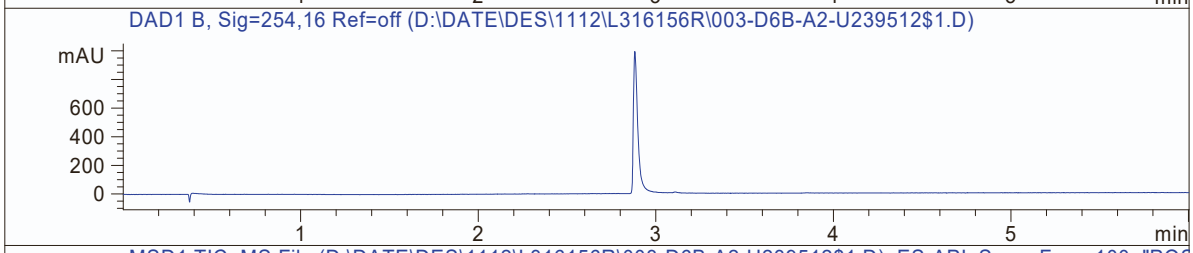

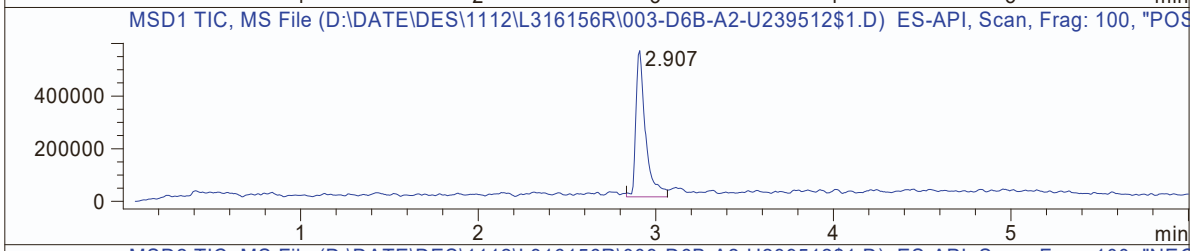

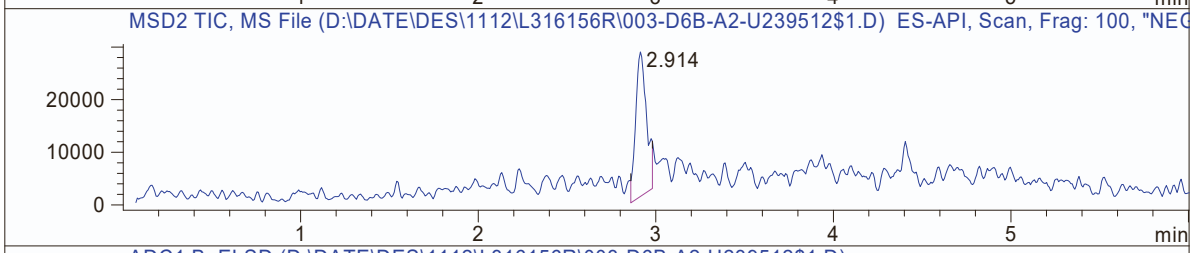

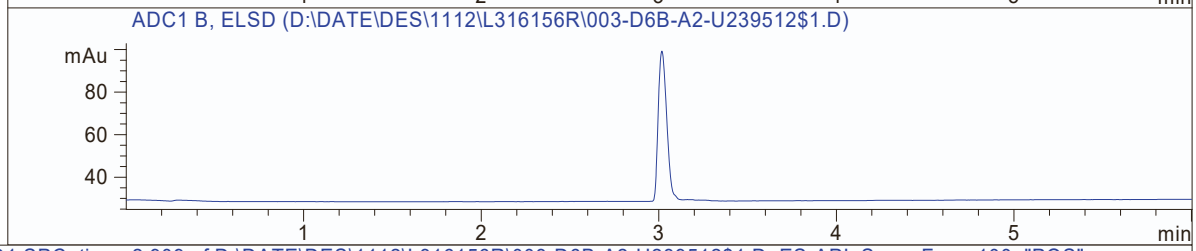

RT 2.907

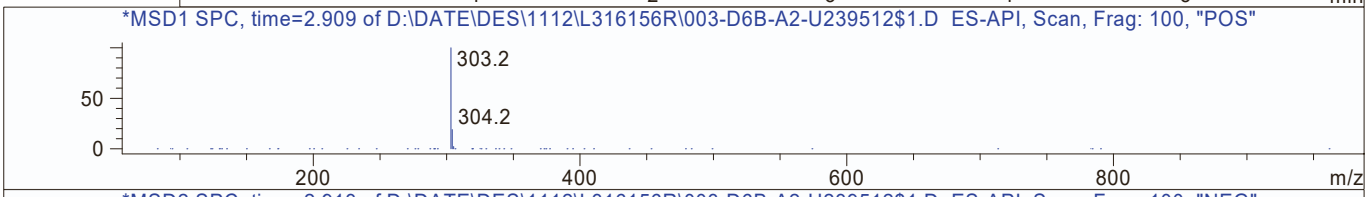

RT 2.914

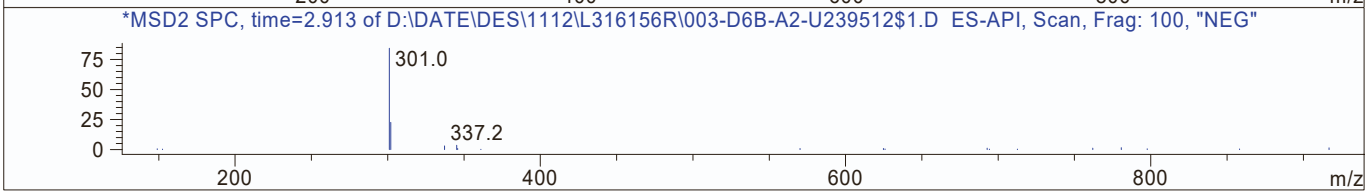

MaxPeak: 100.00%
Ret_Time: 1.932 min

MW01-E11
Z4623297038

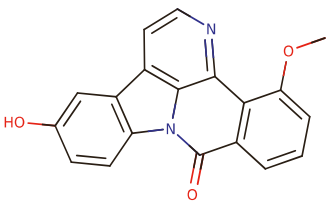

Mol Wt 316.31
Exact Mass 316.09

#	Time	Area%
1	1.932	100.00

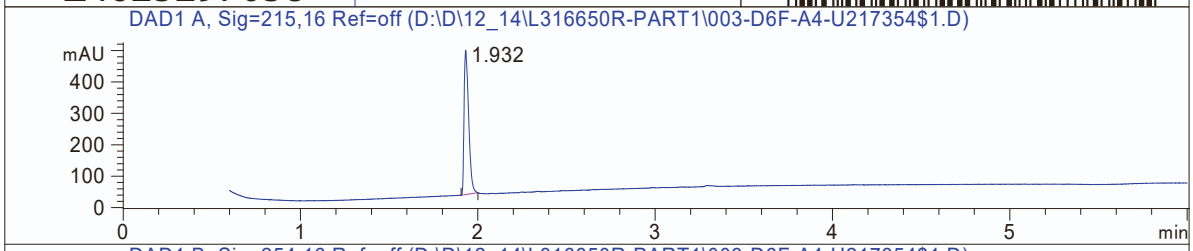

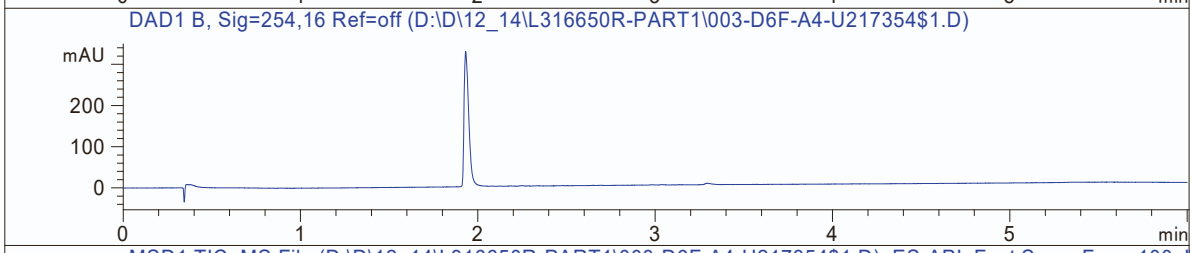

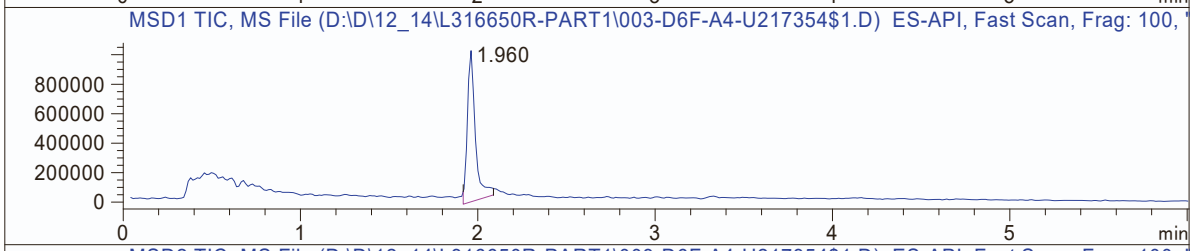

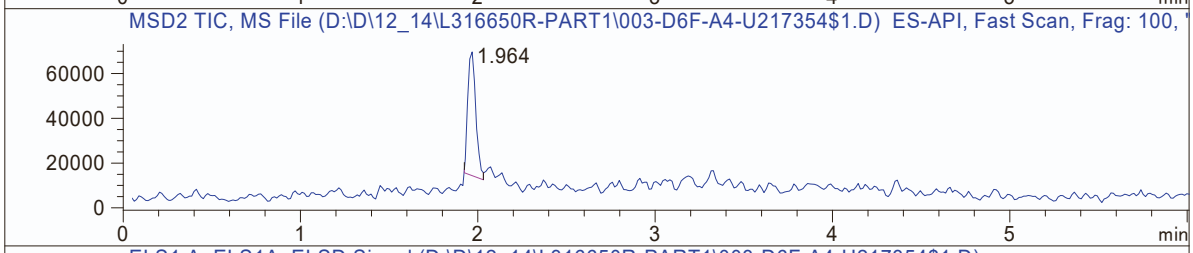

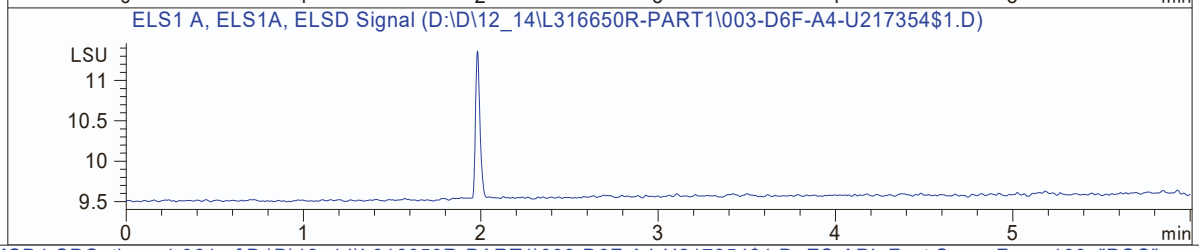

RT 1.960

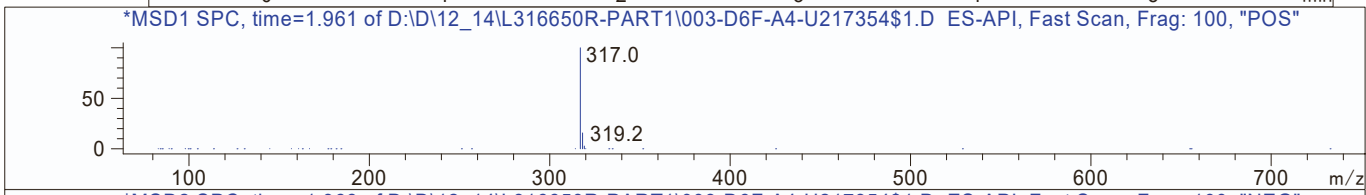

RT 1.964

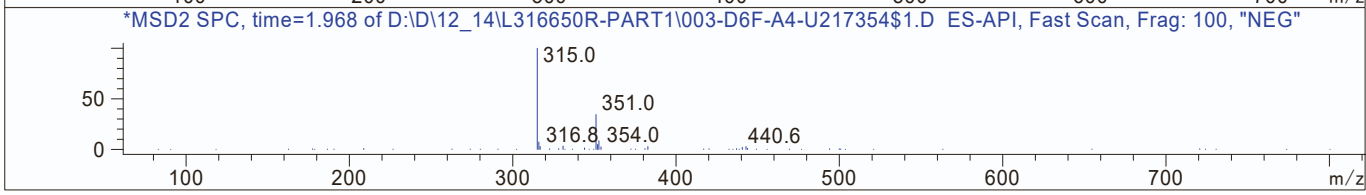

Inj.Date 12/14/2020 N Acq. Method C:\Users\ -> ->

MaxPeak: 97.66%
Ret_Time: 2.769 min

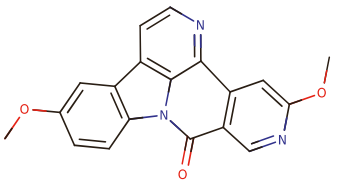

Mol Wt 331.32
Exact Mass 331.1

#	Time	Area%
1	2.769	97.66
2	2.905	2.34

MW01-E12
Z4613897071

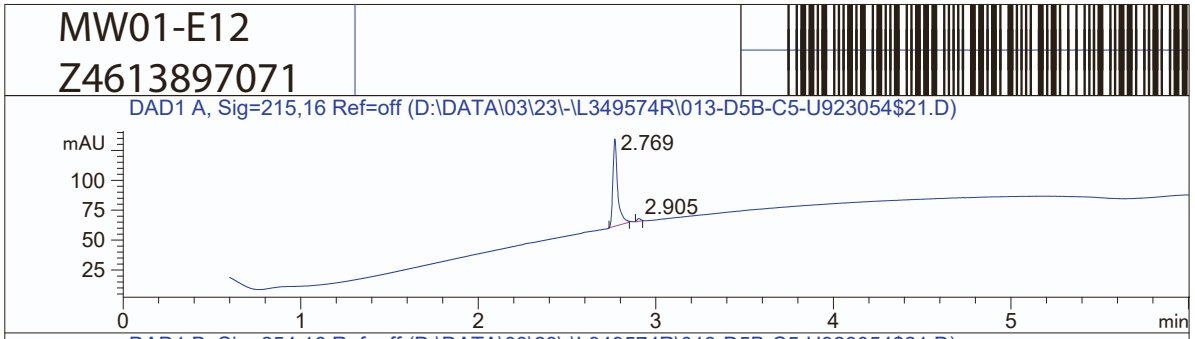

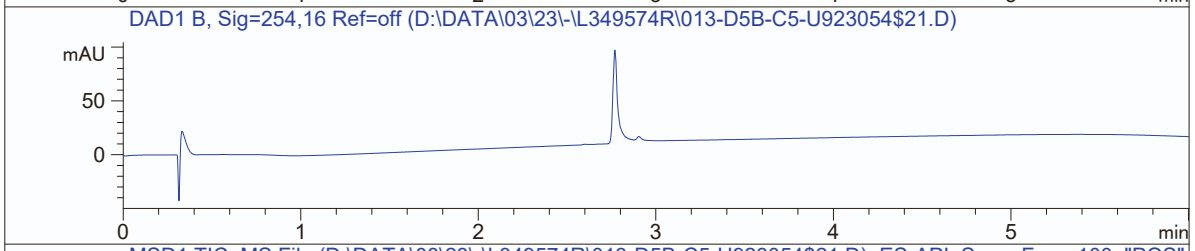

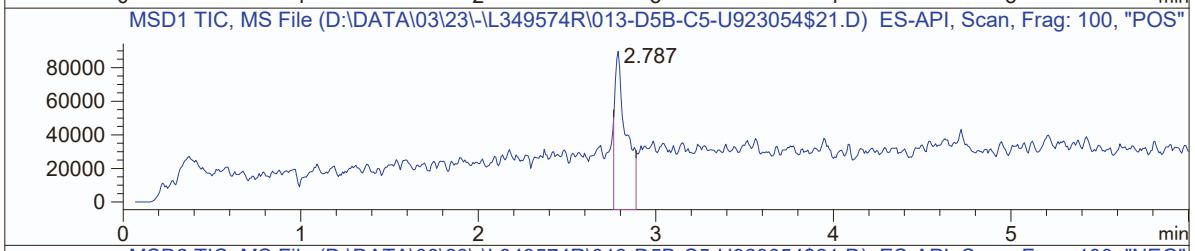

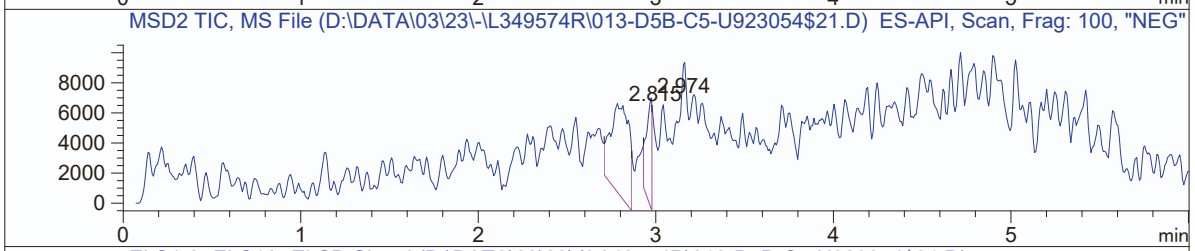

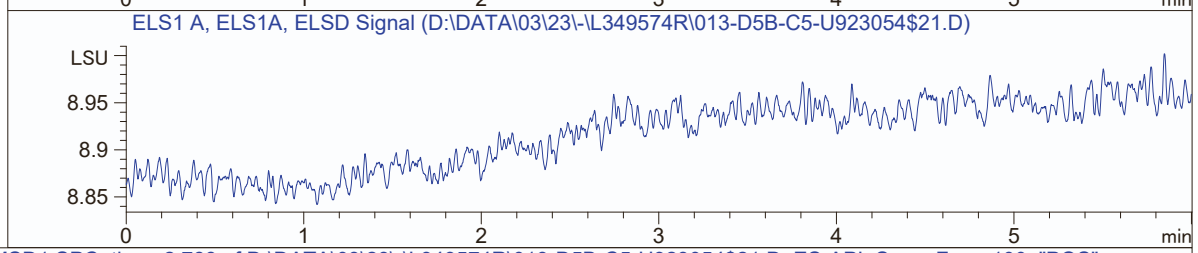

RT 2.787

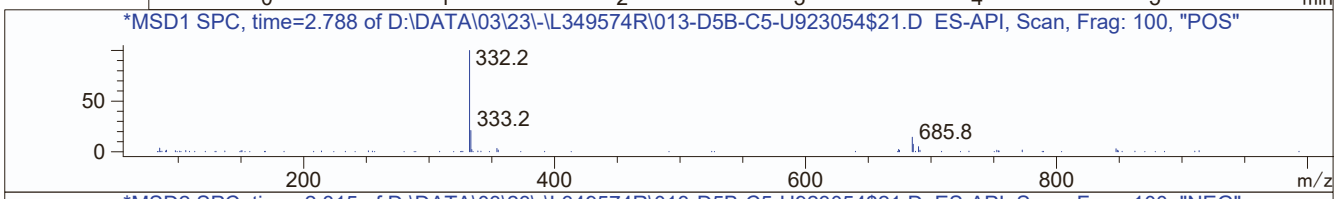

RT 2.815

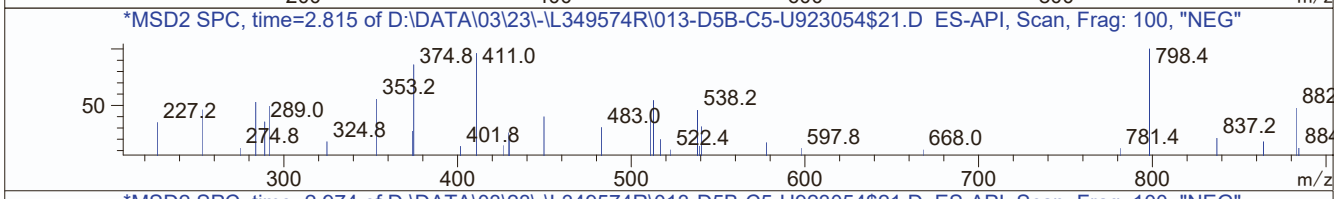

RT 2.974

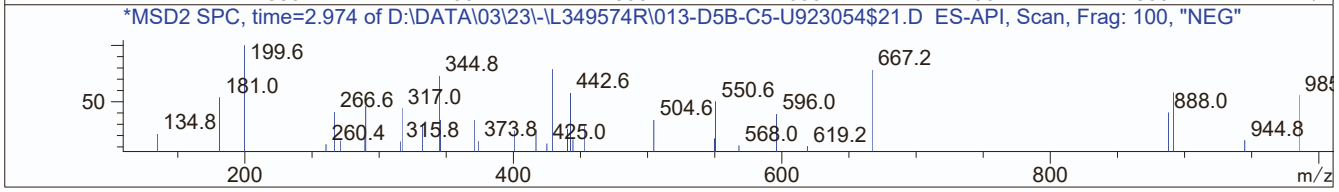

MaxPeak: 100.00%
Ret_Time: 3.000 min

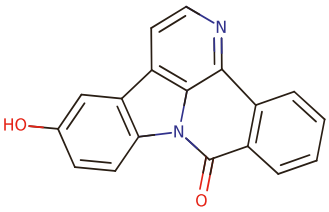

Mol Wt 286.28
Exact Mass 286.08

#	Time	Area%
1	3.000	100.00

MW01-E13
Z3243812160

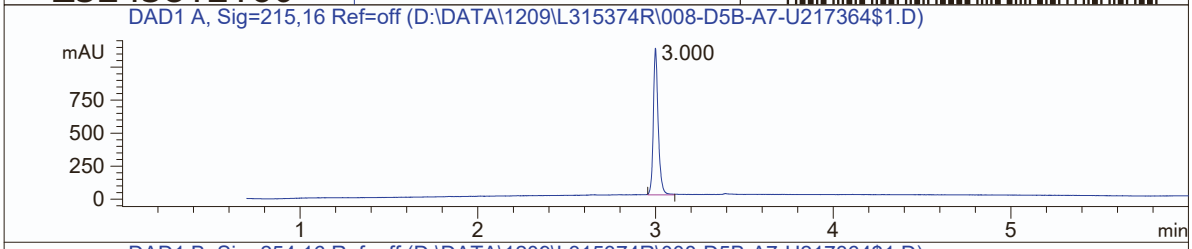

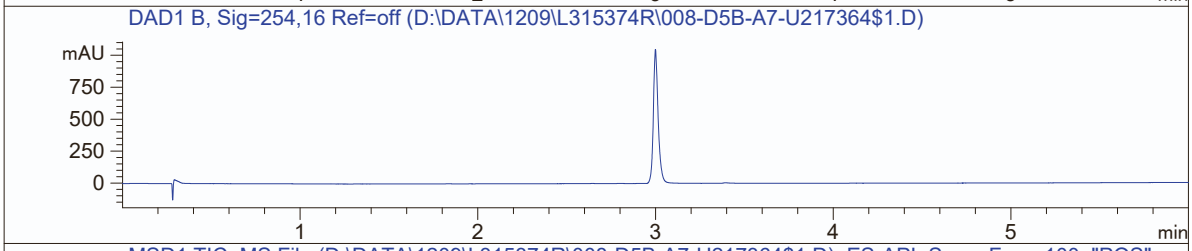

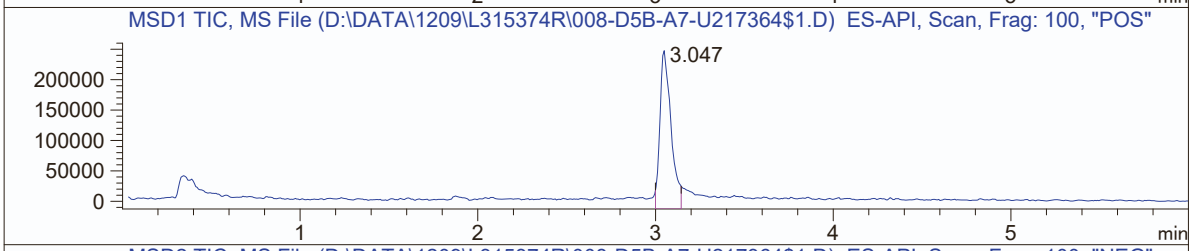

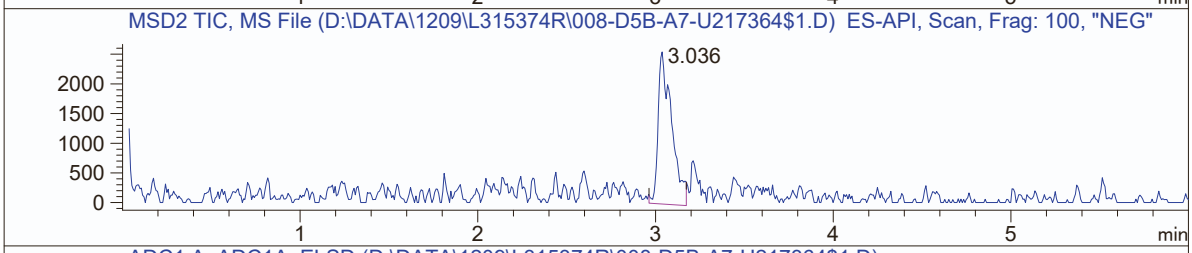

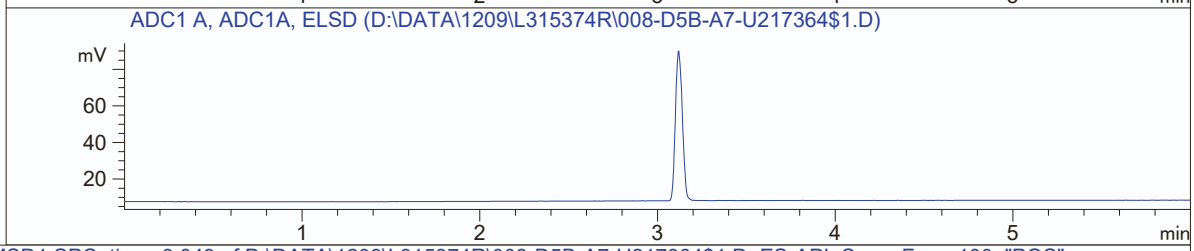

RT 3.047

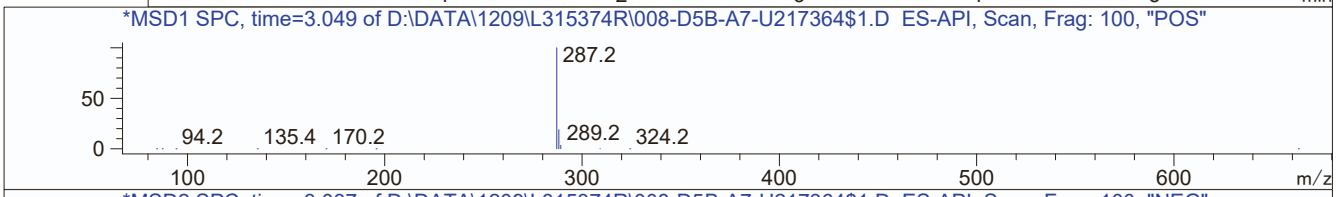

RT 3.036

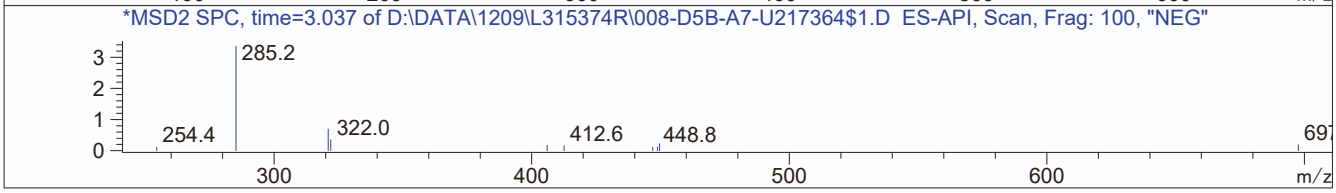

MaxPeak: 100.00%
Ret_Time: 3.454 min

MW01-E14
Z4613898542

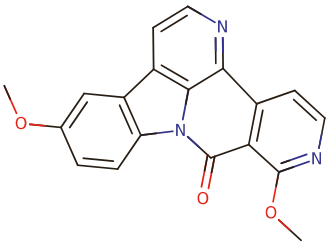

Mol Wt 331.32
Exact Mass 331.1

#	Time	Area%
1	3.454	100.00

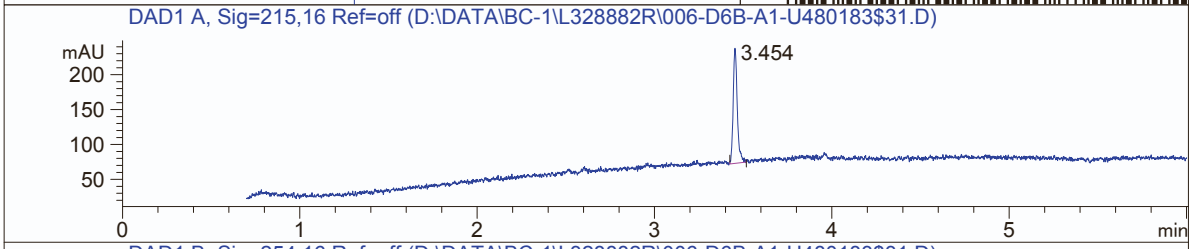

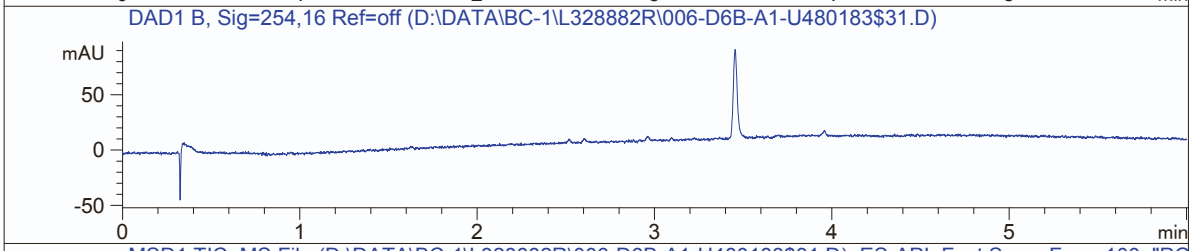

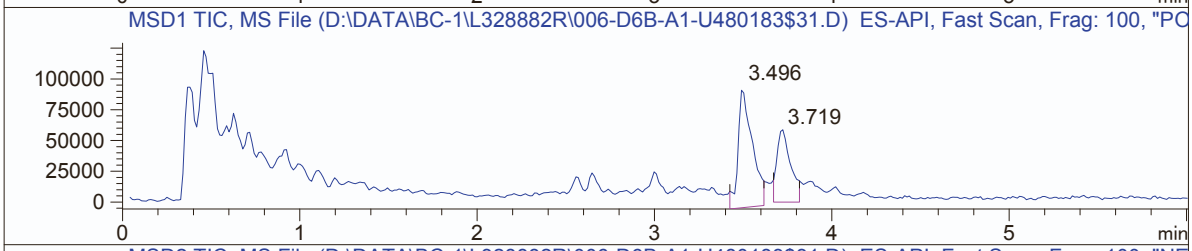

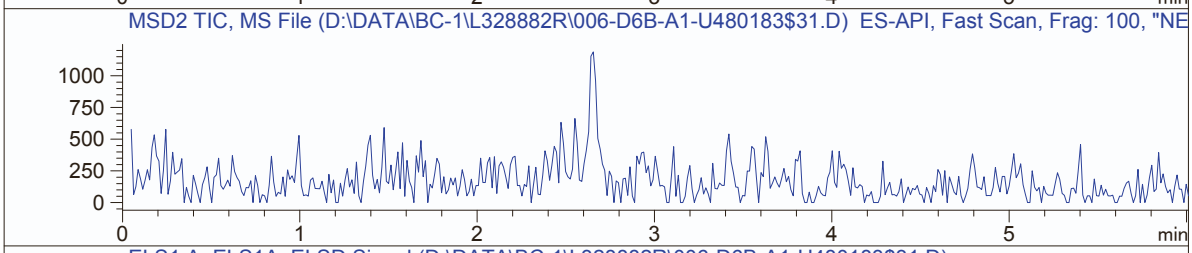

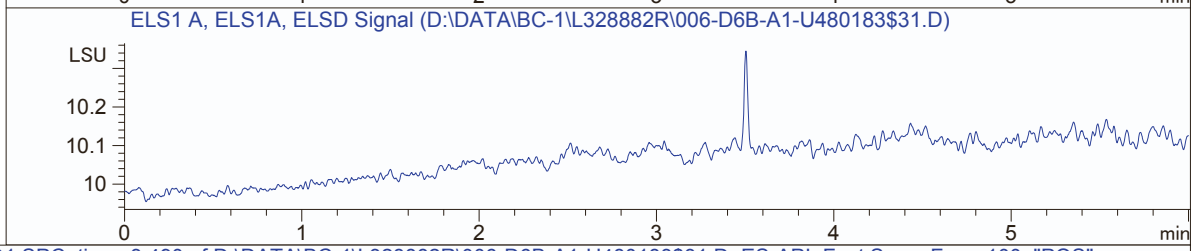

RT 3.496

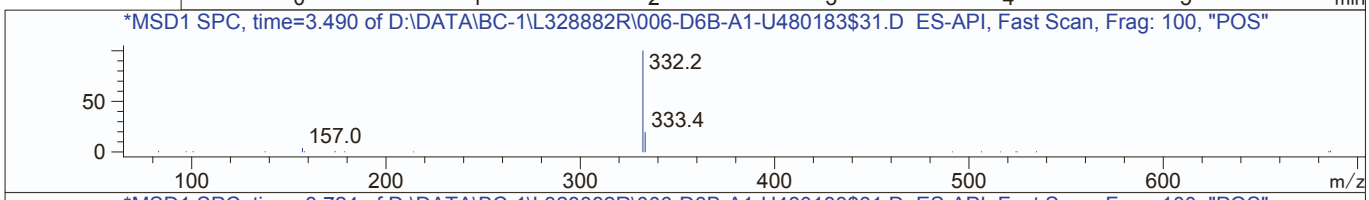

RT 3.719

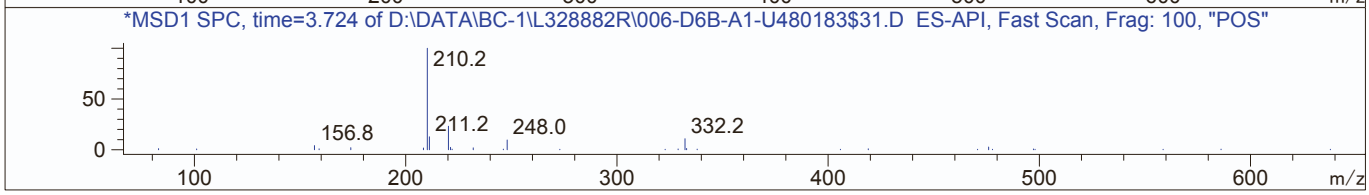

Inj.Date 1/25/2021 M Acq. Method C:\Users\ -> ->

MaxPeak: 100.00%
Ret_Time: 3.026 min

MW01-E15
Z4615451237

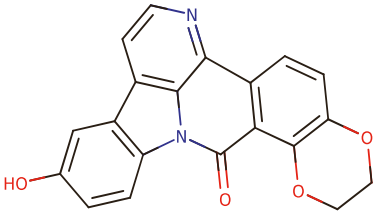

Mol Wt 344.32
Exact Mass 344.08

#	Time	Area%
1	3.026	100.00

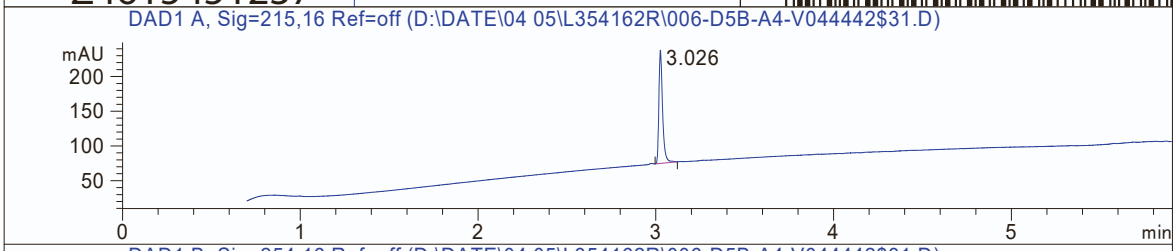

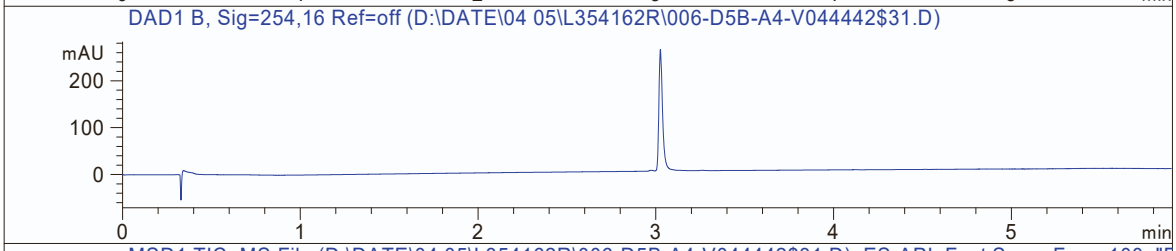

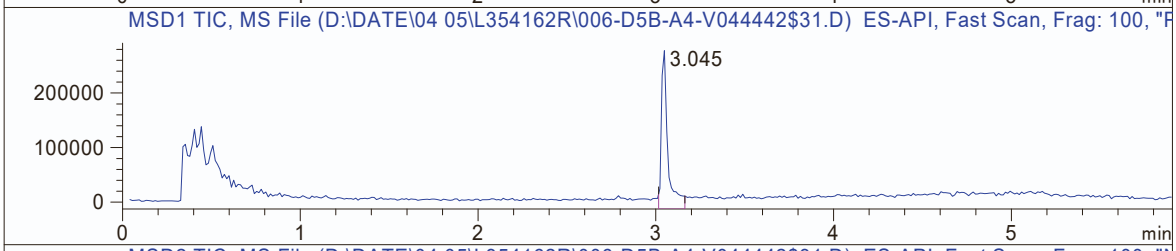

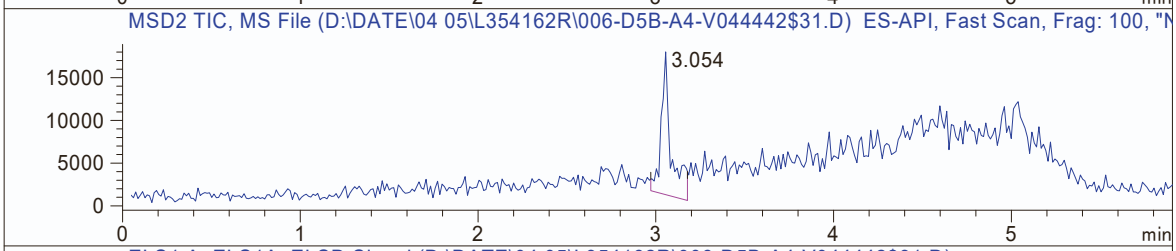

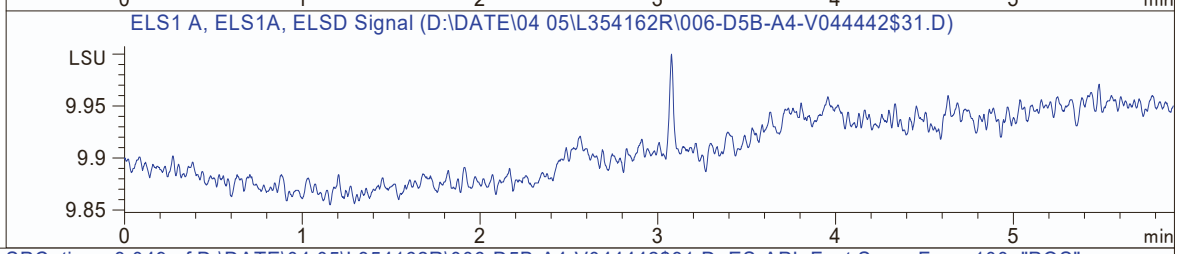

RT 3.045

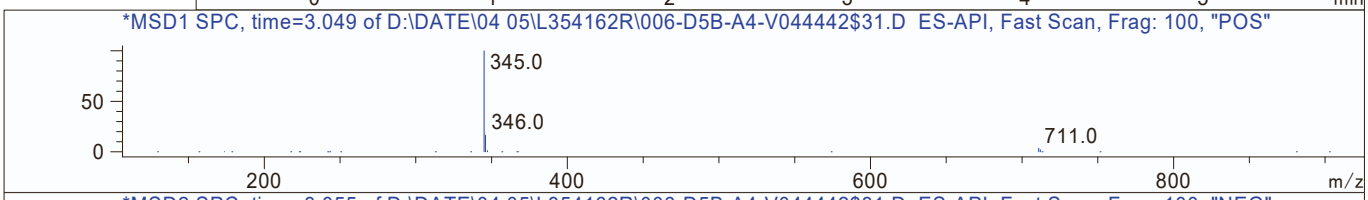

RT 3.054

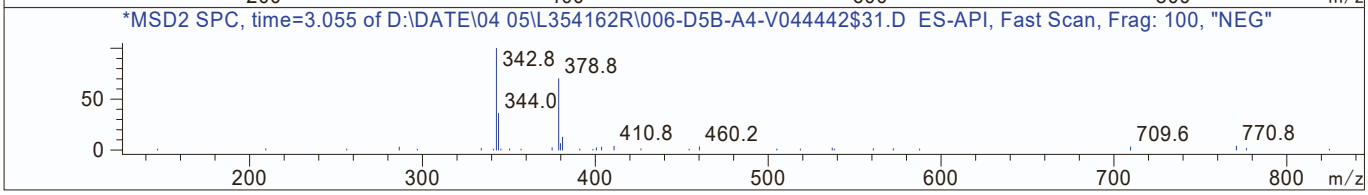

Inj.Date 4/5/2021 E Acq. Method C:\Users\ -> ->

MaxPeak: 97.37%
Ret_Time: 2.809 min

MW01-E16
Z4613449794

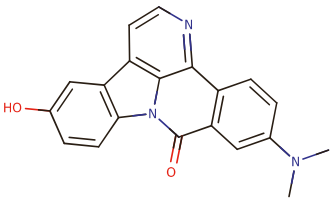

Mol Wt 329.35
Exact Mass 329.13

#	Time	Area%
1	2.509	1.66
2	2.809	97.37
3	3.194	0.97

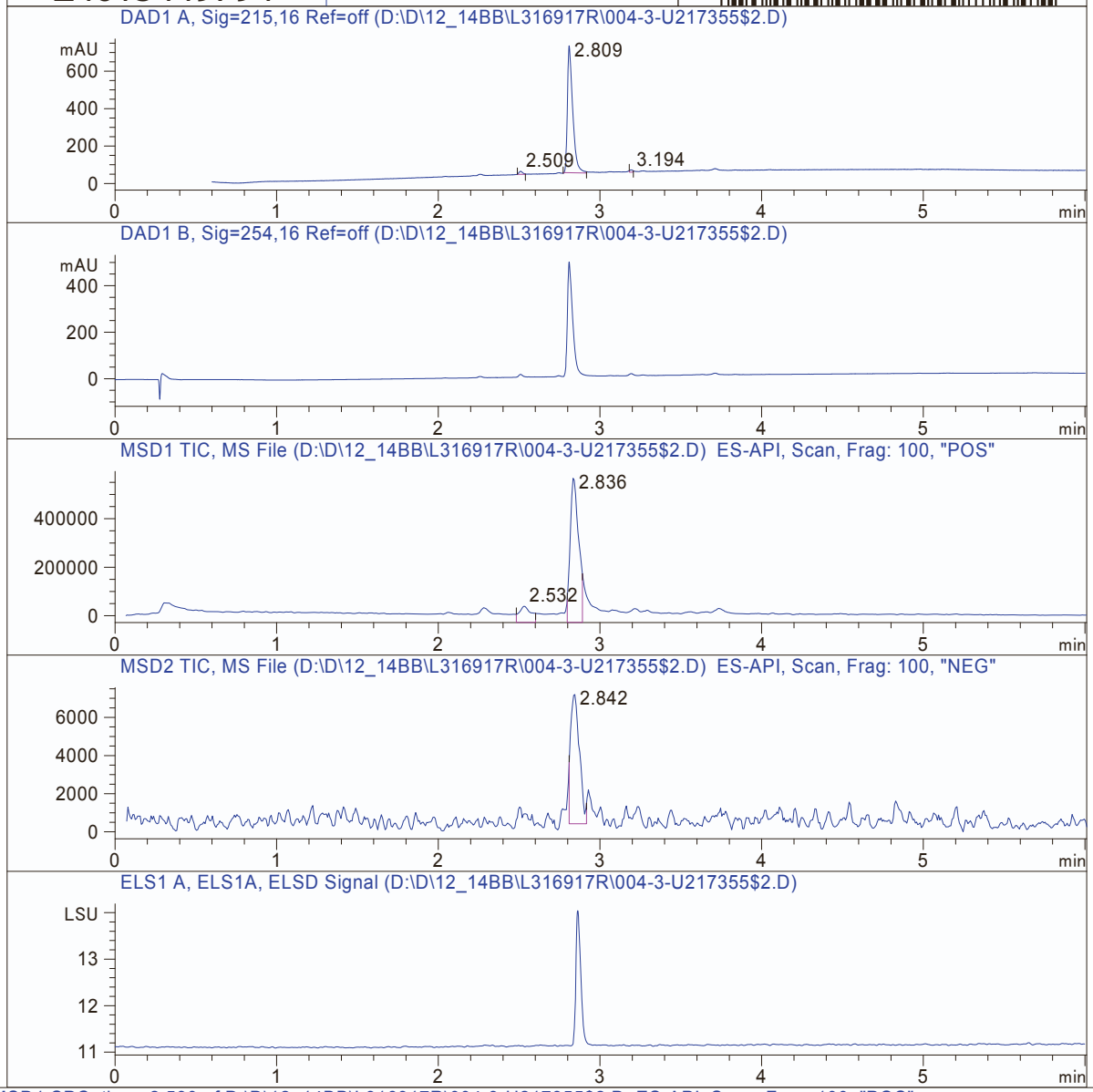

RT 2.532

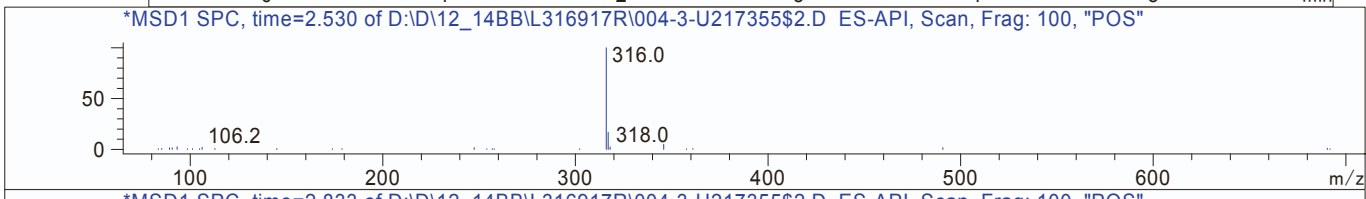

RT 2.836

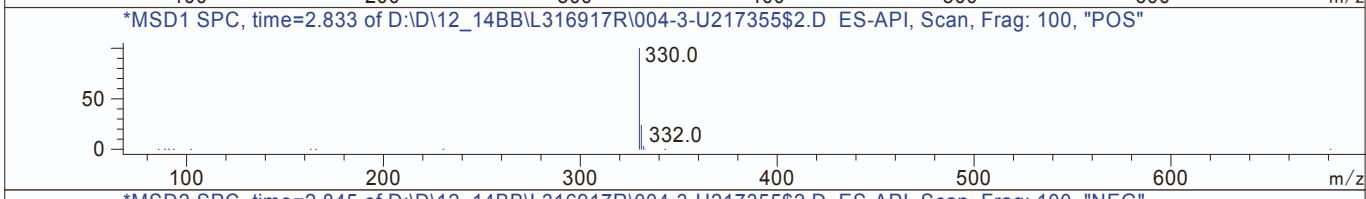

RT 2.842

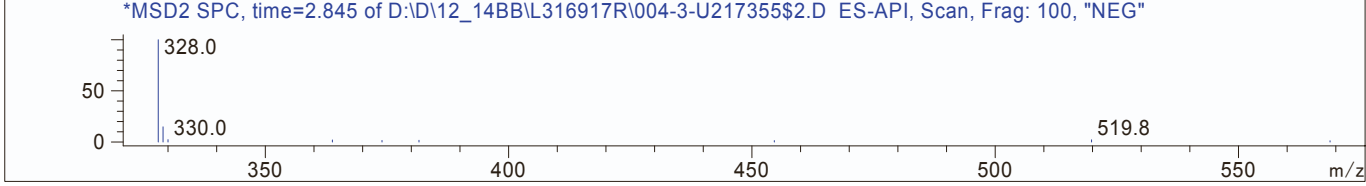

Inj.Date 12/14/2020 N 13 Acq. Method C:\Chem32\-> ->

MW01-E17
EN300-27707803

MaxPeak: 98.76%
Ret_Time: 3.413 min

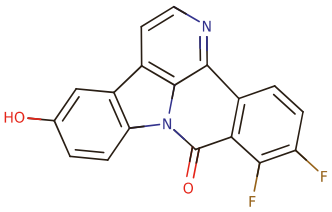

Mol Wt 322.26
Exact Mass 322.06

#	Time	Area%
1	2.585	1.24
2	3.413	98.76

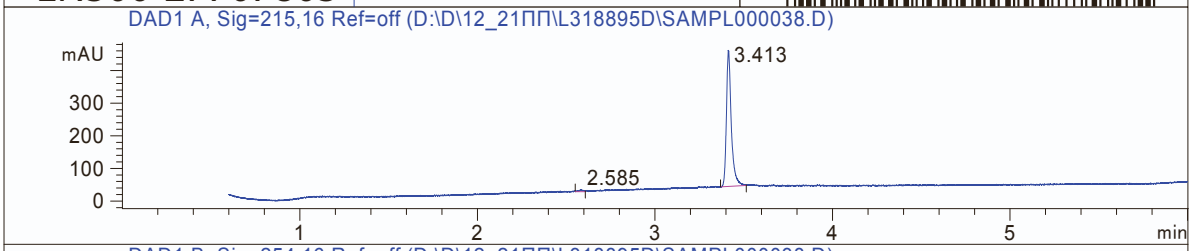

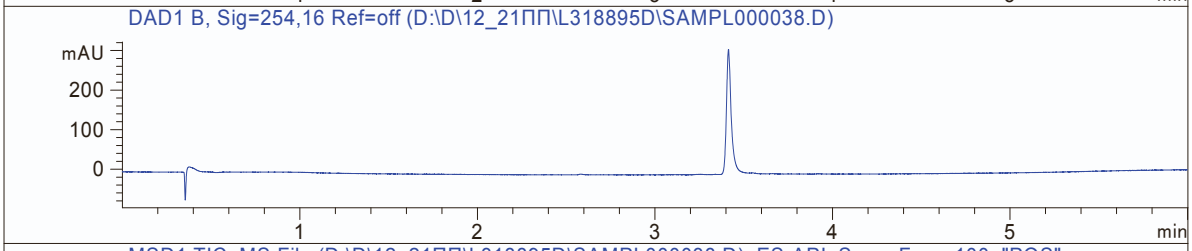

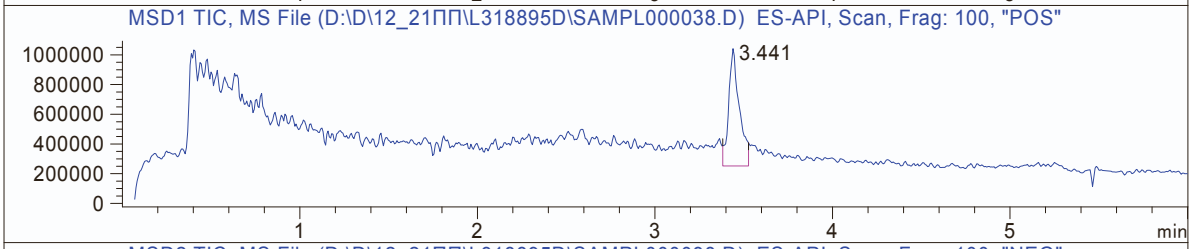

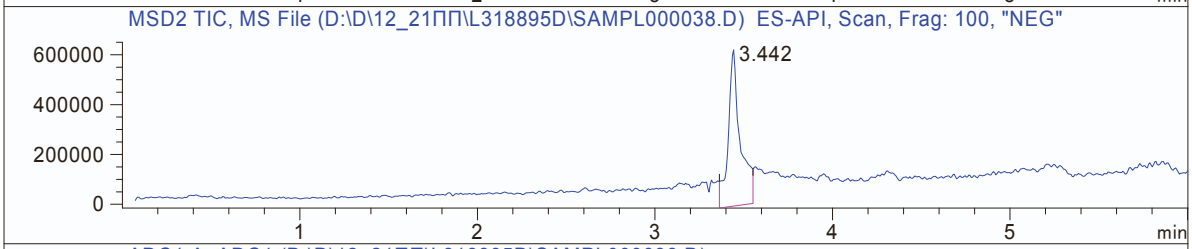

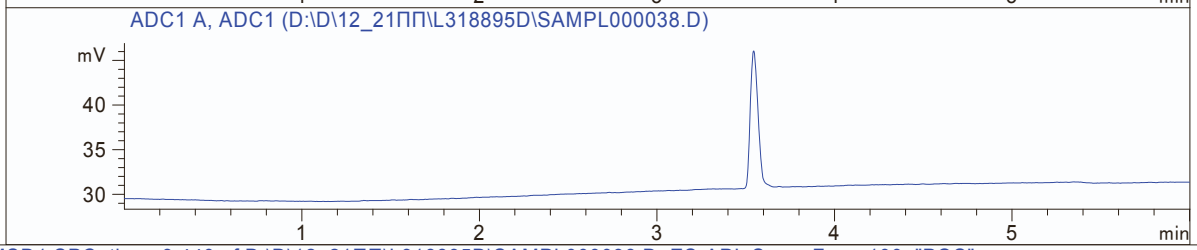

RT 3.441

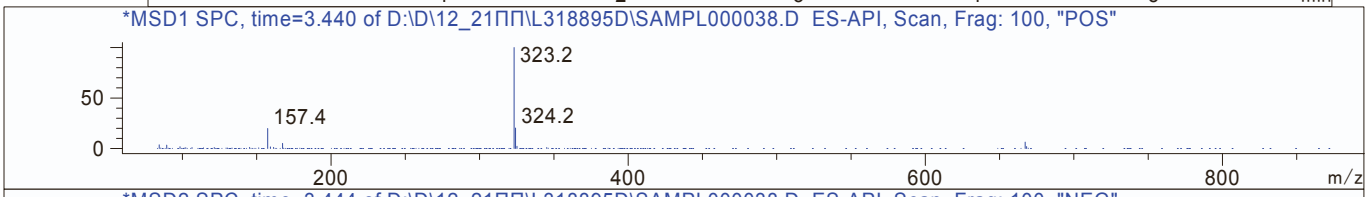

RT 3.442

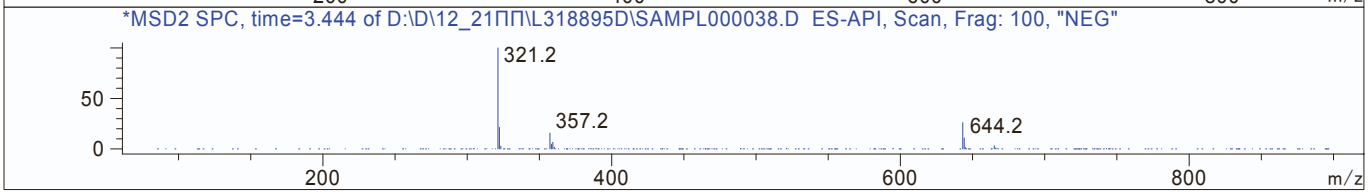

MW01-E18
EN300-27707927

MaxPeak: 87.58%
Ret_Time: 2.385 min

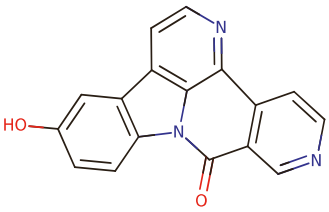

Mol Wt 287.27
Exact Mass 287.07

#	Time	Area%
1	2.385	87.58
2	2.450	8.01
3	2.707	4.41

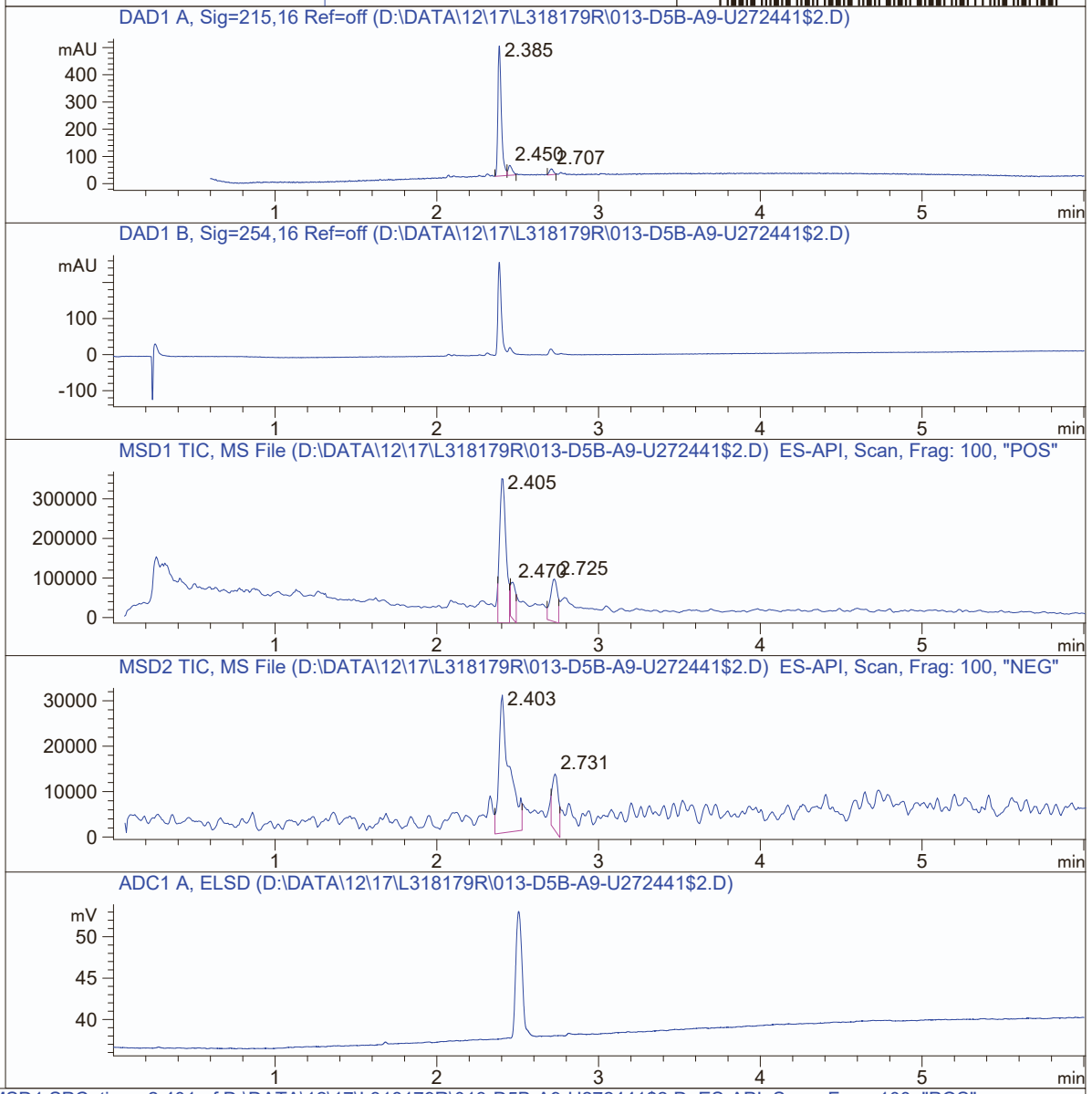

RT 2.405

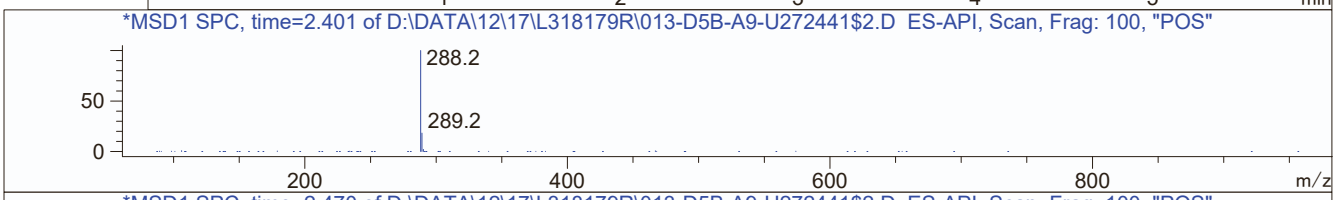

RT 2.470

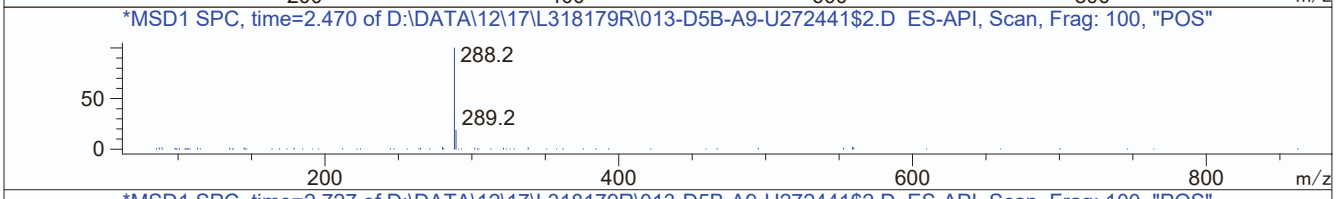

RT 2.725

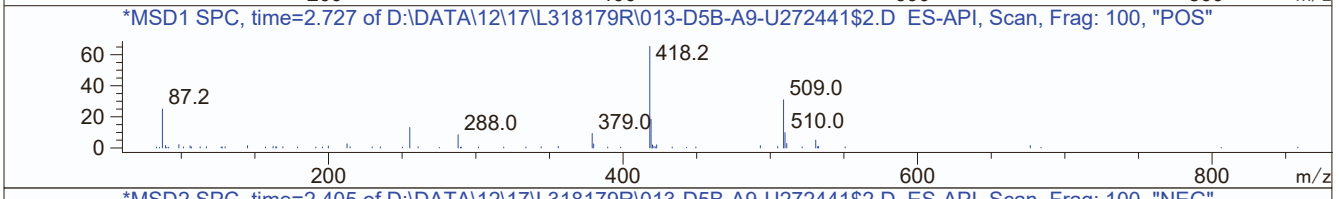

RT 2.403

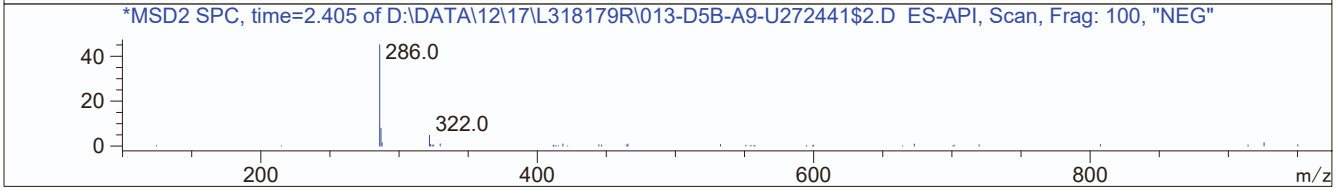

MaxPeak: 100.00%
Ret_Time: 2.662 min

MW01-E19
EN300-27716224

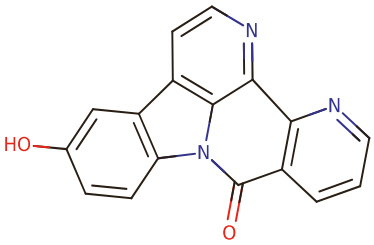

Mol Wt 287.27
Exact Mass 287.07

#	Time	Area%
1	2.662	100.00

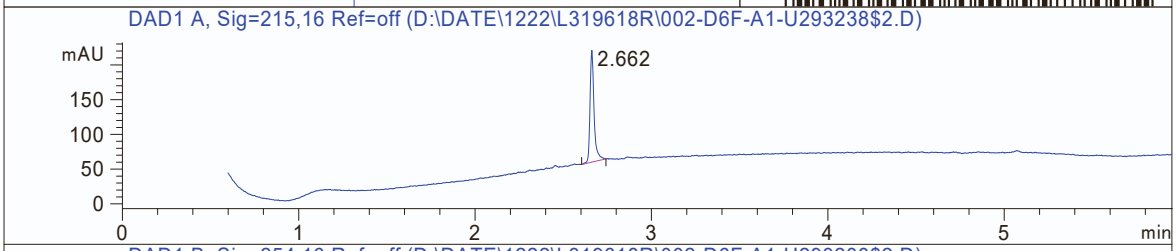

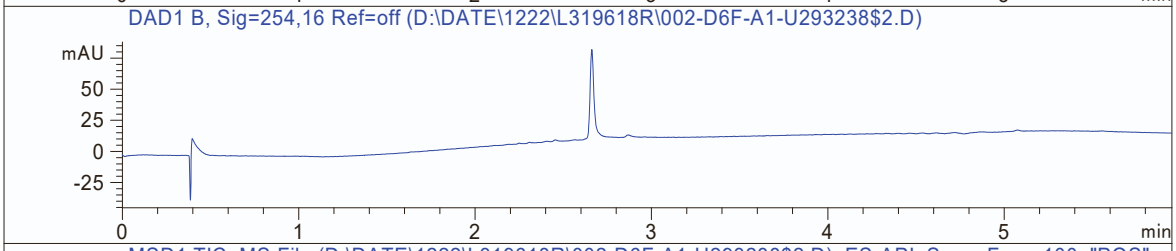

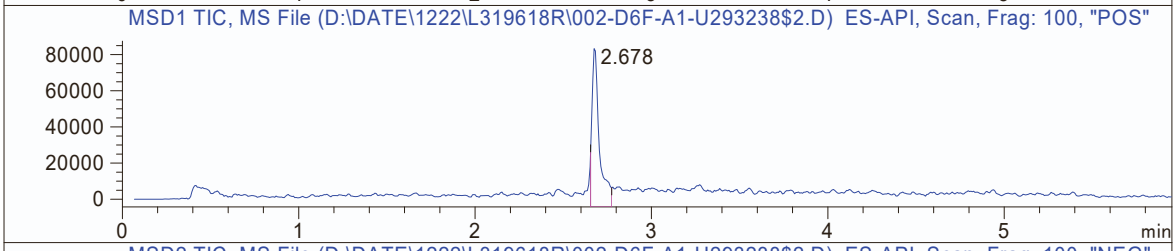

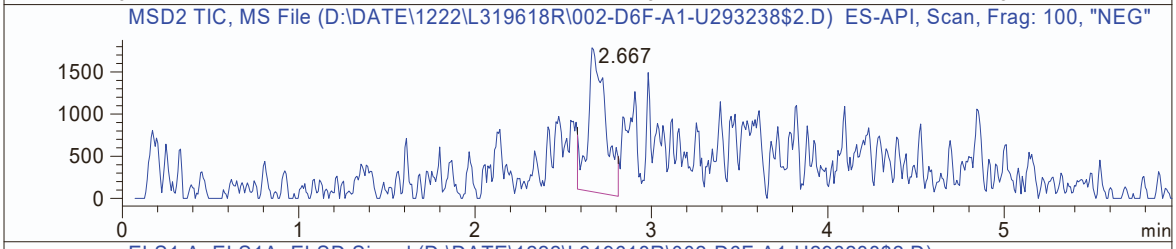

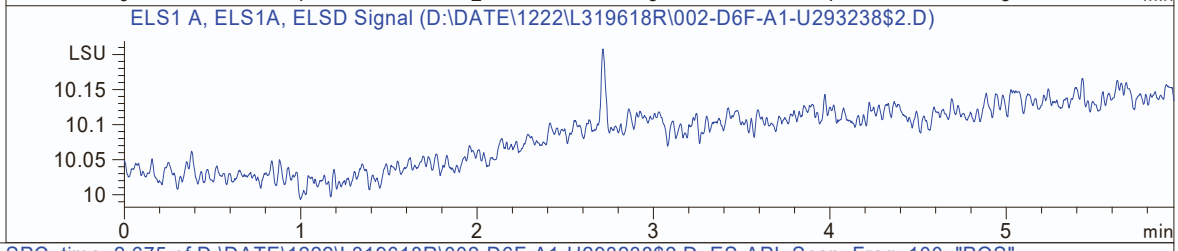

RT 2.678

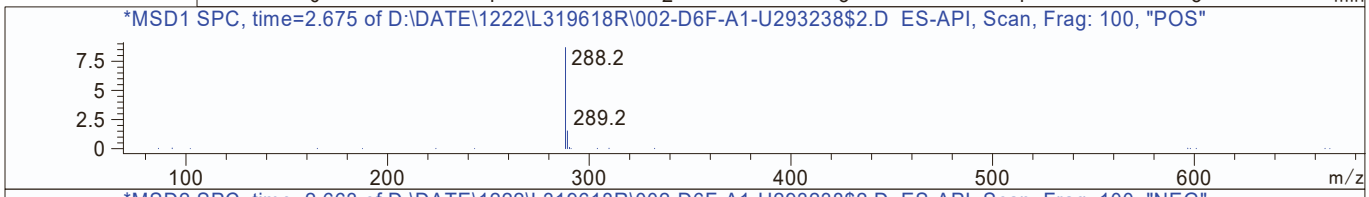

RT 2.667

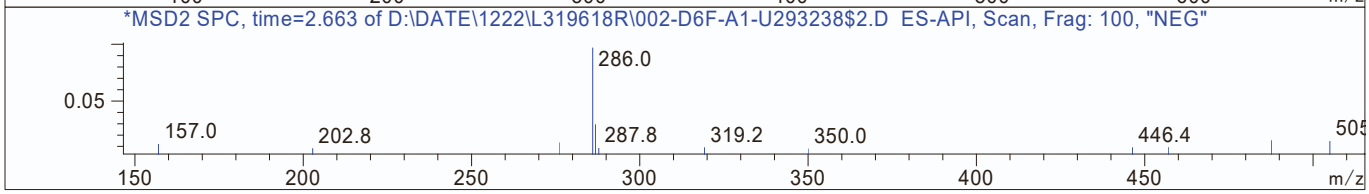

MaxPeak: 100.00%
Ret_Time: 2.562 min

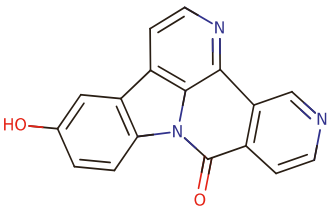

Mol Wt 287.27
Exact Mass 287.07

#	Time	Area%
1	2.562	100.00

MW01-E20
Z4905255295

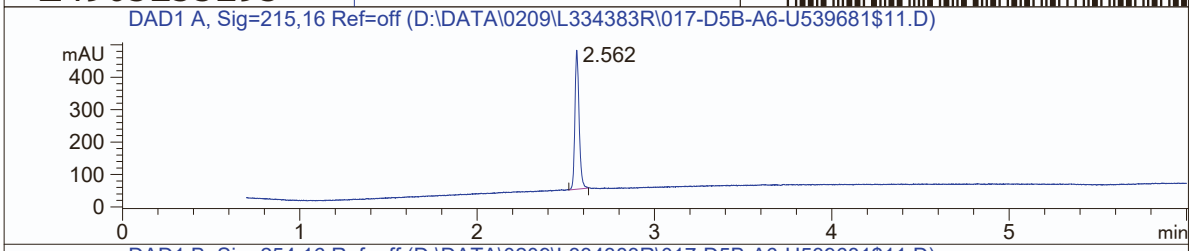

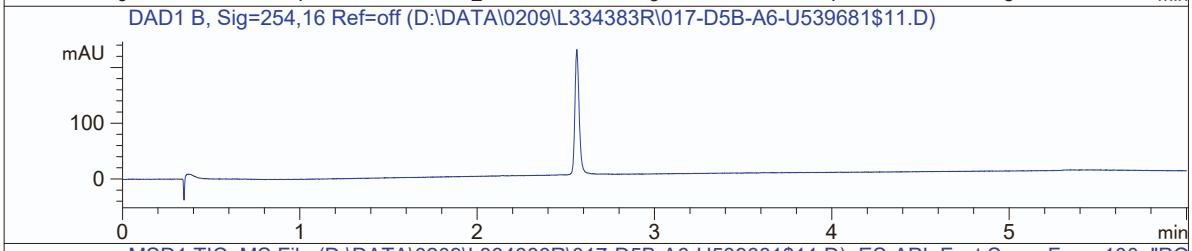

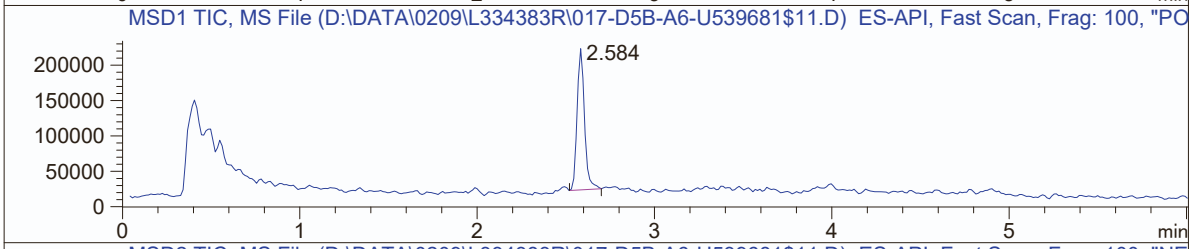

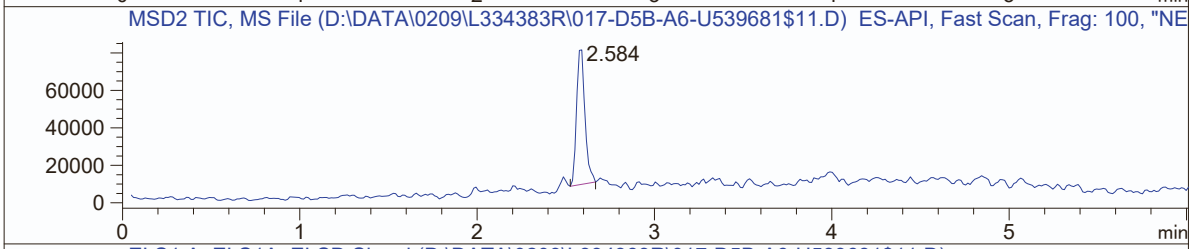

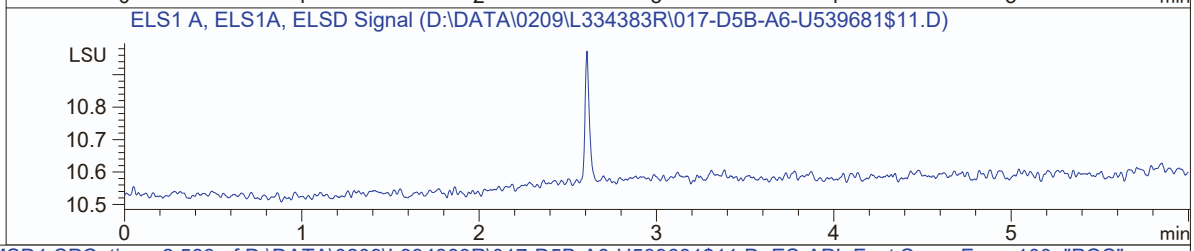

RT 2.584

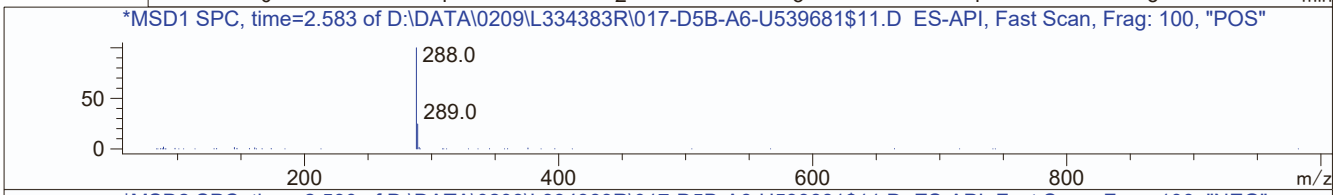

RT 2.584

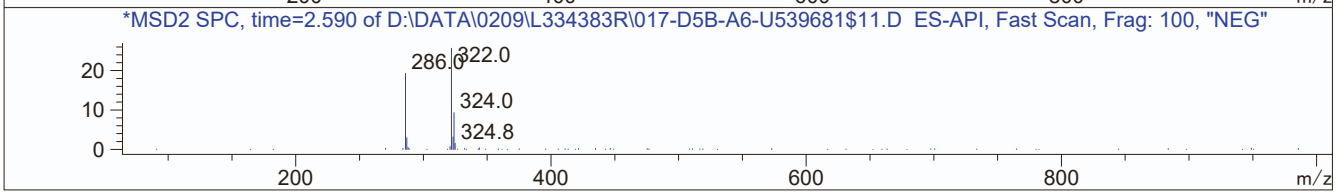

Inj.Date 2/9/2021 OA Acq. Method C:\Users\ -> ->

MaxPeak: 100.00%
Ret_Time: 3.562 min

MW01-E21
Z4905255587

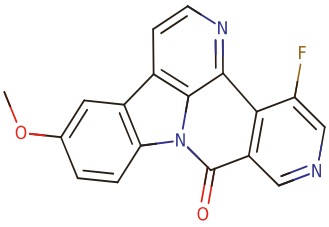

Mol Wt **319.29**
Exact Mass **319.08**

#	Time	Area%
1	3.562	100.00

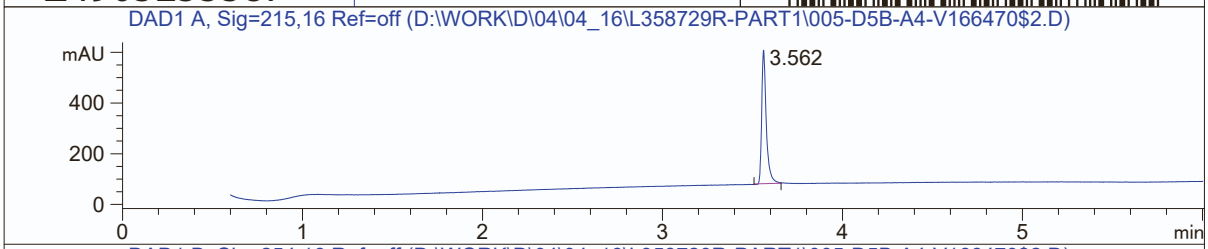

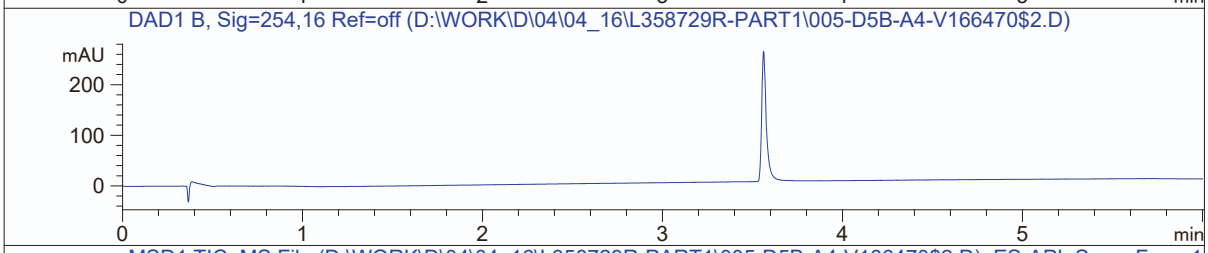

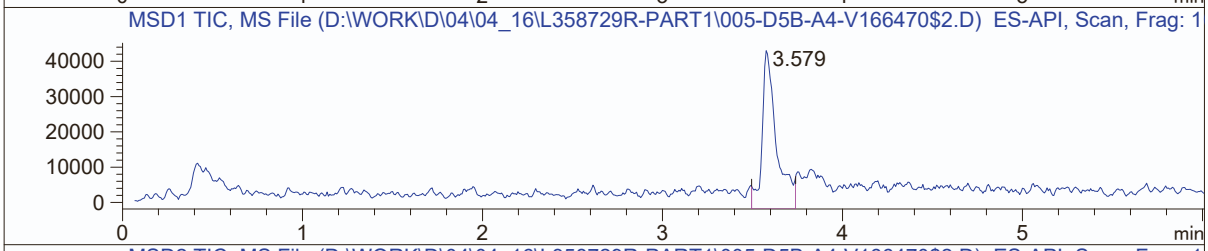

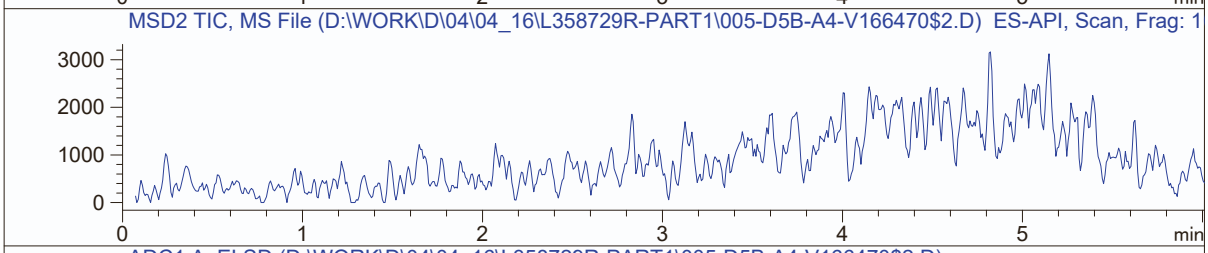

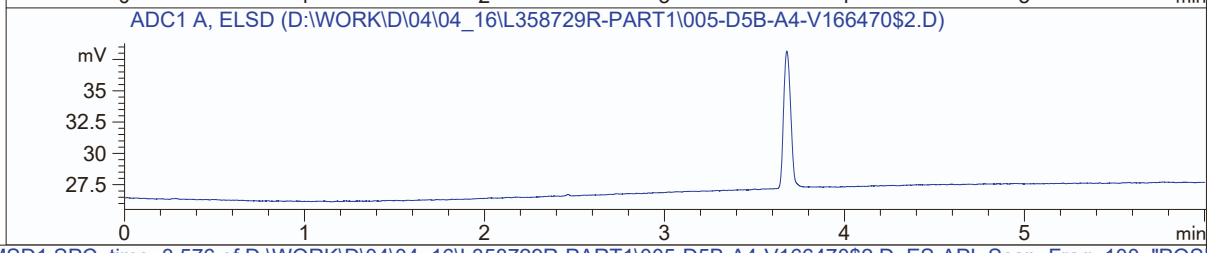

RT 3.579

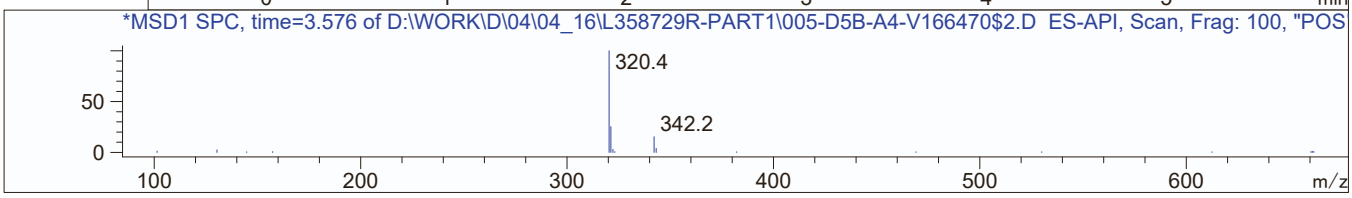

MaxPeak: 91.02%
Ret_Time: 1.112 min

MW05
Z2027896743

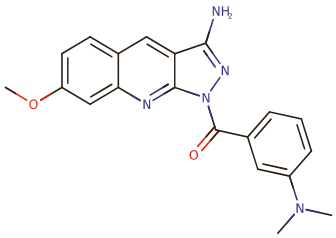

Mol Wt 361.4
Exact Mass 361.17

#	Time	Area%
1	0.662	3.70
2	1.013	5.29
3	1.112	91.02

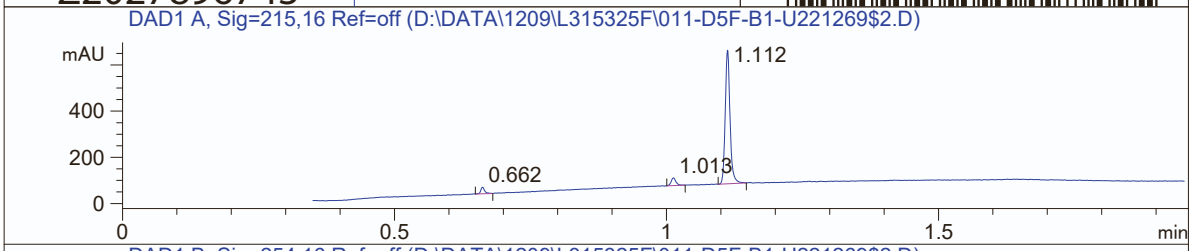

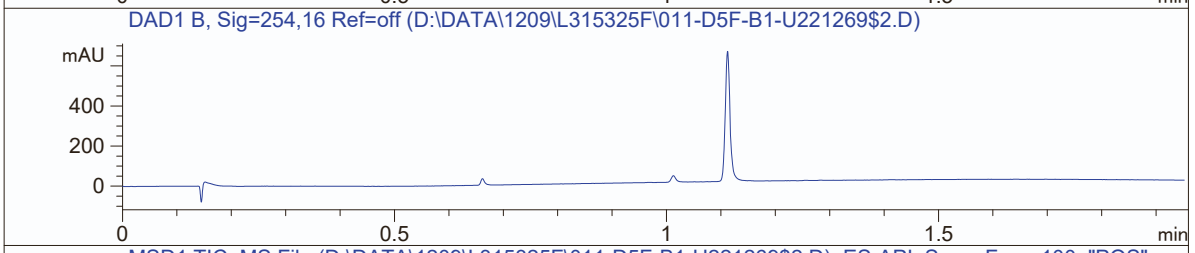

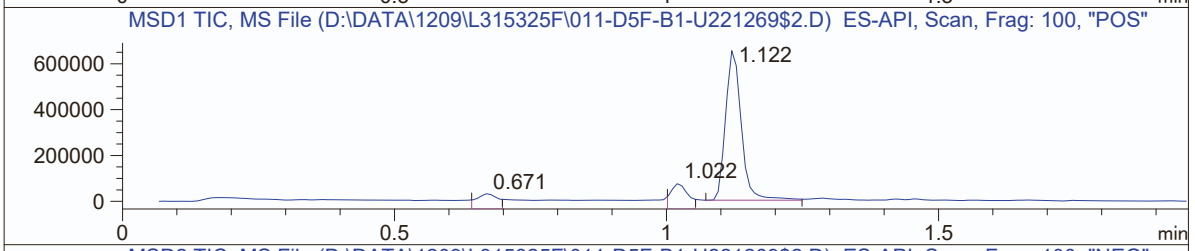

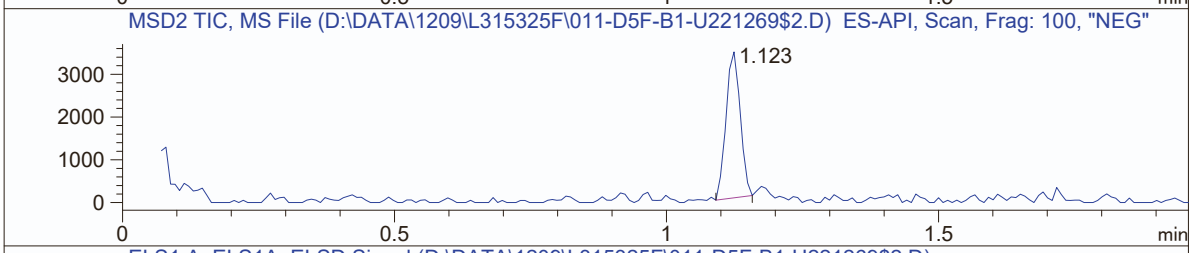

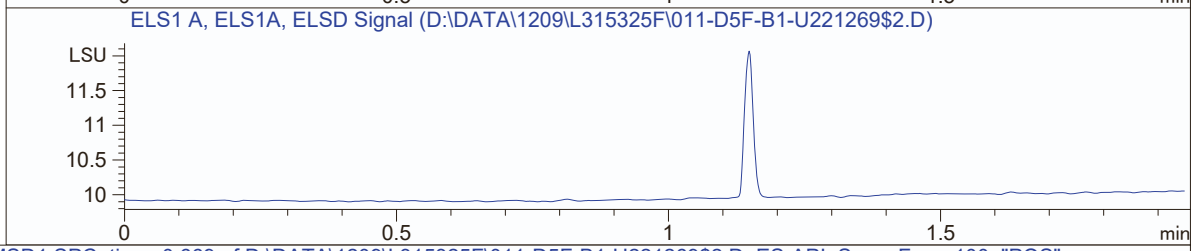

RT 0.671

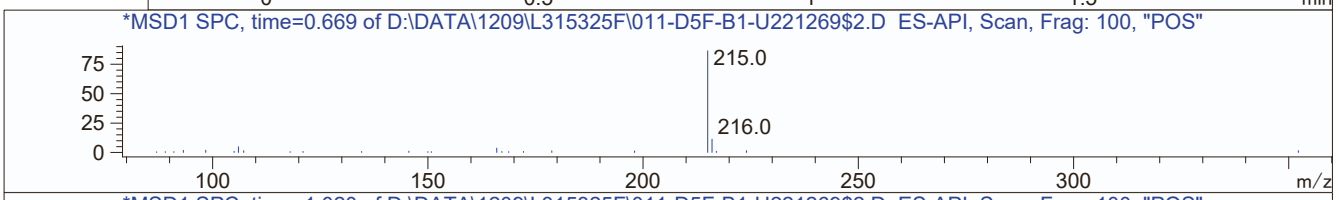

RT 1.022

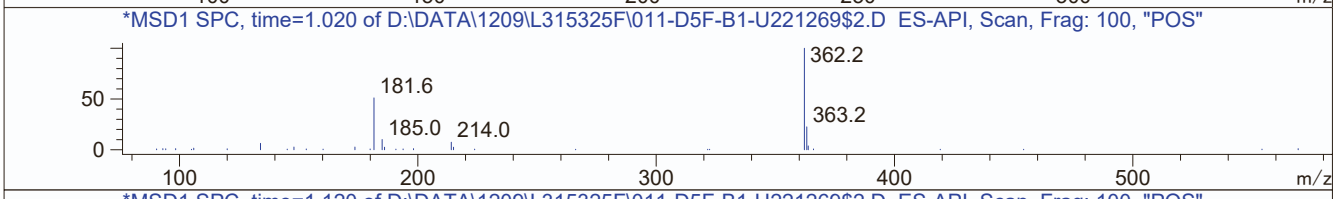

RT 1.122

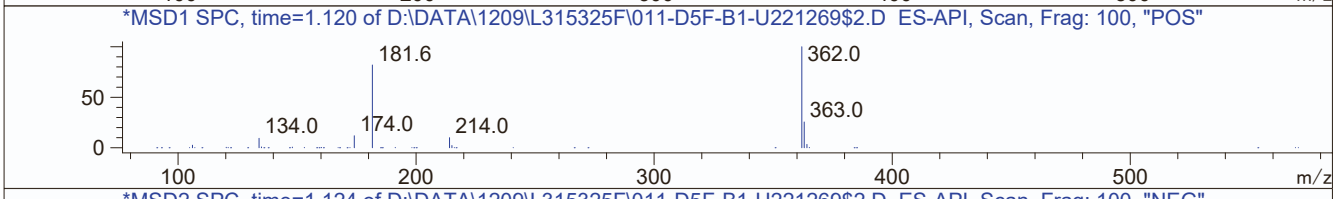

RT 1.123

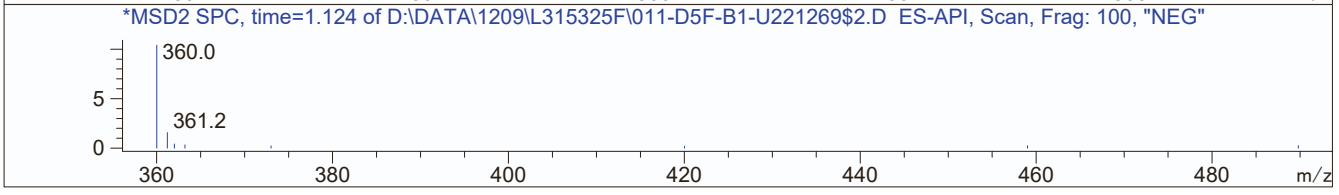

MaxPeak: 100.00%
Ret_Time: 0.973 min

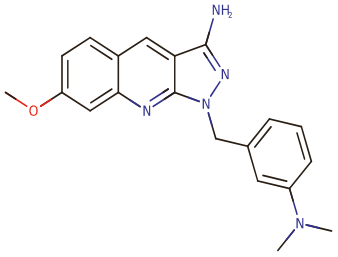

Mol Wt 347.41
Exact Mass 347.2

#	Time	Area%
1	0.973	100.00

MW05-E1
Z4619432587

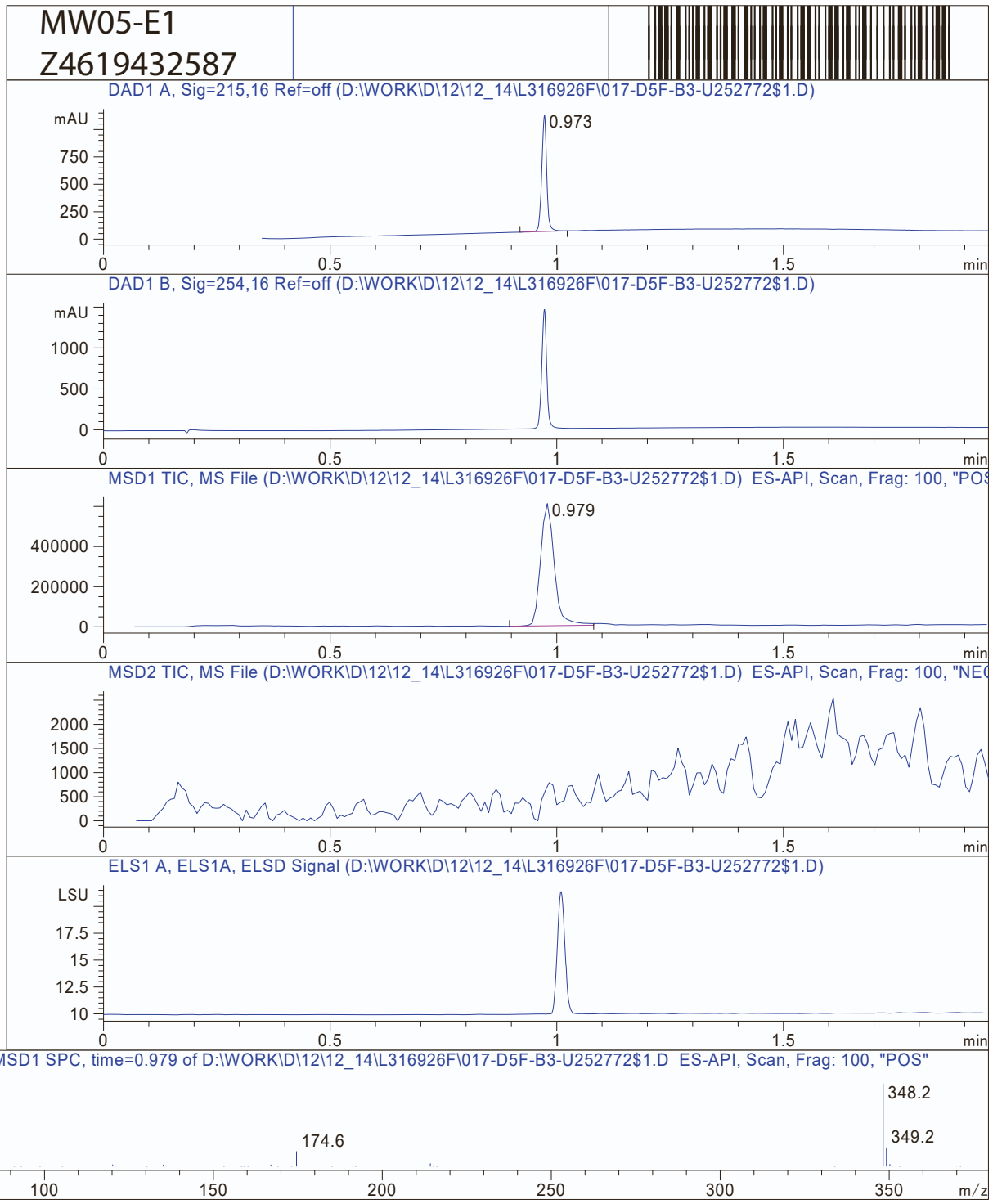

RT 0.979

MaxPeak: 100.00%
Ret_Time: 1.119 min

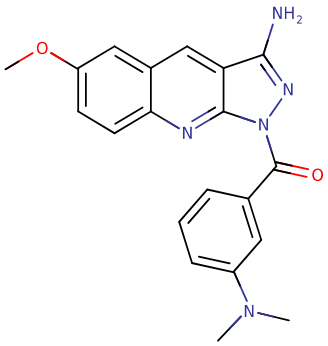

Mol Wt **361.4**
Exact Mass **361.17**

#	Time	Area%
1	1.119	100.00

MW05-E2
Z4619442527

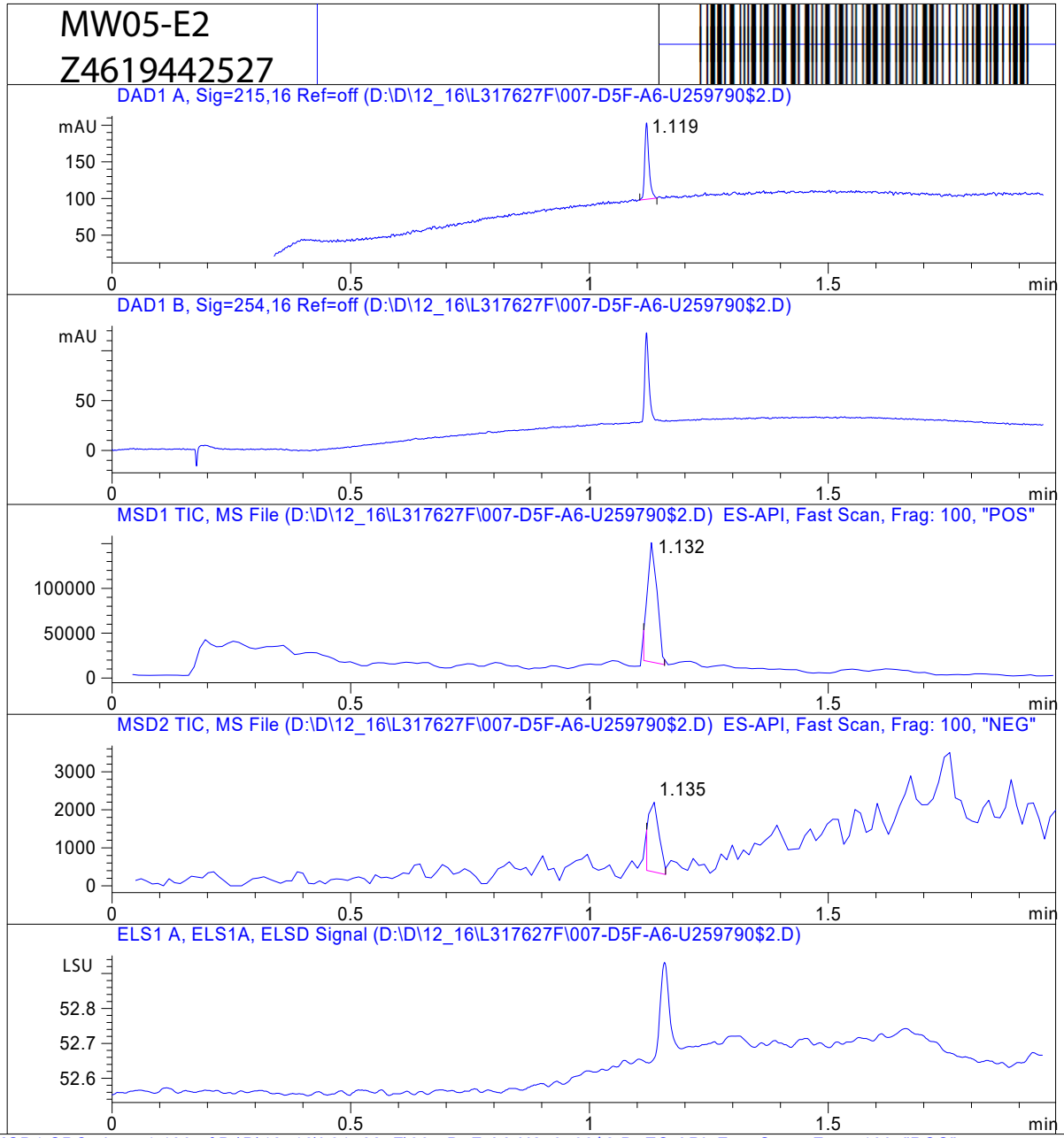

RT 1.132

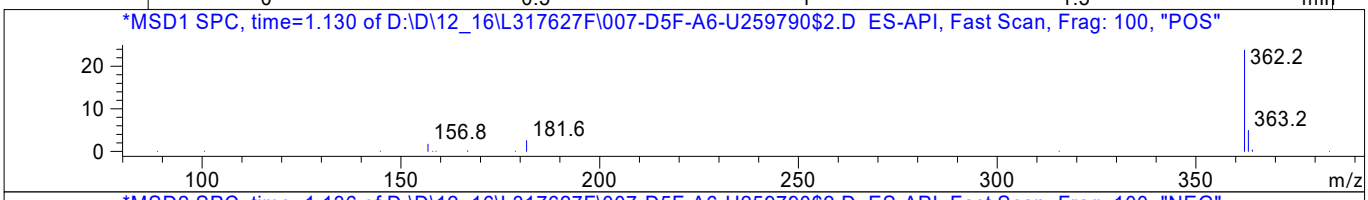

RT 1.135

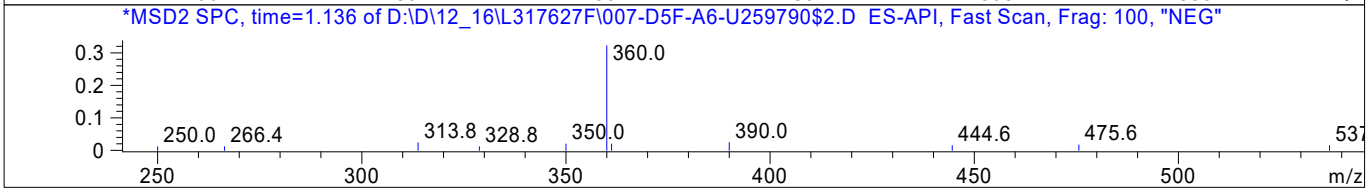

Inj.Date 12/16/2020 N Acq. Method C:\Users\ -> ->

MaxPeak: 96.59%
Ret_Time: 0.843 min

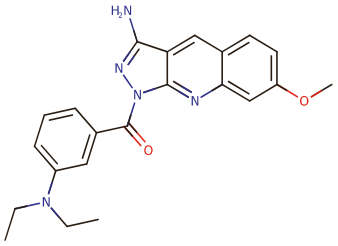

Mol Wt 389.45
Exact Mass 389.21

#	Time	Area%
1	0.585	3.41
2	0.843	96.59

MW05-E3
Z4619437296

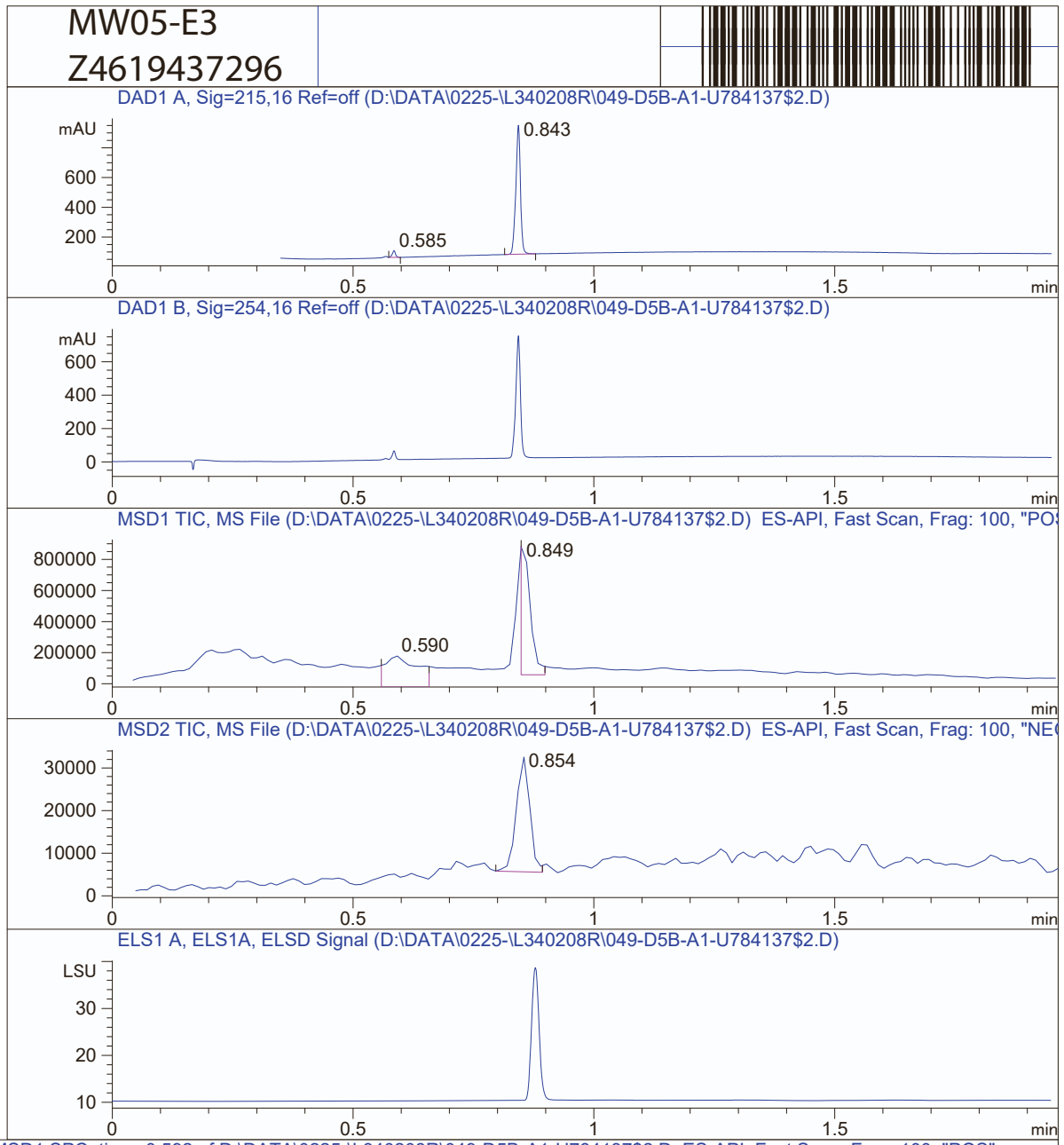

RT 0.590

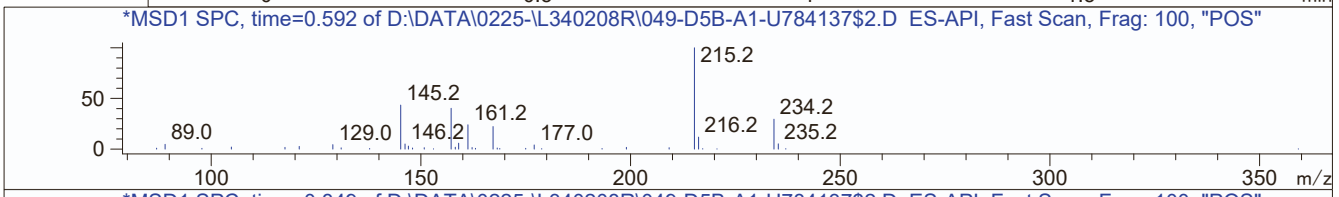

RT 0.849

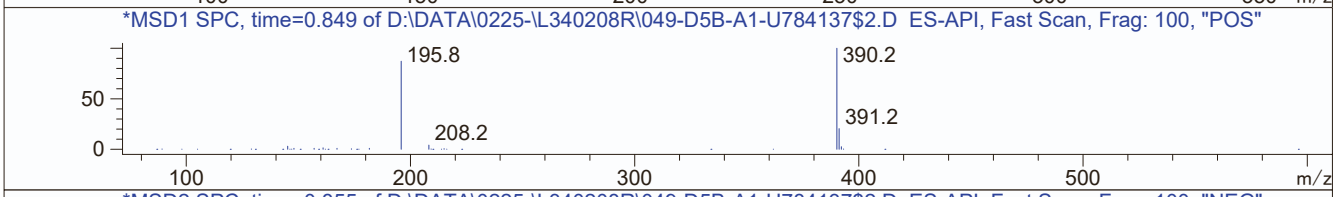

RT 0.854

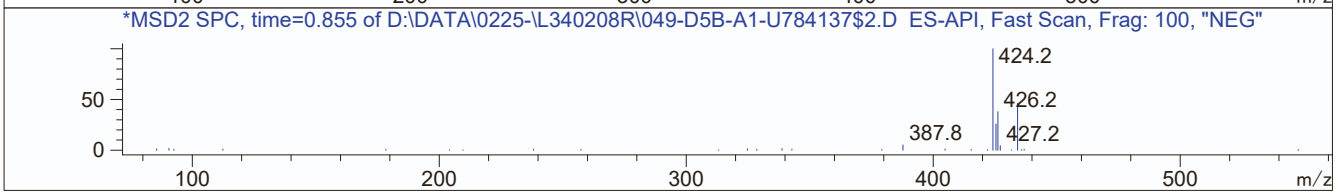

MaxPeak: 100.00%
Ret_Time: 1.311 min

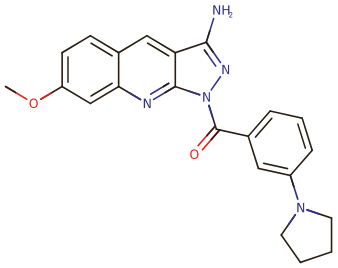

Mol Wt 387.43
Exact Mass 387.19

#	Time	Area%
1	1.311	100.00

MW05-E4
Z4619437299

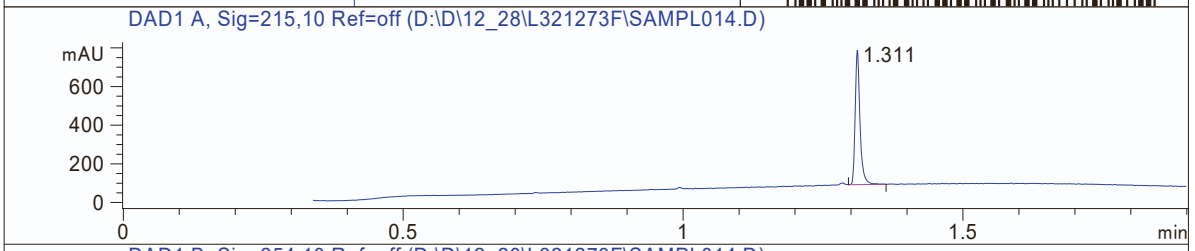

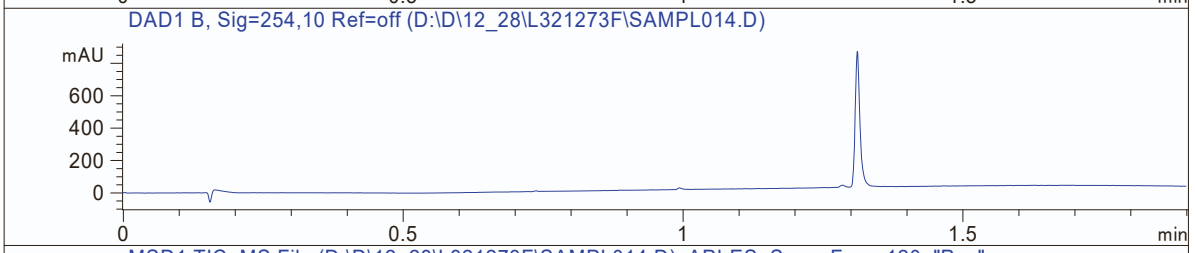

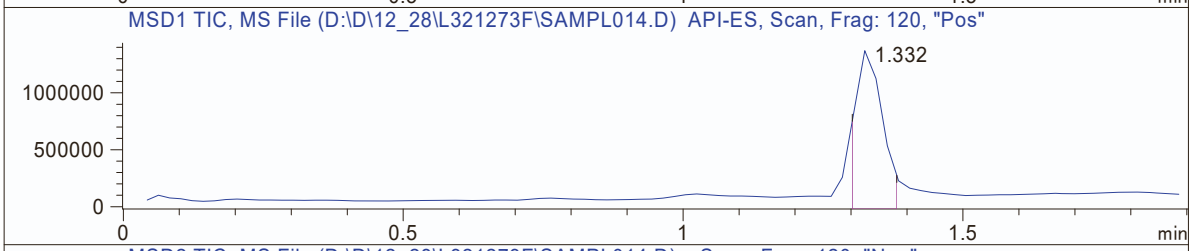

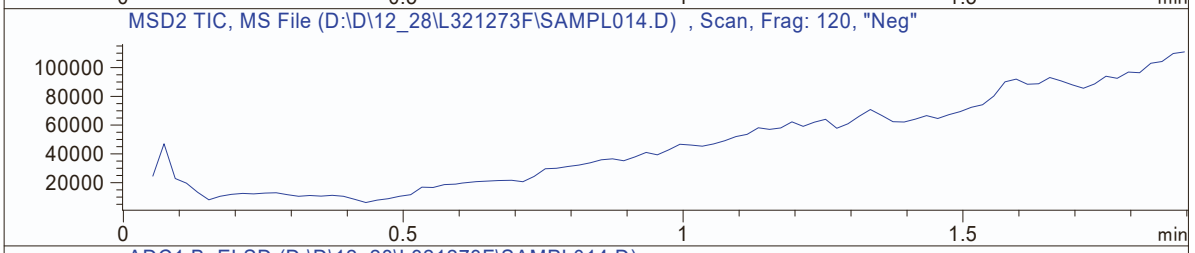

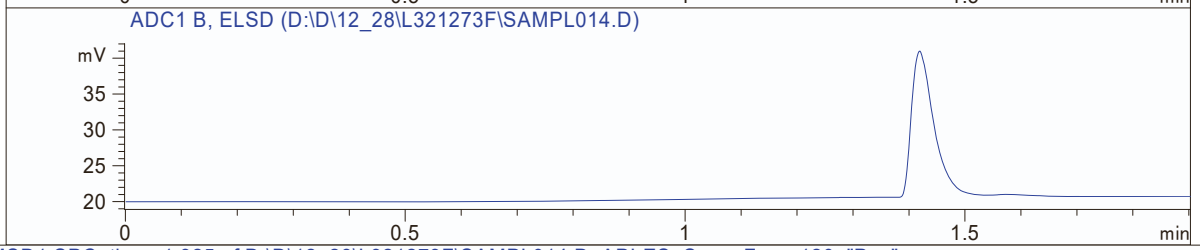

RT 1.332

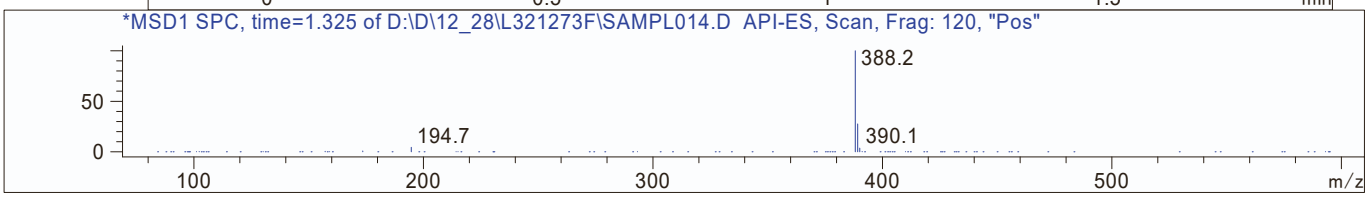

Inj.Date 12/28/2020 N -SL- Acq. Method C:\HPCHEM\-> ->

MaxPeak: 96.51%
Ret_Time: 0.939 min

MW05-E5
Z4619437298

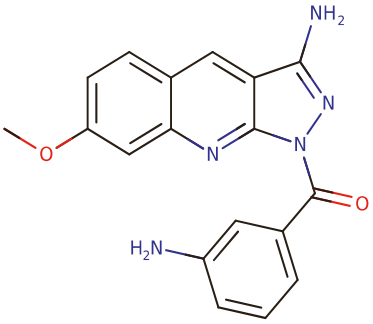

Mol Wt 333.34
Exact Mass 333.13

#	Time	Area%
1	0.939	96.51
2	0.972	3.49

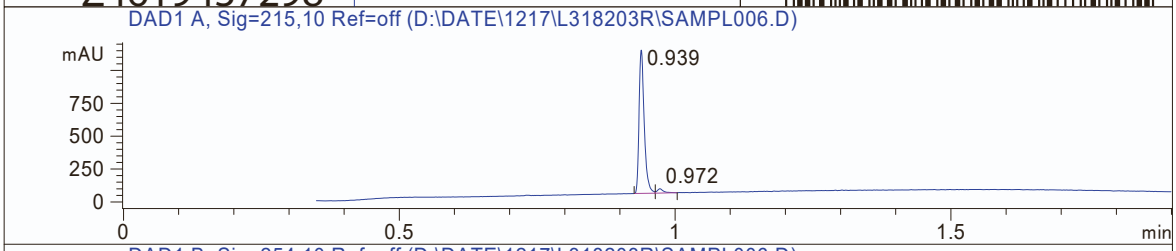

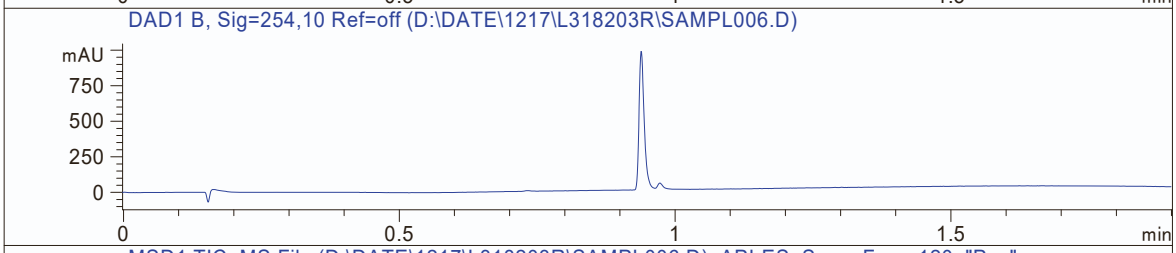

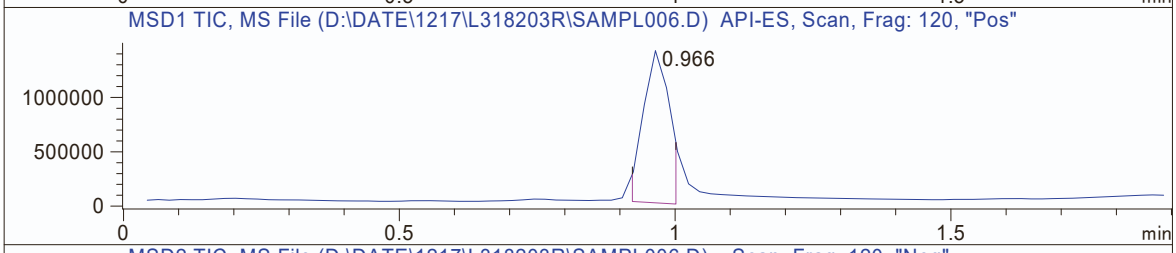

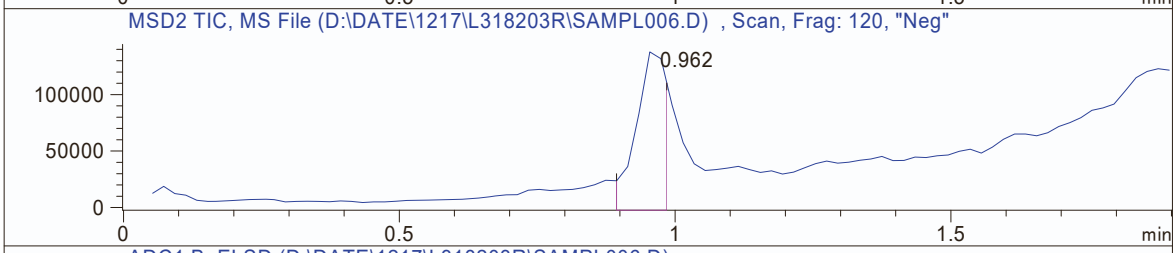

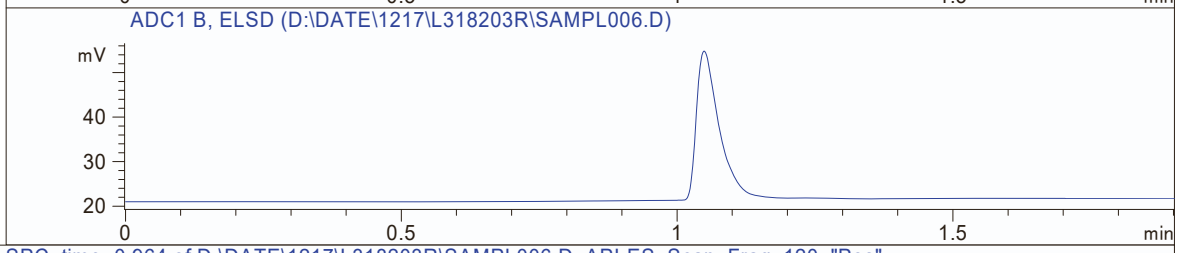

RT 0.966

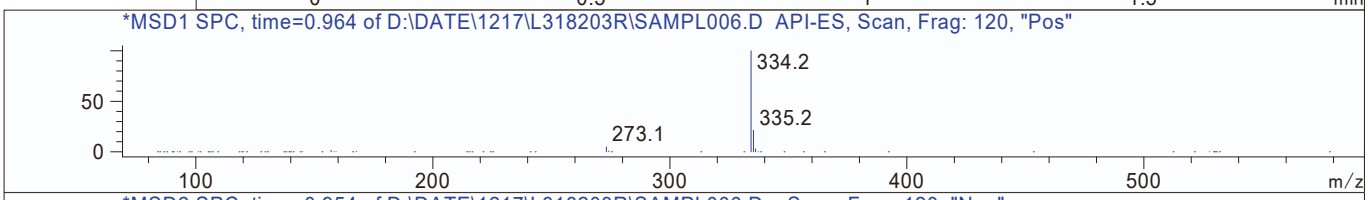

RT 0.962

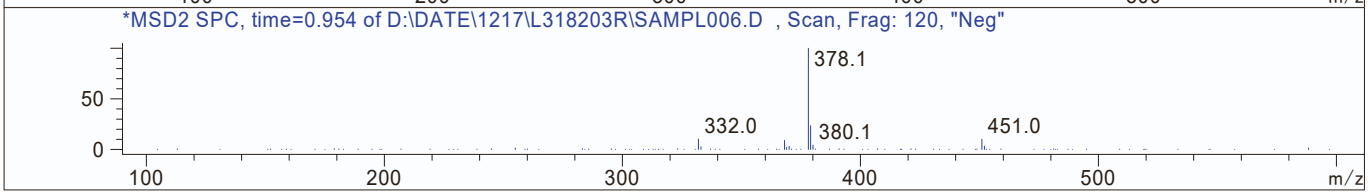

Inj.Date 12/18/2020 E -SL- Acq. Method C:\HPCHEM\-> ->

MaxPeak: 96.16%
Ret_Time: 0.991 min

MW05-E6
Z4619437297

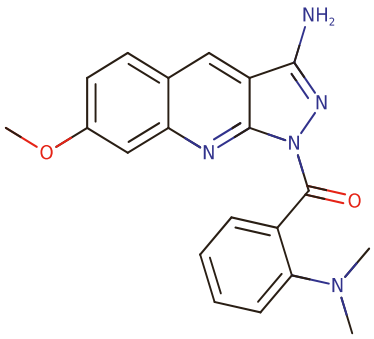

Mol Wt 361.4
Exact Mass 361.17

#	Time	Area%
1	0.670	3.84
2	0.991	96.16

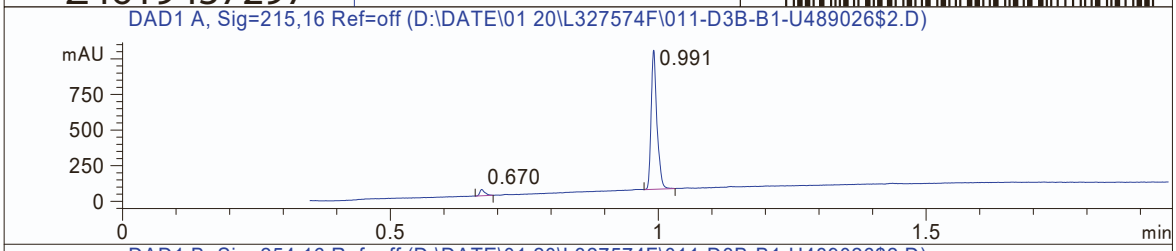

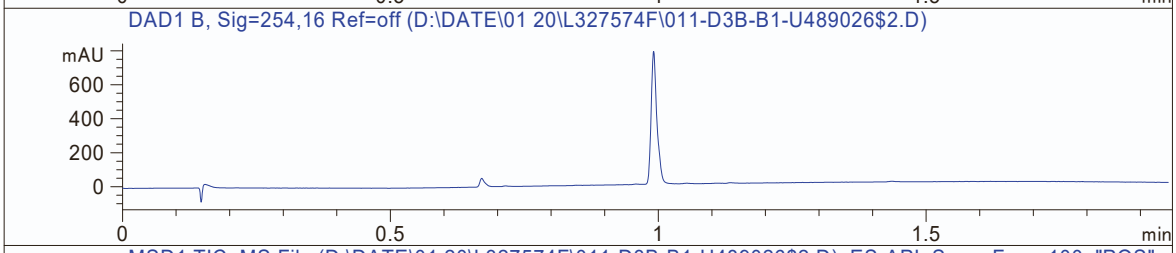

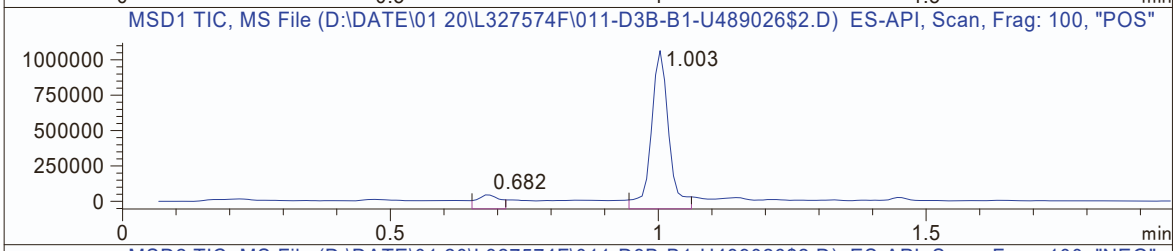

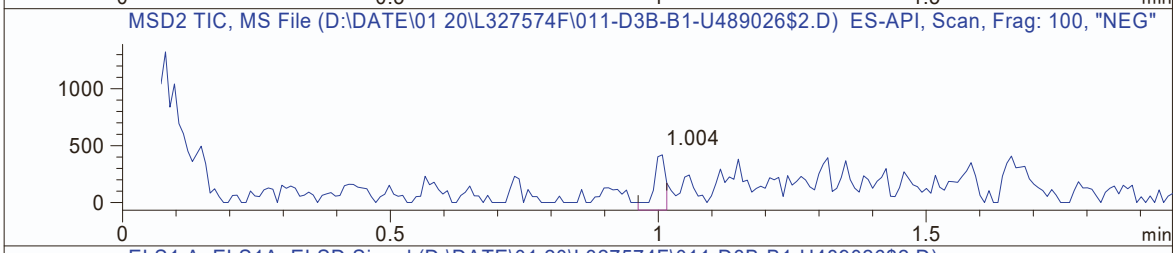

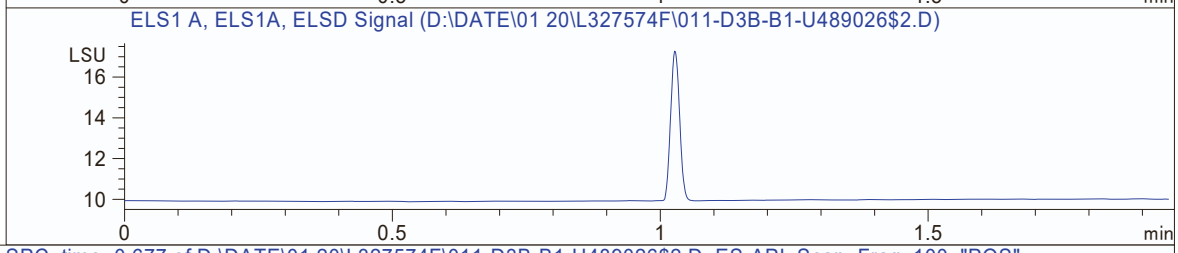

RT 0.682

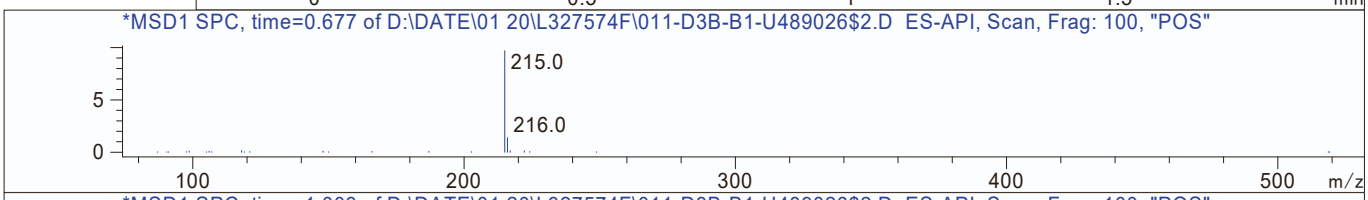

RT 1.003

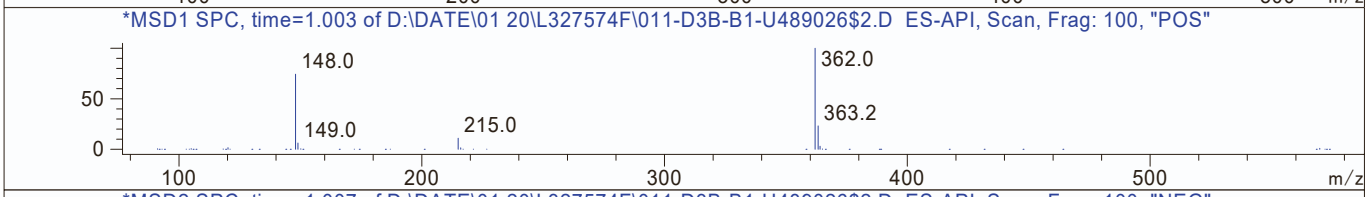

RT 1.004

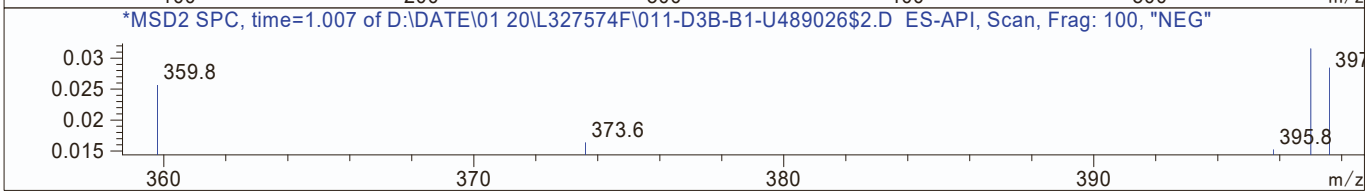

MaxPeak: 95.10%
Ret_Time: 1.221 min

MW05-E7
Z4619443254

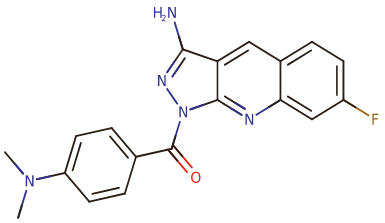

Mol Wt 349.36
Exact Mass 349.15

#	Time	Area%
1	1.221	95.10
2	1.341	4.90

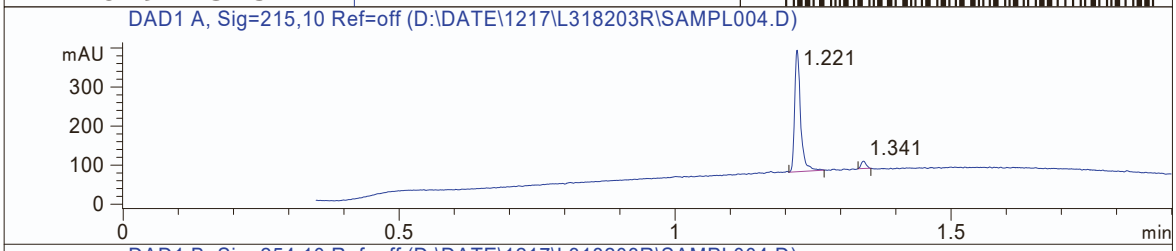

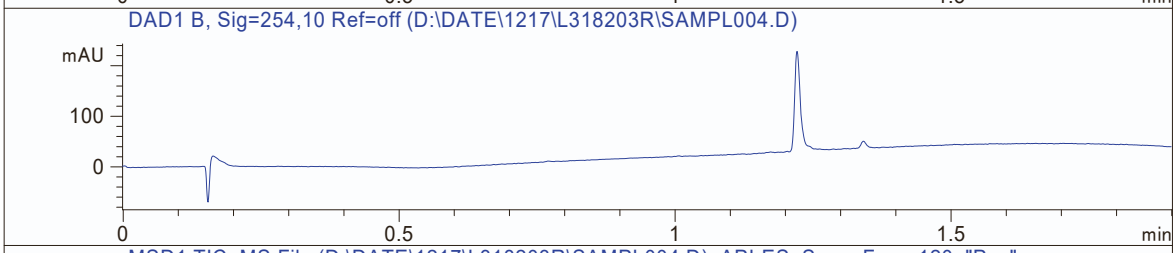

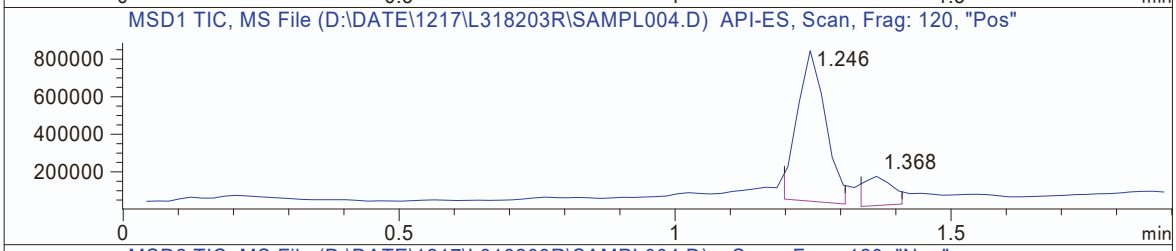

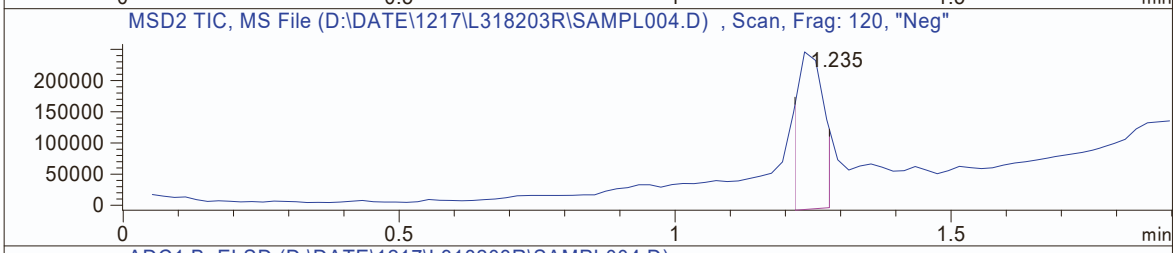

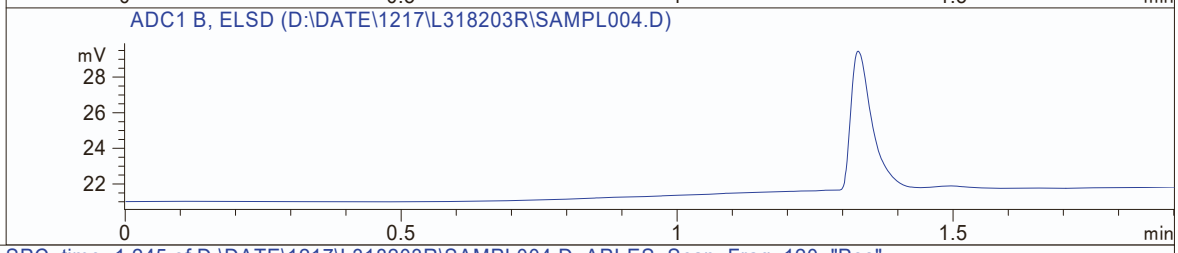

RT 1.246

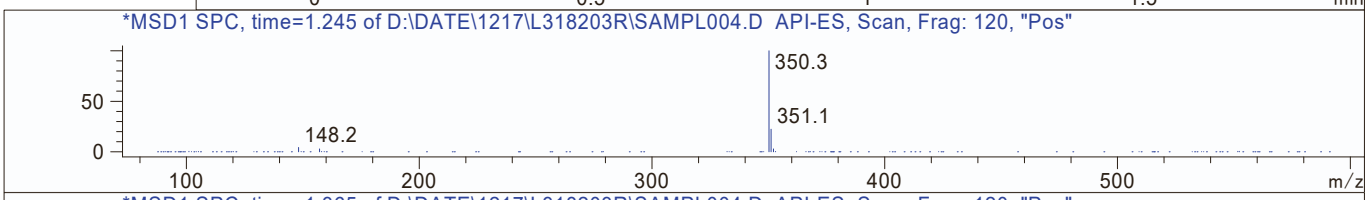

RT 1.368

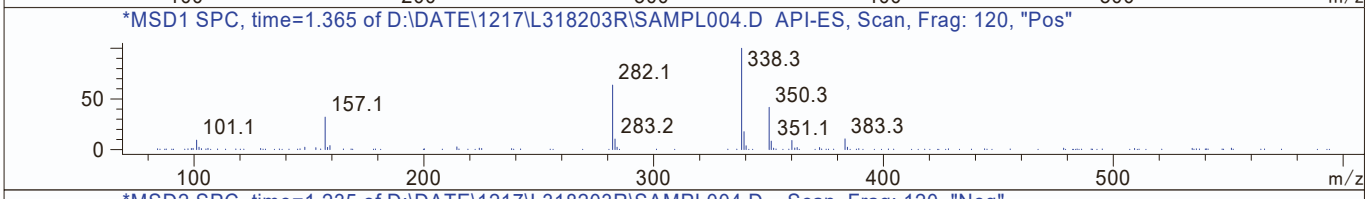

RT 1.235

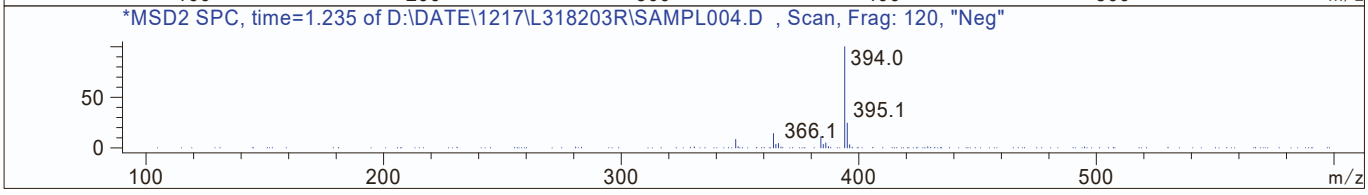

Inj.Date 12/18/2020 E -SL- Acq. Method C:\HPCHEM\-> ->

MaxPeak: 100.00%
Ret_Time: 1.119 min

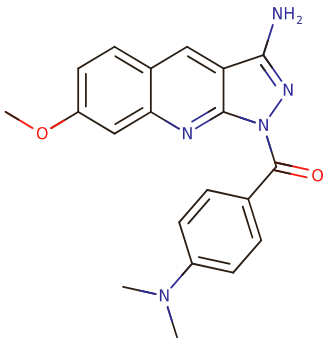

Mol Wt 361.4
Exact Mass 361.17

#	Time	Area%
1	1.119	100.00

MW05-E8
Z4619437300

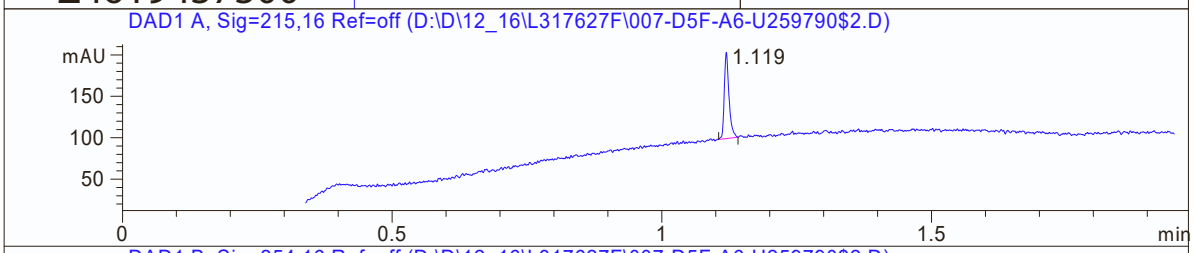

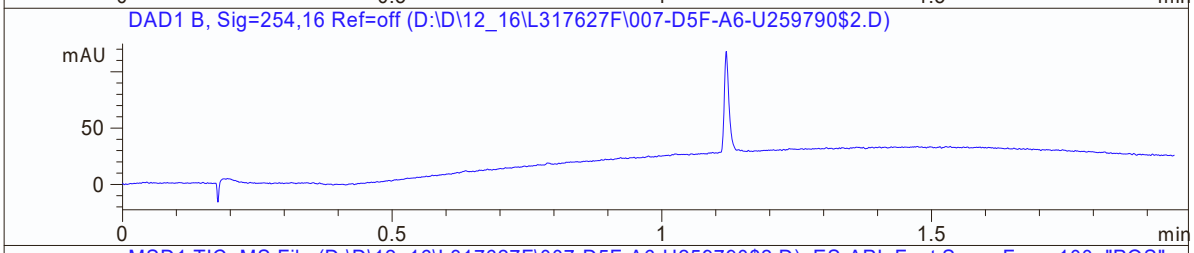

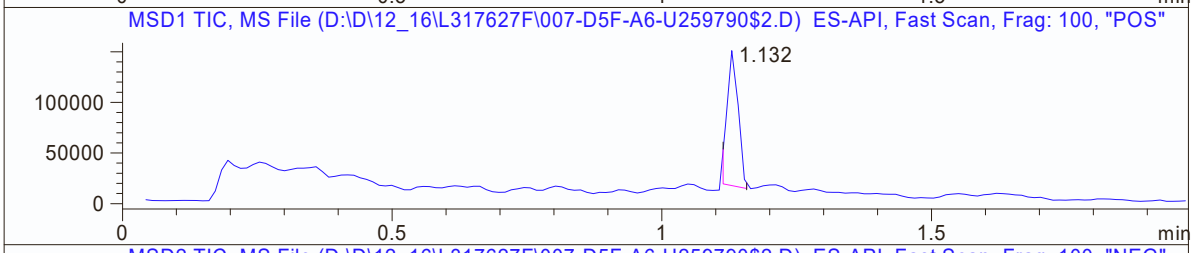

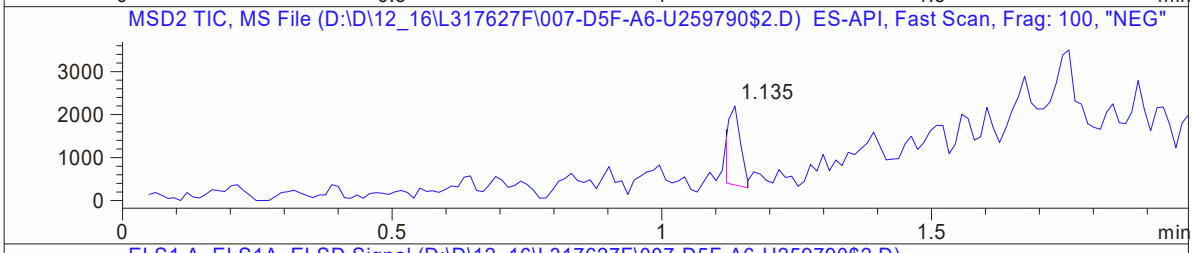

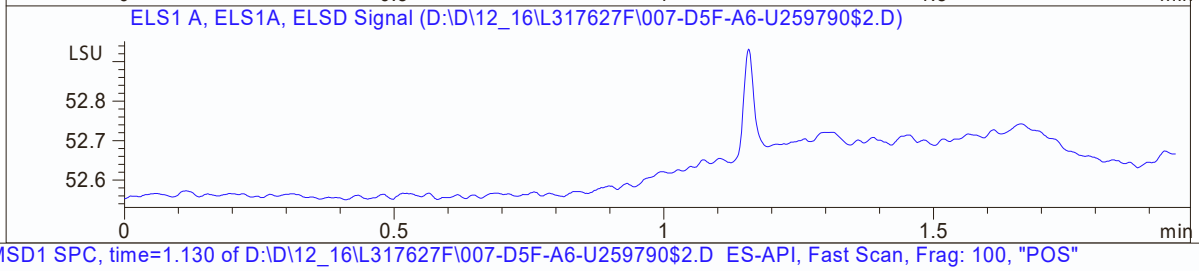

RT 1.132

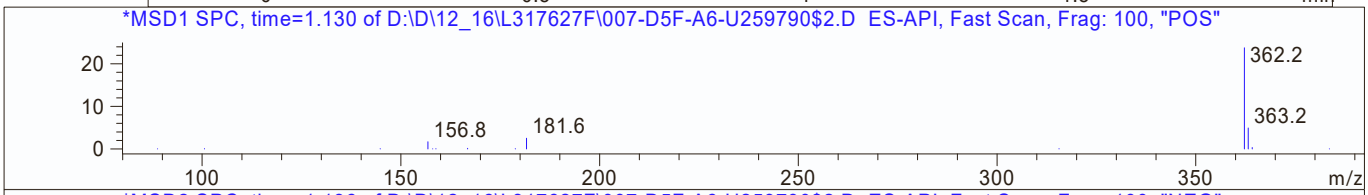

RT 1.135

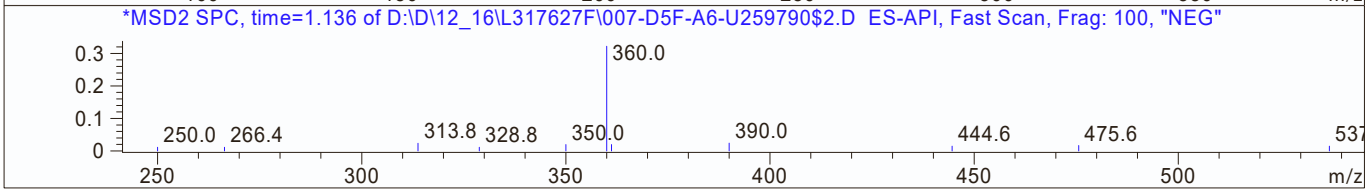

Inj.Date 12/16/2020 N Acq. Method C:\Users\ -> ->

MaxPeak: 100.00%
Ret_Time: 0.921 min

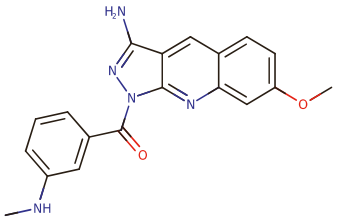

MW05-E9
Z4619432589

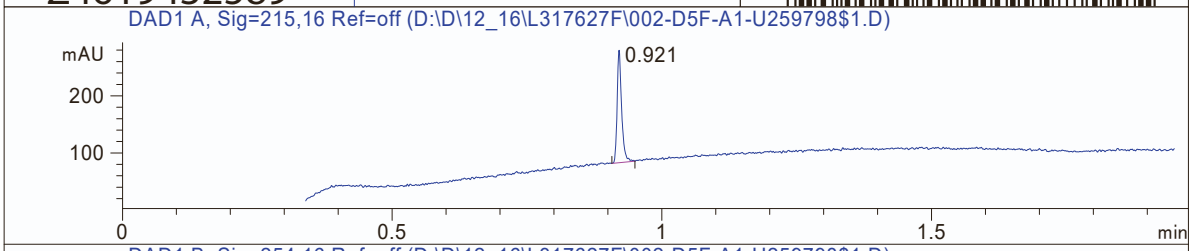

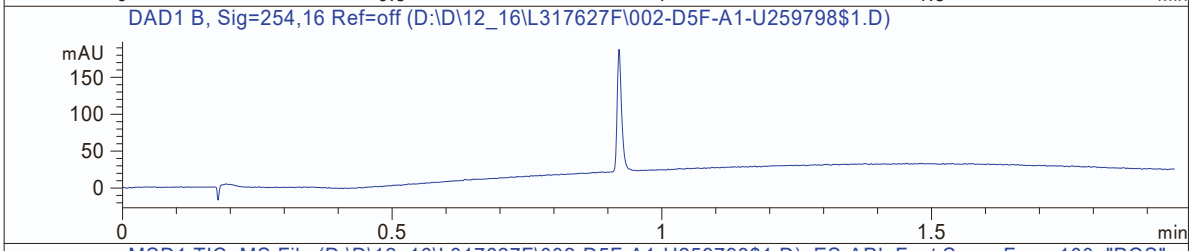

Mol Wt 347.37
Exact Mass 347.15

#	Time	Area%
1	0.921	100.00

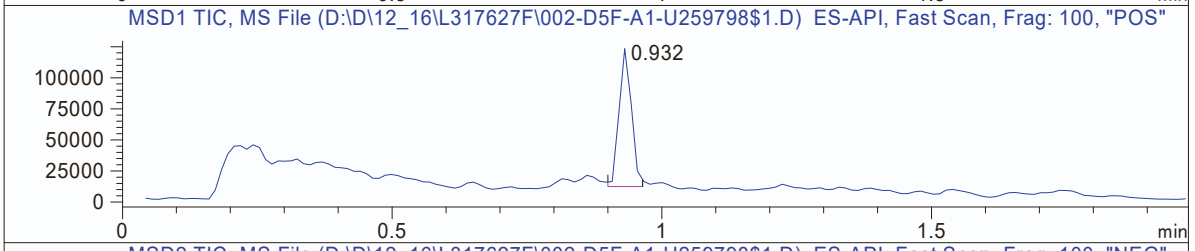

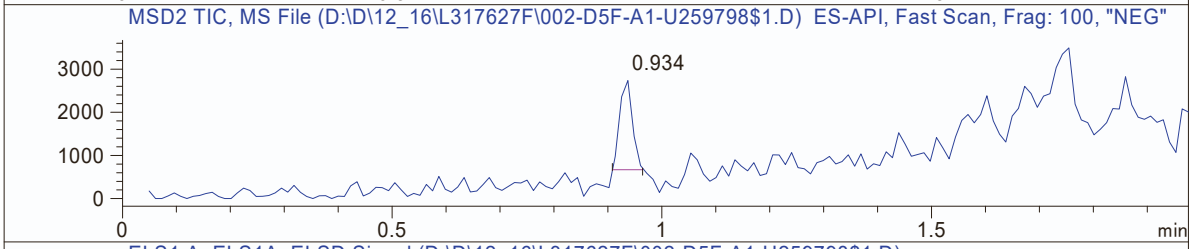

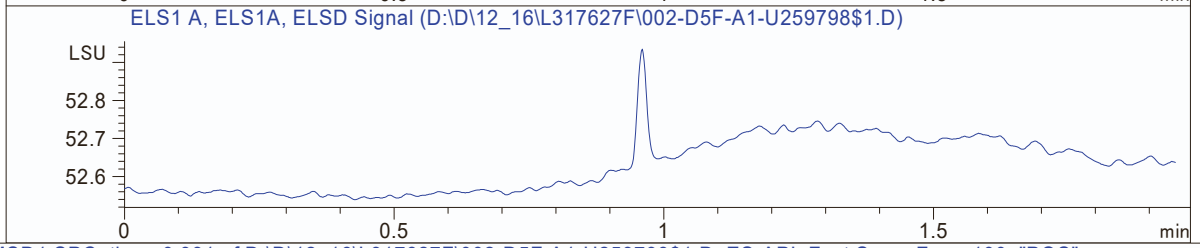

RT 0.932

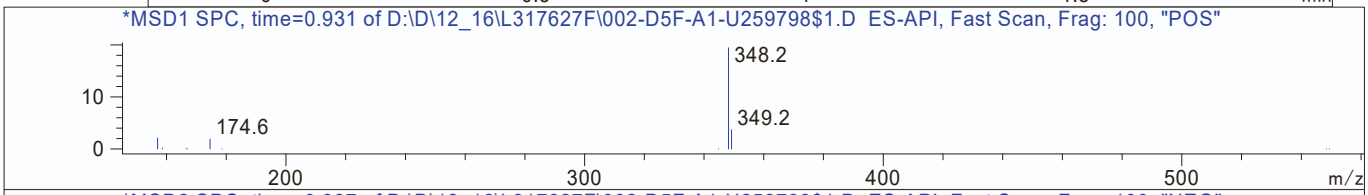

RT 0.934

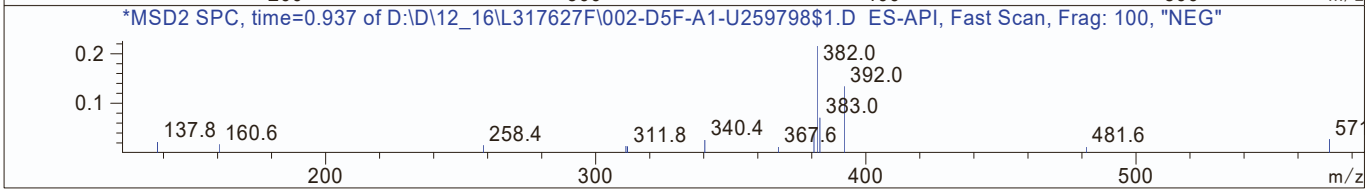

Inj.Date 12/16/2020 N Acq. Method C:\Users\ -> ->

MaxPeak: 97.07%
Ret_Time: 1.311 min

MW05-E10
Z4619432582

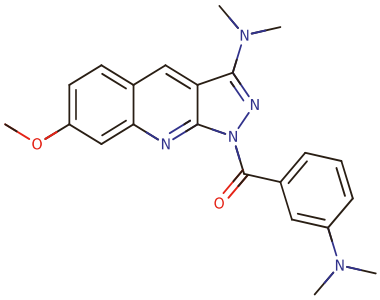

DAD1 A, Sig=215,10 Ref=off (D:\DATE\1217\L318203R\SAMPL008.D)

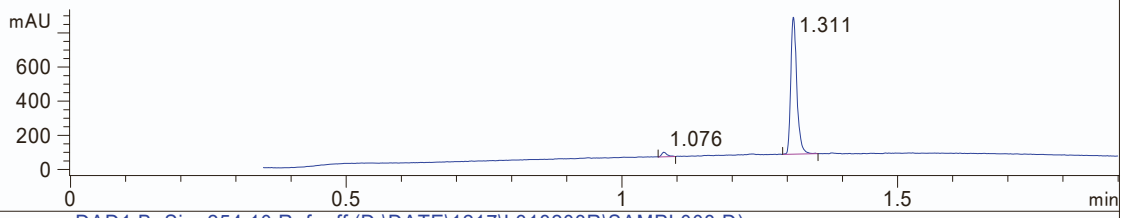

DAD1 B, Sig=254,10 Ref=off (D:\DATE\1217\L318203R\SAMPL008.D)

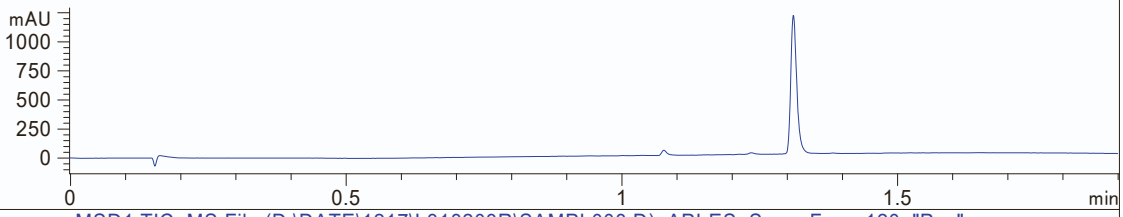

Mol Wt **389.45**
Exact Mass **389.21**

#	Time	Area%
1	1.076	2.93
2	1.311	97.07

MSD1 TIC, MS File (D:\DATE\1217\L318203R\SAMPL008.D) API-ES, Scan, Frag: 120, "Pos"

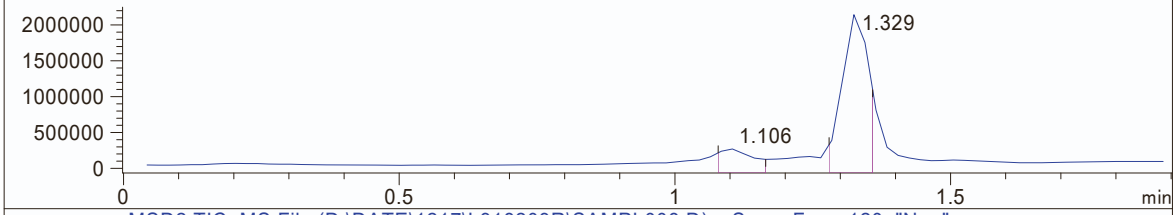

MSD2 TIC, MS File (D:\DATE\1217\L318203R\SAMPL008.D) , Scan, Frag: 120, "Neg"

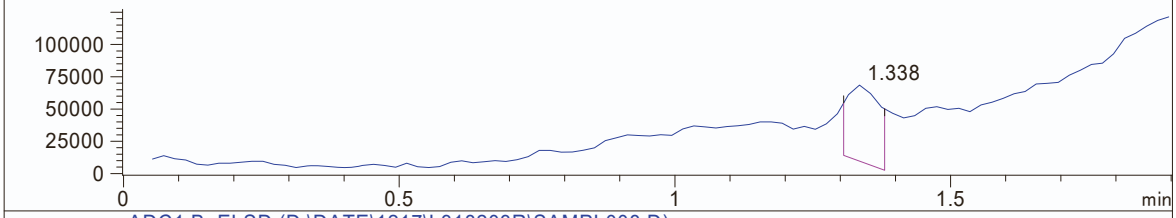

ADC1 B, ELSD (D:\DATE\1217\L318203R\SAMPL008.D)

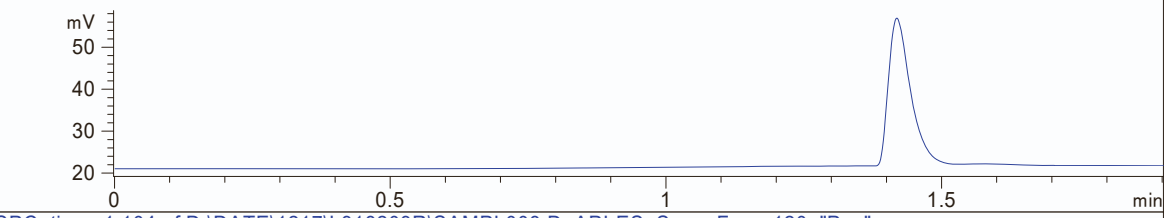

RT 1.106

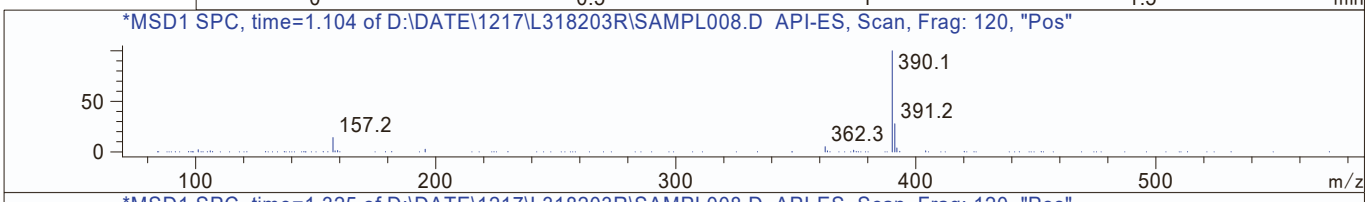

RT 1.329

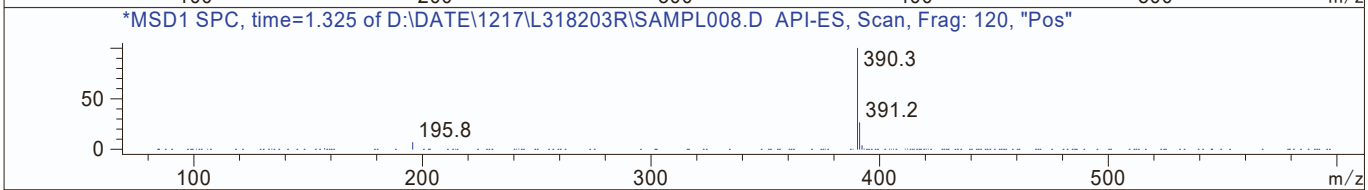

RT 1.338

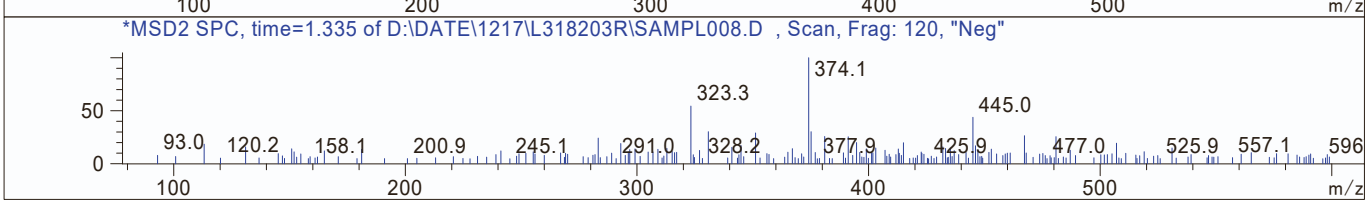

Inj.Date 12/18/2020 E -SL- Acq. Method C:\HPCHEM\-> ->

MaxPeak: 99.06%
Ret_Time: 1.007 min

MW05-E11
Z4619432588

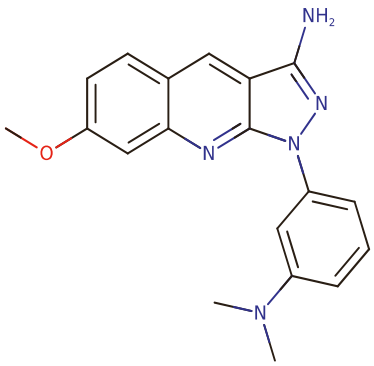

Mol Wt 333.39
Exact Mass 333.18

#	Time	Area%
1	1.007	99.06
2	1.145	0.94

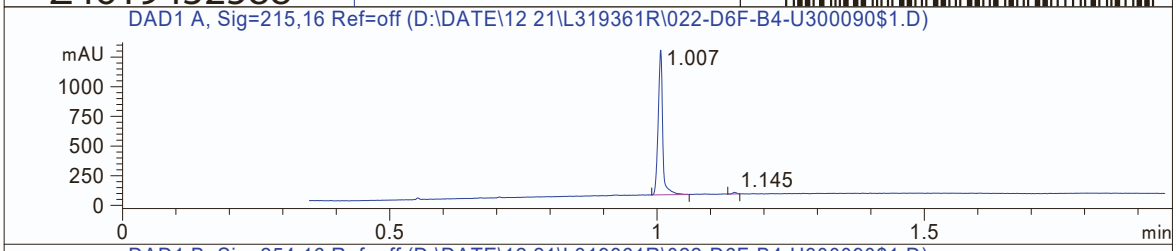

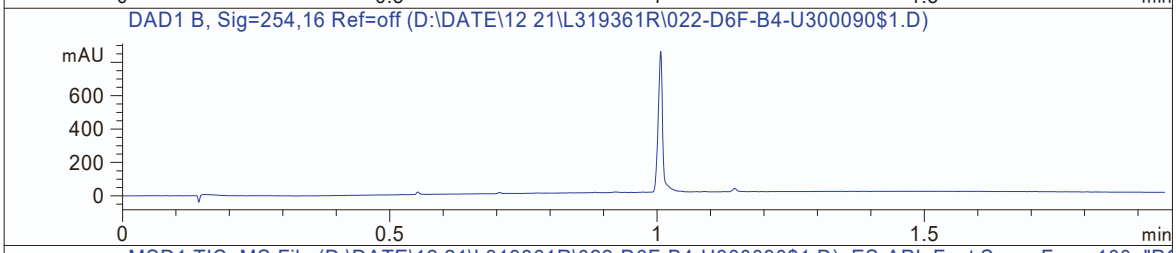

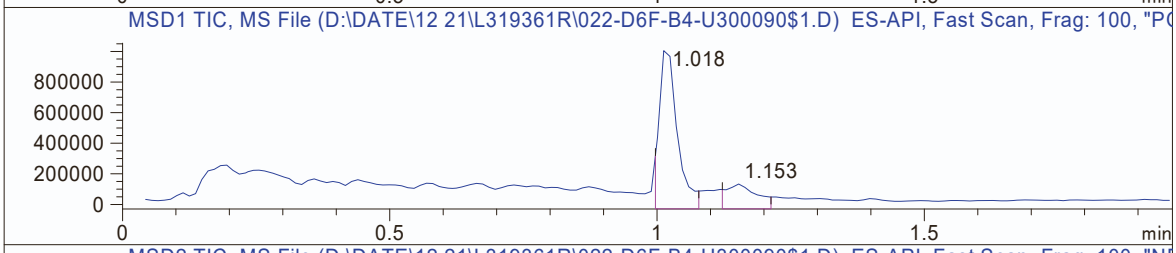

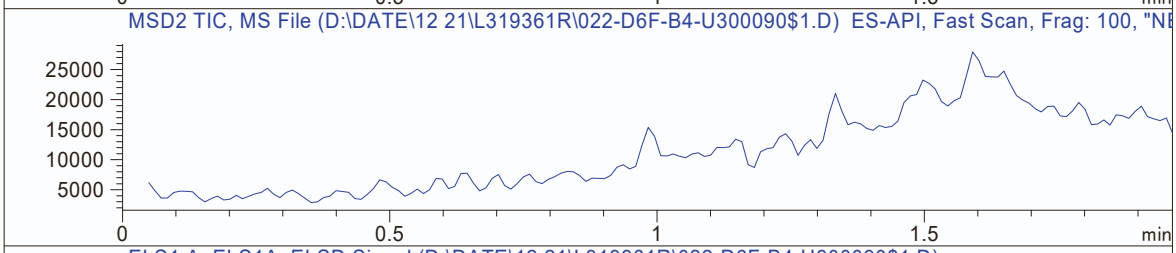

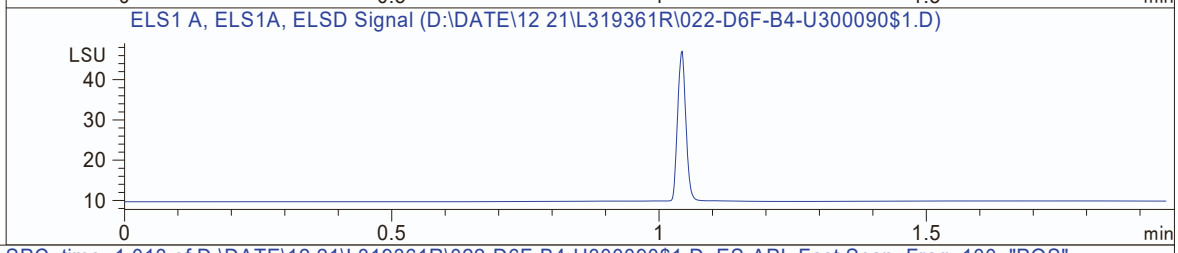

RT 1.018

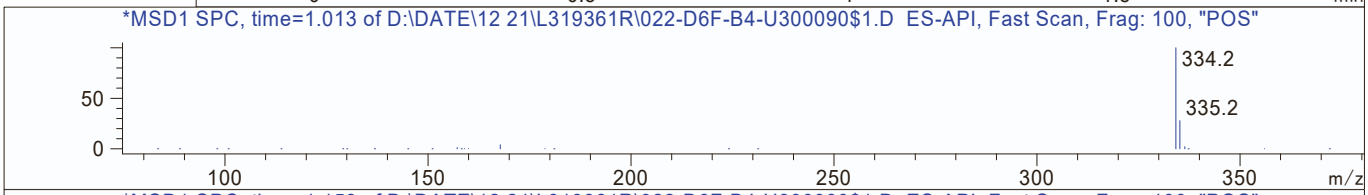

RT 1.153

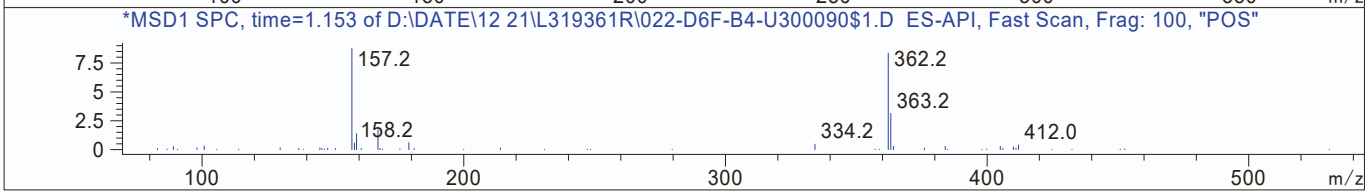

Inj.Date 12/21/2020 E Acq. Method C:\Users\ -> ->

MaxPeak: 100.00%
Ret_Time: 1.148 min

MW05-E13
Z4619442257

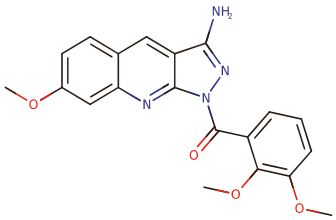

Mol Wt **378.38**
Exact Mass **378.14**

#	Time	Area%
1	1.148	100.00

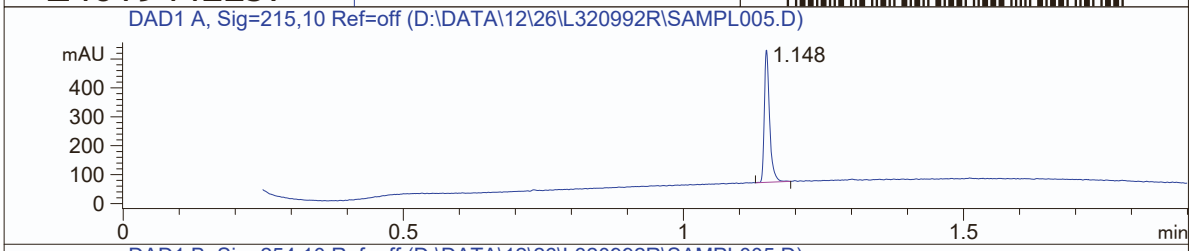

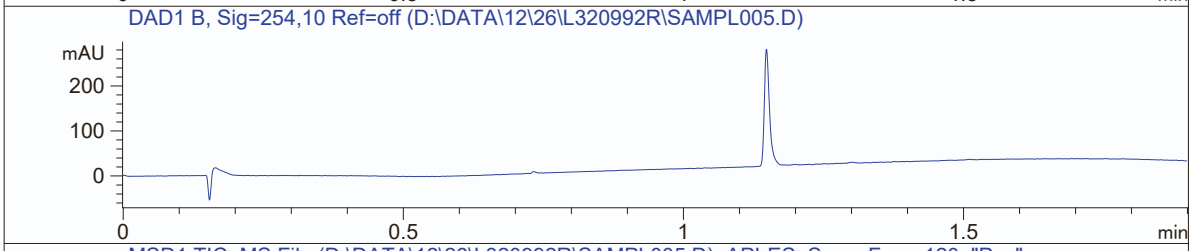

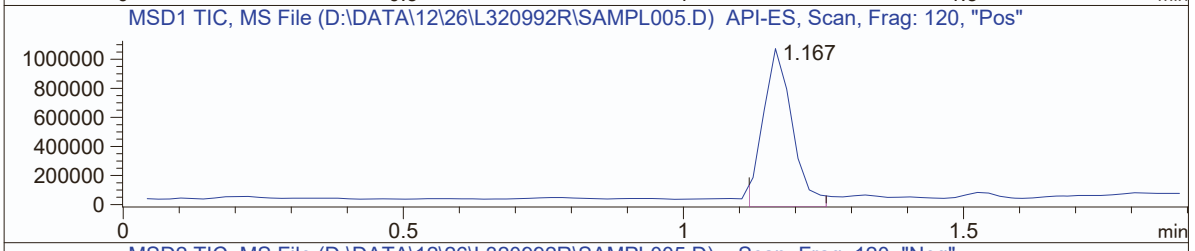

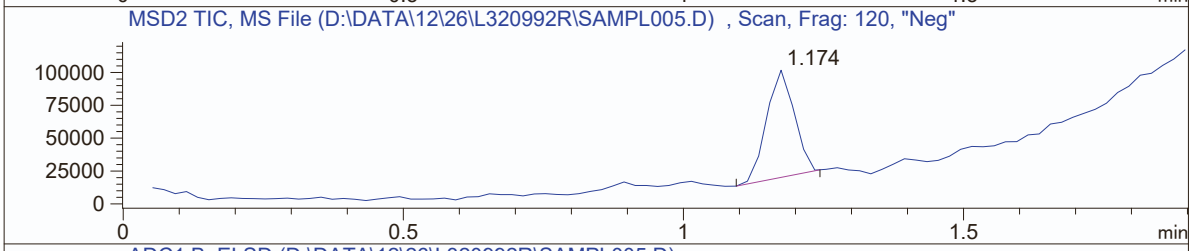

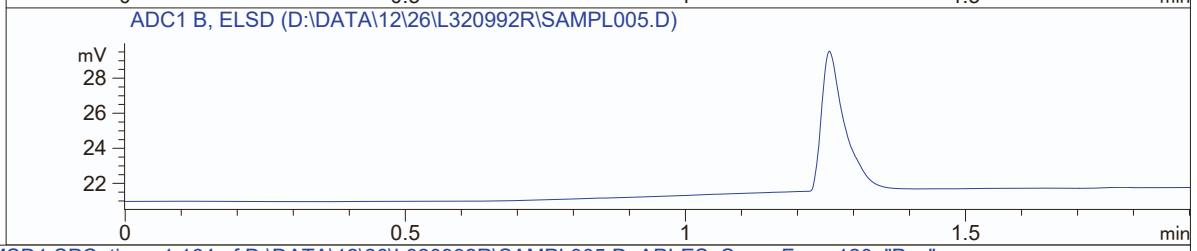

RT 1.167

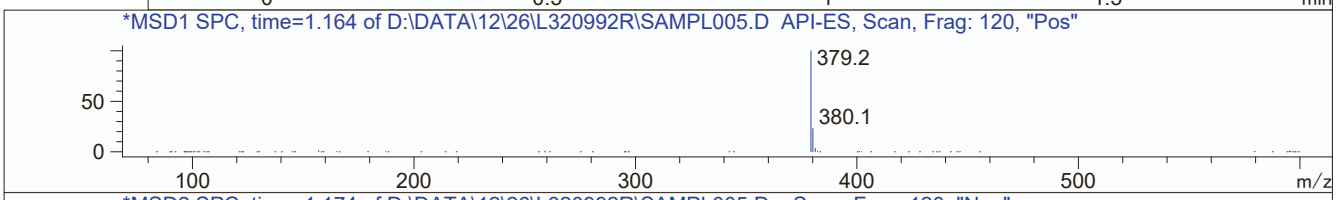

RT 1.174

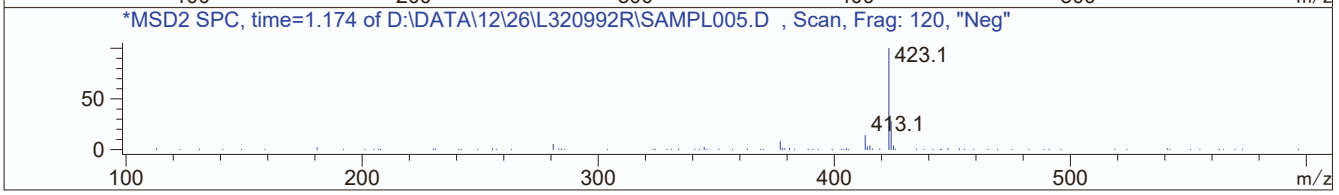

Inj.Date 12/25/2020 LB -SL- Acq. Method C:\HPCHEM\-> ->

MaxPeak: 100.00%
Ret_Time: 0.778 min

MW05-E14
Z3221672719

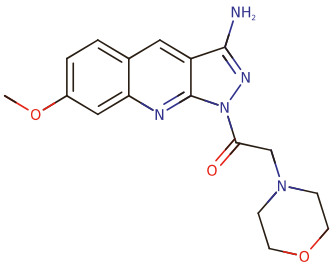

Mol Wt 341.36
Exact Mass 341.16

#	Time	Area%
1	0.778	100.00

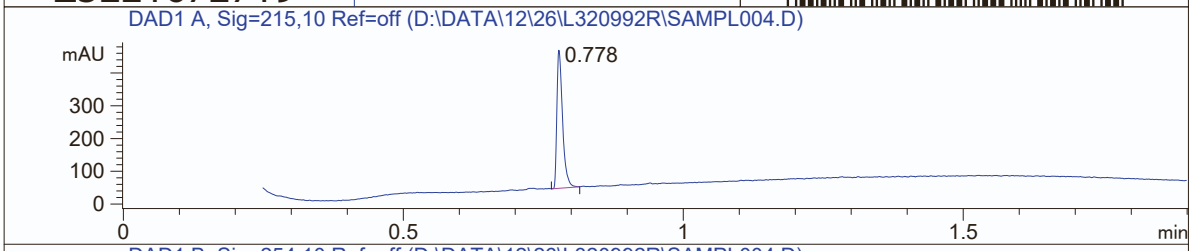

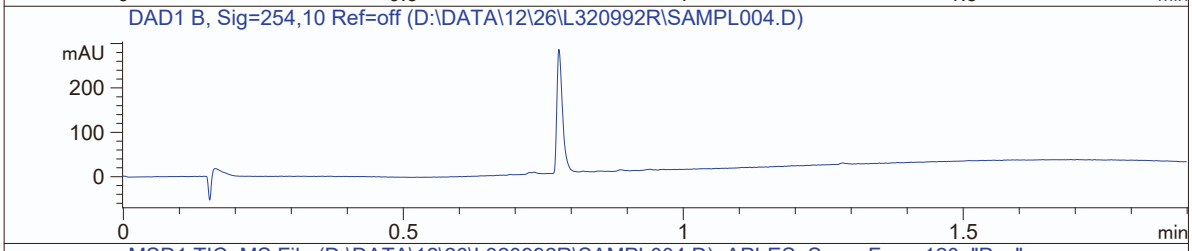

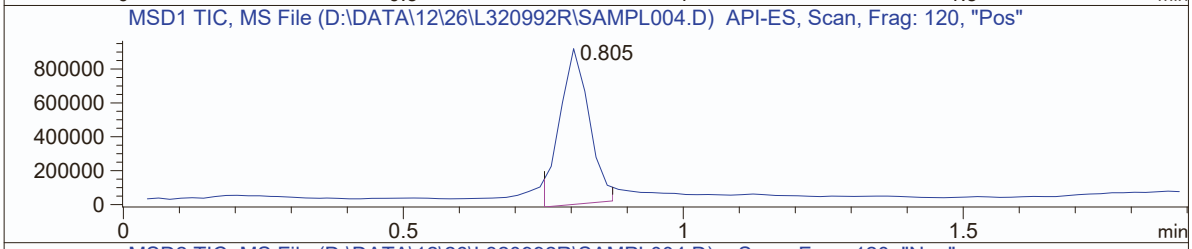

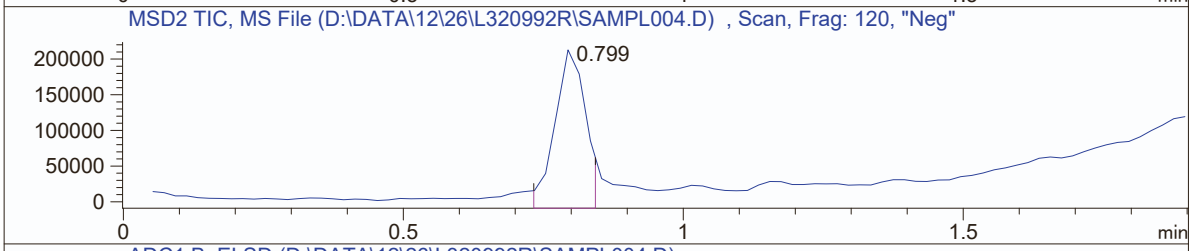

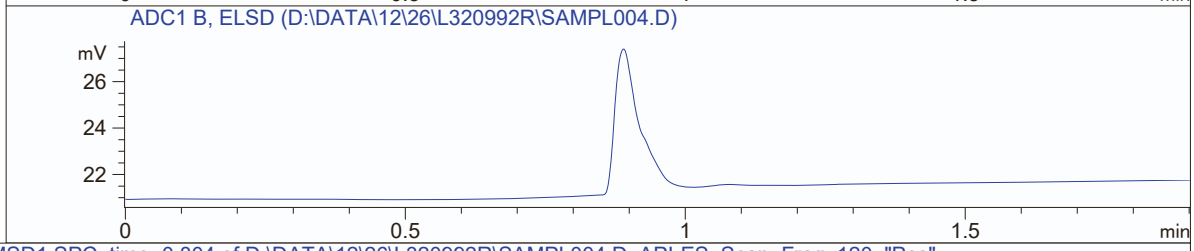

RT 0.805

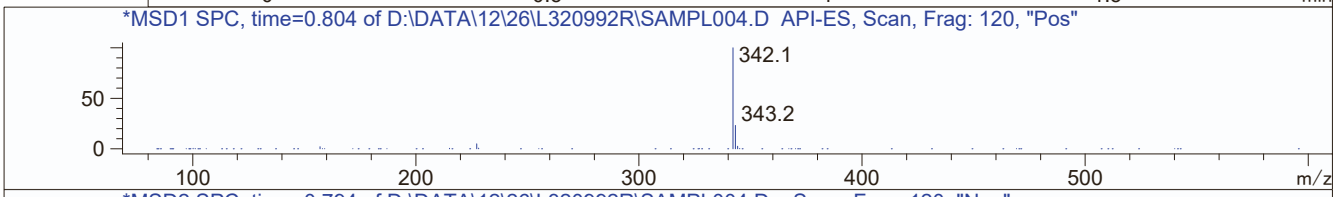

RT 0.799

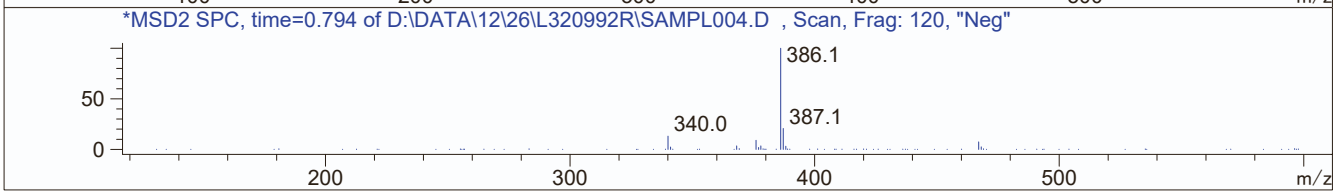

Inj.Date 12/25/2020 LB -SL- Acq. Method C:\HPCHEM\-> ->

MW05-E15
Z3221672536

MaxPeak: 95.10%
Ret_Time: 0.945 min

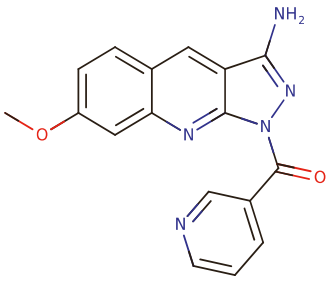

Mol Wt 319.32
Exact Mass 319.11

#	Time	Area%
1	0.945	95.10
2	0.978	2.28
3	1.098	2.62

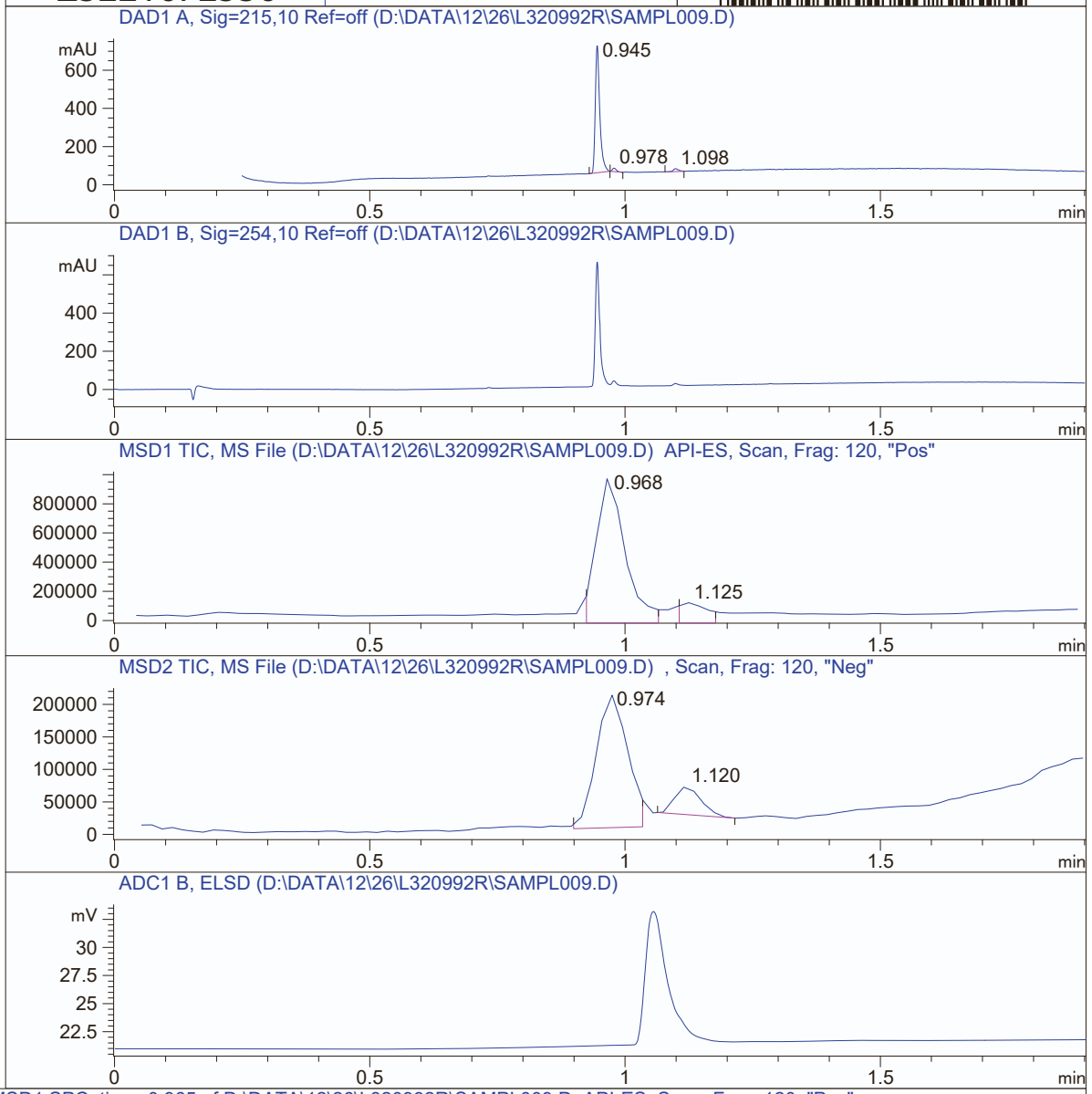

RT 0.968

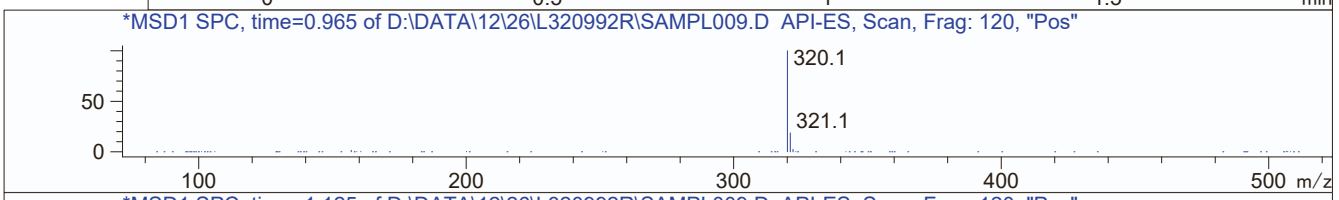

RT 1.125

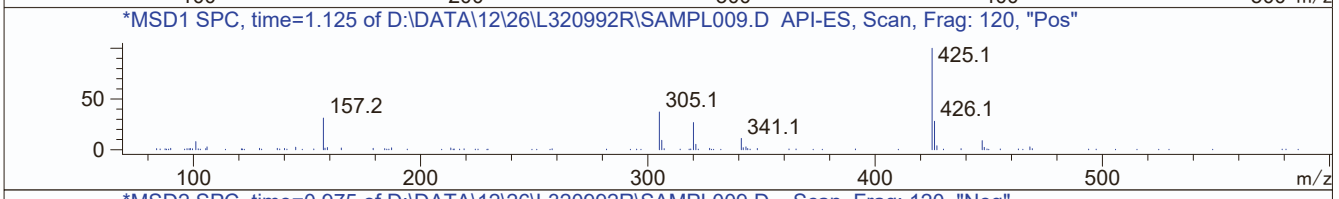

RT 0.974

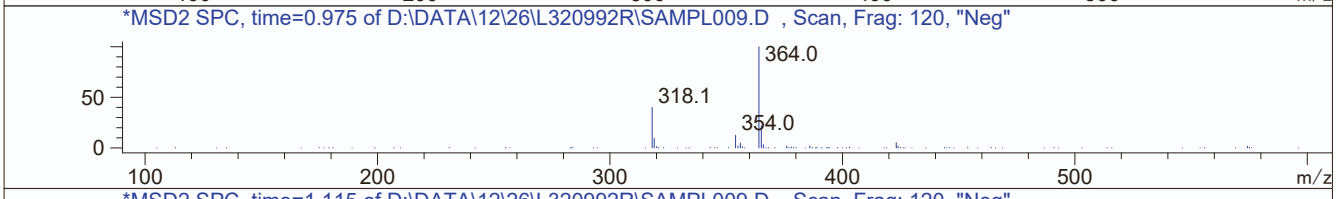

RT 1.120

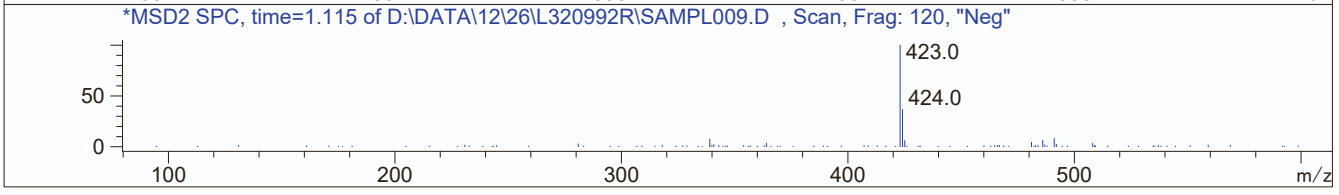

Inj.Date 12/25/2020 LB -SL- Acq. Method C:\HPCHEM\-> ->

Compound	^{1}H NMR Description
MW01	^{1}H NMR (300 MHz, DMSO-d_6) δ 8.65 – 8.56 (m, 2H), 8.40 (dd, J = 8.9, 2.2 Hz, 1H), 8.29 (dd, J = 6.3, 2.2 Hz, 1H), 7.64 (dd, J = 9.0, 2.3 Hz, 1H), 7.45 (dt, J = 9.1, 2.4 Hz, 1H), 4.10 (d, J = 2.2 Hz, 3H), 4.05 (d, J = 2.4 Hz, 4H)
MW01-E10	^{1}H NMR (400 MHz, DMSO-d_6) δ 10.57 (s, 1H), 9.93 (s, 1H), 8.75 (d, J=5.5 Hz, 1H), 8.59 (d, J=5.5 Hz, 1H), 8.45 (d, J=8.4 Hz, 1H), 8.15 (d, J=8.5 Hz, 1H), 7.83 (d, J=1.6 Hz, 1H), 7.65 (d, J=1.6 Hz, 1H), 7.42 (dd, J=8.4, 1.6 Hz, 1H), 7.20 (dd, J=8.4, 1.6 Hz, 1H)
MW01-E18	^{1}H NMR(500 MHz, DMSO-d_6) δ 10.01 (s, 1H), 9.59 (s, 1H), 9.08 (dd, J=8.3, 1.7 Hz, 1H), 8.85 (d, J=5.6, 1H), 8.53 (dd, J=5.5, 1.7 Hz, 1H), 8.38 (m, 2H), 7.72 (s, 1H), 7.22 (dd, J=8.5, 1.8 Hz, 1H)
MW01-E6	^{1}H NMR(500 MHz, DMSO-d_6) δ 8.92 (d, J=8.6 Hz, 1H), 8.65 (d, J=5.6 Hz, 1H), 8.45 (d, J=5.6 Hz, 1H), 8.35 (d, J=8.5 Hz, 1H), 8.00 (d, J=1.6 Hz, 1H), 7.33 (dd, J=8.5, 1.6 Hz, 1H), 7.20 (d, J=8.6 Hz, 1H), 4.15 (s, 3H), 3.91 (s, 3H)
MW01-E14	^{1}H NMR (300 MHz, DMSO-d_6) δ 8.88 (d, J = 4.9 Hz, 1H), 8.64 (d, J = 5.1 Hz, 1H), 8.51 (d, J = 8.8 Hz, 1H), 8.38 (d, J = 5.0 Hz, 1H), 8.21 (d, J = 5.3 Hz, 1H), 8.02 (d, J = 1.6 Hz, 1H), 7.46 – 7.38 (m, 1H), 4.09 (s, 3H), 3.93 (s, 3H)
MW05	^{1}H NMR(300 MHz, DMSO-d_6) δ 8.81 (s, 1H), 8.03 (d,J = 9.08Hz, 1H), 7.39 (d,J = 2.67Hz, 1H), 7.33 – 7.23 (m, 2H), 7.17 – 7.06 (m, 2H), 6.91 (dd,J = 2.90, 8.32Hz, 1H), 6.69 (s, 2H), 3.97 (s, 3H), 2.93 (s, 6H).
MW05-E3	^{1}H NMR (400 MHz, DMSO-d_6) δ 8.84 (s, 1H), 8.09 (d, J=8.2 Hz, 1H), 7.37 (m, 1H), 7.25 (m, 2H), 7.10-6.95 (m, 2H), 6.84 (m, 1H), 6.65 (s, 2H), 4.00 (s, 3H), 3.32 (m, 4H), 1.10 (m, 6H)
MW05-E9	^{1}H NMR (400 MHz, DMSO-d_6) δ 8.85 (s, 1H), 8.05 (d, J=8.2 Hz, 1H), 7.42 (d, J=1.9 Hz, 1H), 7.33-7.12 (m, 2H), 7.00 (m, 2H), 6.70 (m, 3H), 5.87 (m, 1H), 4.00 (s, 3H), 2.70 (m, 3H)
MW05-E2	^{1}H NMR (400 MHz, DMSO-d_6) δ 8.80 (s, 1H), 7.95 (d, J=8.2 Hz, 1H), 7.60-7.45 (m, 2H), 7.30 (m, 1H), 7.10 (m, 2H), 6.90 (d, J=8.2 Hz 1H), 6.75 (s, 2H), 4.00 (s, 3H), 2.95 (s, 6H)
MW05-E10	^{1}H NMR(500 MHz, DMSO-d_6) δ 8.72 (s, 1H), 7.92 (d, J=8.4 Hz, 1H), 7.30 (s, 1H), 7.15 (m, 1H), 6.95 (m, 1H), 6.72 (s, 1H), 6.65 (m, 1H), 6.53 (m, 1H), 4.00 (s, 6H), 3.50 (s, 3H), 2.65 (s, 6H)